WEIKAI ZHANG

Application of Nanotechnology-based MRI and Gene Delivery in Treatment of Sensorineural Hearing Loss

ACADEMIC DISSERTATION
To be presented, with the permission of
the board of the School of Medicine of the University of Tampere,
for public discussion in the Jarmo Visakorpi Auditorium,
of the Arvo Building, Lääkärinkatu 1, Tampere,
on November 1st, 2011, at 12 o'clock.

UNIVERSITY OF TAMPERE

UNIVERSITY
OF TAMPERE

ACADEMIC DISSERTATION
University of Tampere, School of Medicine
Finland

Supervised by
Docent Jing Zou
University of Tampere
Finland
Professor Ilmari Pyykkö
University of Tampere
Finland

Reviewed by
Docent Petri Mattila
University of Helsinki
Finland
Docent Maija Vihinen-Ranta
University of Jyväskylä
Finland

Distribution
Bookshop TAJU
P.O. Box 617
33014 University of Tampere
Finland

Tel. +358 40 190 9800
Fax +358 3 3551 7685
taju@uta.fi
www.uta.fi/taju
http://granum.uta.fi

Cover design by
Mikko Reinikka

Acta Universitatis Tamperensis 1661
ISBN 978-951-44-8584-8 (print)
ISSN-L 1455-1616
ISSN 1455-1616

Acta Electronica Universitatis Tamperensis 1124
ISBN 978-951-44-8585-5 (pdf)
ISSN 1456-954X
http://acta.uta.fi

Tampereen Yliopistopaino Oy – Juvenes Print
Tampere 2011

CONTENCES

ABSTRACT 5
ABBREVIATIONS 7
LIST OF ORIGINAL PUBLICATIONS 9
1. INTRODUCTION 10
2. REVIEW OF THE LITERATURE 12
2.1 Anatomy of the inner ear 12
2.2 Sensorineural hearing loss 12
2.2.1 The causes of sensorineural hearing loss 12
2.2.2 Treatment of sensorineural hearing loss 13
2.3 MRI 14
2.3.1 Magnetic resonance basics 14
2.3.2 MRI contrast agents 14
2.3.3 Application of MRI in diagnosis and treatment 15
2.3.3.1 Application of MRI in diagnosis 15
2.3.3.2 SPIONs-labelled stem cell tracking 17
2.4 Gene therapy 19
2.4.1 Math1 gene and inhibitor of DNA binding/differentiation proteins 20
2.4.1.1 Math1 gene 20
2.4.1.2 Inhibitor of DNA binding/differentiation proteins 21
2.4.2 Gene delivery system 21
2.4.2.1 Electroporation 22
2.4.2.2 Viral vector 23
2.4.2.3 Nonviral vector 23
2.4.2.3.1 Liposome and polymers 24
2.4.3 Cellular targeting 27
2.5 Stem cell-based therapy 28
2.5.1 In situ differentiation of inner ear stem cells 29
2.5.2 Exogenous stem cell transplantation 29
2.5.3 Autologous transplantation 30
2.5.4 Perspectives for future research 31
3. AIM OF THE STUDY 32
4. MATERIALS AND METHODS 33

4.1 Plasmid preparation 33
4.1.1 Math1 Plasmid construction 33
4.1.2 Id2.3 shRNA plasmid preparation 33
4.2 Cell cultures and treatment 33
4.3 Cochlear organotypic culture 35
4.4 In vivo experiment 35
4.5 Confocal microscopy 36
4.6 Statistical analysis 36
4.7 Synthesis of different nanoparticles 36
4.7.1 Synthesis of lipoplex nanoparticles 36
4.7.1.1 Synthesis of lipoplexes with TrkB ligand 36
4.7.1.2 Synthesis of lipoplexes with Math1 plasmid 37
4.7.2 Synthesis of hyperbranched polylysine nanoparticles 37
4.7.3 Synthesis of POA@SPIONs 38
4.8 MRI measurements 38
4.8.1 MRI measurement of Gd-DOTA 38
4.8.2 MRI measurement of POA@SPIONs 39
5. RESULTS 42
5. 1. Passage of gadolinium through the mouse inner ear barriers 42
5. 2. MRI manifestation of novel POA@SPIONs in the rat inner ear 45
5. 3. Internalization of HPNPs in the cochlear cells both in vitro and in vivo 47
5. 4. Math1 expression in vitro and intracellular trafficking of the Math1 protein 51
5. 5. Internalization of liposome nanoparticles functionalized with the TrkB ligand 54
6. DISCUSSION 58
6. 1. Difference in gadolinium permeability of perilymphatic and endolym- phatic barriers and indication for diagnosis 58
6. 2. POA@SPION are a “super” MR contrast agent for inner ear imaging 59
6. 3. Nuclear entry of HPNPs into the cochlear cells 61
6. 4. Importance of nuclear localization of Math1 in transcription 63
6. 5. Targetability of TrkB ligand-functionalized liposome nanoparticles 66
7. SUMMARY AND CONCLUSIONS 68
8. ACKNOWLEDGEMENTS 69
9. REFERENCES 71
10. ORIGINAL PUBLICATIONS 90

// ABSTRACT

Sensorineural hearing loss (SNHL) is a common sensory defect that has an enormous impact on the affected individual as well as on all of society. Approximately 13% of EU citizens, over 60 million individuals, suffer from hearing loss. The human cochlea is buried deeply in the temporal bone, and its access is limited by membranous partitions. This fact makes the diagnosis of inner ear disorders using imaging techniques, such as MRI, challenging. The traditional treatment strategy for SNHL has not been successful. Cochlear implant (CI) has certain indications and problems. A cure for SNHL would thus depend on novel concepts, such as CI in combination with gene delivery or stem cell therapy.

Herein, contrast agent or nanoparticles are evaluated using 4.7 T MRI *in vivo*. The contrast agent gadolinium, administered either by intravenous injection or an intratympanic route, was studied to demonstrate the limits of MR imaging resolution of the fine inner ear structures in the mouse and to explore intracochlear barriers permeability. The MRI manifestation of superparamagnetic iron oxide nanoparticles hierarchically coated with oleic acid and Pluronic®F127 copolymers (POA@SPIONs) was investigated in the rat inner ear. Internalization and of nuclear entry capacity for hyperbranched polylysine nanoparticles (HPNPs) were tested *in vitro* and *in vivo*. Math1 was selected as the model gene and was cloned into the pCDNA6.2/C-EmGFP vector, which is designed for non-viral vector mediated gene expression in mammalian cells. Neuron directed-differentiation of bone marrow mesenchymal stem cells (MSCs) via Math1 gene engineering was investigated. Internalization and targetability of TrkB ligand-functionalized multifunctional liposome nanoparticles were analyzed in primary cochlear cell culture, cochlear explants, and rats.

Based on this series of five studies, contrast agent MRI is capable of discerning the inner ear structures of the mouse and intracochlear barrier function. The normal blood-endolymph barrier is tighter than the blood-perilymph barrier. POA@SPIONs are a promising T2 negative contrast agent that is detectable within the rat inner ear using MRI. The normal blood-perilymph, blood-endolymph, and perilymph-endolymph barriers restrict passage of POA@SPIONs. HPNPs were efficiently internalized by the cochlear cells in primary cell culture, in organotypic culture, and *in vivo*. Both cytoplasm and nucleus showed the distribution of HPNPs. This finding suggests that HPNPs have a potential use in gene delivery to the cochlea. Plasmid pcDNA6.2/C-EmGFP-Math1 is suitable for non-viral gene delivery of Math1. Unique intracellular trafficking for Math1 was demonstrated using this novel plasmid. Neuron-like cell differentiation of MSCs transfected with the Math1 plasmid was observed. HPNP-mediated gene transfection efficiency was higher than liposome nanoparticles in dividing cells, and both induced poor gene transfection efficiency in primary cochlea cells. Likely targetability of TrkB ligand-functionalized liposome nanoparticles was observed in rat

cochlea, but not in primary cochlear cell culture and cochlear explants.

Taken together, the results reported here demonstrate that contrast agent MRI can evaluate inner ear biological barrier function. The novel POA@SPIONs are a promising T2 negative contrast agent, which may be further surface-modified by either peptides or antibodies to increase their use as a diagnostic agent and as traceable therapeutic nanoparticles in SNHL molecular imaging. The nuclear localization of the Math1 protein is important for their function. Neuron-like MSC differentiation mediated by Math1 provides information for future studies of the spiral ganglion neuron-orientated stem cell differentiation. The nuclear entry and efficient endosomal escape of HPNPs result in high gene transfection efficiency. TrkB ligand-functionalized liposome nanoparticles can potentially be used for the targeted delivery of genes or drugs to spiral ganglion cells. Transfection efficacy and targetability may be improved by using multifunctional nanoparticles, functionalized with peptides or antibodies. Nanoparticle-mediated biological treatment of SNHL is a very promising strategy.

ABBREVIATIONS

2D	Two-dimensional
3D	Three-dimensional
Am	Ampulla
bHLH	Basic helix-loop-helix
CA	Cochlear aqueduct
CI	Cochlear implant
DAPI	4', 6-diamidino-2-phenylindole
DLS	Dynamic light scattering
DMEM	Dulbecco's Modified Eagle's Medium
DOPE	1, 2-dioleoyl-sn-glycero-3 phosphoethanolamine
ESCs	Embryonic stem cells
FBS	Fetal bovine serum
GFP	Green fluorescent protein
Gd-DOTA	Gadolinium-tetra-azacyclododecane-tetra-acetic acid
HPNPs	Hyperbranched polylysine nanoparticles
IC	Intracochlear
Ids	Inhibitor of DNA binding/differentiation proteins
iPSs	induced pluripotent stem cells
IT	Intratympanic
IV	Iintravenous
LW	Lateral wall
MFNPs	Multifunctional nanoparticles
Mn	Manganese
Mod	Modiolus
MPR	Multiplanar reconstruction
MR	Magnetic resonance
MRI	Magnetic resonance imaging
MSCs	Mesenchymal stem cells
NLS	Nuclear localization signal
NPC	Nuclear pore complex
NSCs	Neural stem cells
OHC	Outer hair cell
OSL	Osseous spiral lamina
PBS	Phosphate-buffered saline
PC	Polyurethane catheter
PCR	Polymerase chain reaction
pDNA	Plasmid DNA

PEI	Polyethylenimine
POA@SPIONs	SPIONs coated with Pluronic® F127 copolymers and oleic acid
RWM	Round window membrane
SC	Silicon catheter
SGC	Spiral ganglion cell
shRNA	Short hairpin RNA
siRNA	Small interfereing RNA
SM	Scala media
ST	Scala tympani
SV	Scala vestibuli
SNHL	Sensorineural hearing loss
SPIONs	Super paramagnetic iron nanoparticles
Vest	Vestibulum

LIST OF ORIGINAL PUBLICATIONS

The thesis is based on the following original publications, which are referred to in the text using their roman numerals:

I. Jing Zou, Ya Zhang[1], **Weikai Zhang[1]**, Sanjeev Ranjan[1], Rohit Sood, Andrey Mikhailov, Paavo Kinnunen, Ilmari Pyykkö. Internalization of liposome nanoparticles functionalized with TrkB ligand in rat cochlear cell populations. Eur J Nanomedicine; 2009; 2(2): 7-13.

II. Jing Zou, **Weikai Zhang**, Dennis Poe, Ya Zhang, Usama Abo Ramadan, Ilmari Pyykkö. Differential passage of gadolinium through the mouse inner ear barriers evaluated with 4.7 T MRI. Hear Res. 2010; 259(1-2):36-43.

III. Jing Zou, **Weikai Zhang**, Dennis Poe, Jian Qin, Andrea Fornara, Ya Zhang, Usama Abo Ramadan, Mamoun Muhammed, Ilmari Pyykkö. MRI manifestation of novel superparamagnetic iron oxide nanoparticles in the rat inner ear. Nanomedicine (Lond). 2010; 5(5):739-54

IV. **Weikai Zhang**, Ya Zhang, Marian Löbler, Klaus-Peter Schmitz, Aqeel Ahmad, Ilmari Pyykkö, Jing Zou. Nuclear entry of hyperbranched polylysine nanoparticles into cochlear cells. Int J Nanomedicine. 2011; 6:536-46.

V. **Weikai Zhang**, Ya Zhang, Rohit Sood, Sanjeev Ranjan, Elena Surovtseva, Aqeel Ahmad, Paavo kinnunen, Ilmari Pyykkö, Jing Zou. Visualization of intracellular trafficking of Math1 protein in different cell types with a newly-constructed nonviral gene delivery plasmid. J Gene Med. 2011; 13(2):134-44.

[1] Equal contributor.

The original publications are reproduced in this thesis with the permission of the copyright holders.

1. INTRODUCTION

Hearing loss is a major public health problem that ranks 9th among the most severe diseases in the EU. The traditional treatment strategies for SNHL have not been very successful. Cochlea hair cells are mechanosensory receptors that can convert sound signals into electrical impulses. Hair cell loss from overstimulation, ototoxic drugs, bacterial and viral infections, aging and other causes is irreversible and leads to permanent hearing impairment. CI is currently the only therapeutic intervention for patients with severe or profound SNHL. However, CI has its indications and at the same time progressive degeneration of the cochlear neurons (spiral ganglion cells) takes place and may eventually result in complete hearing loss (Rejali et al., 2007; Roehm , Hansen, 2005; Shepherd et al., 2004). A cure for SNHL would thus depend on novel concepts, such as CI in combination with successful gene/drug delivery or stem cell therapy (de Felipe et al., 2011; Ciorba et al., 2009; Okano et al., 2006).

Magnetic resonance imaging (MRI) is a powerful tool for visualizing the anatomy and certain aspects of the physiology of different organs *in vivo*. MRI of the delicated inner ear structure has been realized using higher field strength magnets and contrast agents. The inner ear is housed in dense bone and is subdivided into different fluid-filled compartments; thus, it is possible to evaluate the biological barrier function using MRI. The current challenge in inner ear MRI today is distinguishing the inner ear fluids (endolymph and perilymph) using contrast agents and, eventually, identifying the pathological changes.

Gene therapy offers new treatment possibilities for a large number of common acquired and inherited human inner ear diseases for which conventional therapy is not effective (Maiorana and Staecker, 2005;Van de Water et al., 1999). Identification of effective methods to stimulate either new functional hair cells or spiral ganglion cells regeneration in the cochlear would be of therapeutic value for treating hearing deficits. The bHLH transcription factor Math1 is both necessary and sufficient for hair cell development in the mammalian cochlea (Bermingham et al., 1999; Zheng and Gao, 2000). Math1 has been reported as being the necessary molecule to initiate stem cell differentiation toward both hair cells and neurons (Bermingham et al., 1999; Flora et al., 2007). One potential strategy for hair cell regeneration is to induce the phenotypic transdifferentiation of nonsensory cells that remain in the inner ear (de Felipe et al., 2011; Shibata and Raphael, 2010; Batts SA and Raphael Y, 2007; White er al., 2006). To achieve this goal, gene therapy requires technologies capable of gene transfer into targeted cells within the cochlea in a large quantity. A key factor of successful gene therapy is development of gene delivery systems for efficient gene delivery into target cells. Thus far, two types of gene delivery systems, viral and non-viral vectors, have been employed as vehicles for gene transfer. Viral vectors are still not regarded as safe for inner ear gene

delivery. Nonviral gene transfer techniques represent a simple and, more importantly, safer alternative to viral vectors. Nonviral vectors can circumvent some of the problems associated with viral vectors such as oncogenic effects and unexpected immune response (Nabel et al., 1993; Smith et al., 1993b; Yang et al., 1994). Nanoparticles are one of the most promising gene carriers among the nonviral gene delivery systems (Borkholder DA., 2008). Thus far, there have been no reports of the use of nanoparticles as vectors for Math1 gene transfer in the treatment of hearing deficiencies.

Stem cell-based therapy is a rapidly growing area of research and has potential applications in the treatment of SNHL. Although many major hurdles still exist, stem cell-based therapy has the potential to become the gold standard for the restoration of hearing loss (Pauley et al., 2008). MSCs have been reported to differentiate into inner ear hair cells (Jeon et al., 2007) and neurons (Jiang et al., 2002). Thus, MSCs are attractive candidates for autologous transplantation in replacement of damaged inner ear hair cells and neurons.

The purpose of the present study was to evaluate the effects of different contrast agents on reporting function of the inner ear barrier using MRI; to investigate the nuclear entry of nanoparticles into cochlear cells for potential gene delivery; to demonstrate the efficacy of nanoparticle-mediated delivery of the model gene Math1; and to explore the spiral ganglion cell targetability of TrkB ligand-functionalized liposome nanoparticles.

2. REVIEW OF THE LITERATURE

2.1 Anatomy of the inner ear

The ear is made up of three main parts: the outer ear, the middle ear, and the inner ear. The ear drum separates the outer and middle ear. Behind the ear drum is the middle ear, which is normally filled with air. Three tiny bones inside the middle ear are named for their shapes: the malleus, incus, and stapes. The three bones connect to form a chain. The first bone, the malleus, is connected to the ear drum. The last bone, the stapes, is connected to another membrane called the oval window. The oval window is the beginning of the inner ear or cochlea. When sound hits the ear drum, the tiny bones are set in motion, and the last bone pushes on the oval window, activating the cochlea. The hair cells transform sound waves into electrical impulses that travel along the auditory nerve to the brain. The brain processes these impulses and translates the electrical signal into meaningful message.

The mammalian cochlea is a small spiral snail-shaped organ that measures 9 mm in diameter at the base and 5 mm in height in humans (Popper A, 1996). Its anatomy consists predominantly of fluid-filled chambers that contain endolymph and perilymph. The two larger chambers, the scala tympani and scala vestibuli, contain perilymph, a fluid with high Na^+ content and a similar ionic composition to extracellular fluid. The central chamber or scala media, which houses the auditory receptor hair cells, is separated from the scala tympani and scala vestibuli by the basilar membrane and Reissner's membrane, respectively, and contains the K^+-rich fluid endolymph (Makimoto et al., 1978; Ryan et al., 1979). The isolating structure for the endolymph is watertight in order to maintain the electrolyte homeostasis, which is essential for the normal function of the organ of Corti, the site of sensory neuroepithelium (Hibino et al., 2006; Leonova et al., 1997). Loss of the integrity of these membranes, increase in the permeability of the stria vascularis, or reduce in absorptive functions of the endolymphatic sac may produce a number of disorders, such as endolymphatic hydrops, which can produce pathological changes in the sensory endorgans (Poe et al., 2009).

2.2 Sensorineural hearing loss

2.2.1 The causes of sensorineural hearing loss

SNHL is a common disease, which includes two types of hearing loss: either damage to the hair cells or the auditory nerve and auditory nerve pathways. Typically, it is difficult to know whether the problem is either the hair cell, neural, or both. Thus, we often use the general term, sensorineural hearing loss. SNHL usually typically begins in the high frequencies. As broad damage occurs, the hearing loss will spread towards the lower frequencies.

SNHL may be caused by different mechanisms. The most common pathological change of SNHL arises from either damage to, or loss of, cochlear hair cells or their associated neurons. Cochlear hair cells are mechanosensory receptors, which can convert sound signals into electrical impulses that are transmitted along the auditory nerves to the central nervous system. Their loss, resulting from overstimulation, ototoxic drugs, bacterial and viral infections, aging and other causes, is irreversible and leads to permanent hearing impairment in the mammalian ear (Shibata and Raphael, 2010). SNHL may be divided into genetic and acquired sensorineural hearing loss. Commonly, genetic mutations, which are related to the normal develop- ment or function of the inner ear tissues, may lead to hearing loss. Currently, at least 70 genes that cause hearing loss have been identified (www.hereditaryhearingloss.home-page). Noise-induced hearing loss is a common cause for acquired hearing loss, which refers to any type of hearing loss that is caused or aggravated by environmental factors.

2.2.2 Treatment of sensorineural hearing loss

At present, the traditional treatment strategy for SNHL is often unsuccessful. In the EU, approximately 44 million individuals are significantly handicapped by SNHL and require some treatment (http://www.hear-it.org/multimedia/hear_it_Report_October_2006.pdf). For mild to moderate forms, hearing aids alleviate the communication problems. In severe forms of hearing loss and deafness, the auditory function can only be restored by a cochlear implant which functionally replaces lost inner ear sensory cells by directly stimulating the auditory nerve. Cochlear implants were first developed in France in 1957 by Djourno and Eyries (Djourno, 1957), who described a method to stimulate the cochlear nerve using electric currents. This technique makes use of the topographical arrangement of the cochlea, with high-frequency sounds coded near the base, and low-frequency sounds at the apex of the cochlea. Currently, cochlear implantation has gained widespread acceptance in the profoundly (＞90 dB) and severely (between 70 and 90 dB) deaf patients (Marsot-Dupuch and Meyer, 2001).

However, the cochlear implant does little either to repair or regenerate hair cells and neurons (Patel et al., 2004). Hair cells and associated neurons can not be regenerated in mammals once they are lost. Obviously, a cochlear implant can only be successful when enough functioning spiral ganglion cells (SGCs) are present. More important, a cochlear implant has some indications and at the same time it has the possibility to further degenerate the SGCs, and may eventually result in complete hearing loss (Rejali et al., 2007). Moreover, the cost of a cochlear implant procedure is still too high for most of patients.

As hair cell loss is the major outcome from most acquired and inherited forms of SNHL, their regeneration and repair through application of cellular and molecular therapies represents a

major focus in current hearing research (Patel et al., 2004). Simultaneously, expectations for the development of new therapeutic tools have increased, as research has been conducted on inner ear gene and stem cell therapy. Development of SNHL treatments at the cellular and molecular levels is a promising new research area. In the future, improvements in nanotechnologies, and inner ear regeneration, may yield new devices, such as cochlear implants combined with either local drug/gene therapy or stem cell therapy (Ciorba et al., 2009).

2.3 MRI

Magnetic resonance imaging (MRI) is primarily a noninvasive medical imaging technique. The advent of MRI has provided scientists and clinicians with a powerful tool for visualizing the detailed internal structure and certain aspects of physiology for different organs *in vivo*. MRI is a relatively new technology. The first MR image was published in 1973 (Lauterbur, 1973), and the first studies performed on humans were reported in 1977 (Damadian et al., 1977; Hinshaw et al., 1977). With the development of novel magnetic nanoparticles, MRI has led to various biomedical applications in "theragnostics" (therapeutic and diagnostic) applications such as hyperthermia (Wyatt et al., 2009), stem cell tracking (Thu et al., 2009), gene expression (Klose et al., 2010), cancer detection (Giesel et al., 2009), and inflammation (Yang et al., 2010).

2.3.1 Magnetic resonance basics

MRI is a method for human *in vivo* imaging that uses an external magnetic field to align the nuclear magnetization of water protons, which are responsible for the MRI signals (Schroeder, 2008). When a body is placed in a magnetic field, the proton magnetic moments will orient in the direction of the magnetic field and precess at a resonance frequency. Relaxation is measured in two directions, longitudinal and transverse. Longitudinal, or spin-lattice relaxation, is defined by the time constant T1 and occurs in the direction of the main magnetic field. Signals related to T1 relaxation are obtained after excitation by an external magnetic field, as the proton's dipole moment vector begins to realign, or relax back to its ground state of alignment with the main magnetic field. The spin-spin, or transverse relaxation time, or T2, is the exponential loss of coherence among the spins oriented at an angle to the static magnetic field due to interactions of the spins. The T2* is the loss of phase coherence of the spins in the external magnetic field and is a combination of magnetic field inhomogeneities and T2.

2.3.2 MRI contrast agents

MRI contrast agents are used to improve the visibility of internal body structures in magnetic

resonance imaging. They alter the nuclear magnetic resonance relaxation times of the water protons in solution or tissue known as T1, T2 and T2*. With the help of contrast agents, MRI shows the water distribution in the organ in correlation with the anatomy of the organ (Logothetis, 2008). Thus, MR contrast agents are not directly imaged; rather, they indirectly affect the surrounding water protons that then influence the MRI signal.

Gadolinium (Gd) chelates and manganese (Mn) chloride are paramagnetic positive contrast agents used in experimental and clinical studies. These agents tend to shorten T1 relaxation time more than the T2 and T2* of tissues, generating a signal brightening on MR images. Mn chloride was the first paramagnetic contrast agent used in MRI, and it has been shown *in vivo* that cells can take up Mn chloride through calcium channels in the cell membrane (Mendonca-Dias et al., 1983). The major drawback using Mn as a MRI contrast agent is its narrow therapeutic window and significant cardiotoxicity (Arbab et al., 2006). Gd chelates are commonly used clinically to enhance pathological MRI signals in the brain, heart, and liver as well as tumors, among other tissues. However, the Gd ion is highly toxic in its free form, thus, a number of biocompatible chelating agents have been developed to render the metal ion nontoxic in its chelated form. One class of Gd complexes is macrocyclic chelates. Gadolinium-tetra-azacyclododecane-tetra-acetic acid (Gd-DOTA) is one such chelate that is highly water soluble and thermodynamically stable. Another class of such agents is acyclic chelates, such as gadolinium diethylenetriamine pentaacetic acid dimeglumine salt (Gd-DTPA), which was approved for clinical use in adult patients in 1988 and has since become the most commonly used MRI contrast agent. Intravenously administered Gd-DTPA and Gd-DOTA has relatively low morbidity and minimal side effects. However, patients with poor renal function are considered to have an increased risk for nephrogenic systemic fibrosis when they are exposed to gadolinium-containing contrast agents (Grobner, 2006; High et al., 2007).

Superparamagnetic iron oxide nanoparticles (SPIONs) is one type of superparamagnetic negative contrast agents, which shorten the T2 and T2* much more than the T1, generating a signal darkening on MR images. SPIONs are small superparamagnetic iron-oxide nanoparticles with a crystalline magnetite structure coated either with dextran or more advanced biomaterials. They are a promising group of imaging probes and have been extensively studied in recent years (Mahmoudi et al., 2011).

2.3.3 Application of MRI in diagnosis and treatment

2.3.3.1 Application of MRI in diagnosis

MRI is a new and important tool in the diagnosis of hearing loss (Davidson, 2001). Magnetic resonance imaging of the delicate structure of the inner ear has been addressed using higher field strength magnets. High-resolution MRI on inner ear ultrastructure anatomy may provide

important information for inner ear disease that is otherwise unobtainable. In previous studies, great progress has been made in the evaluation of pediatric SNHL using MRI as a diagnostic tool (Klingebiel et al., 2001; McClay et al., 2008; Simons et al., 2006).

Thus far, the diagnosis of SNHL due to cochlear barrier dysfunction is largely based on patient history and physical examination. A more precise determination of the impairment aetiology and pathology is difficult to achieve in a noninvasive manner. No imaging modality is routinely used to confirm diagnosis of such inner ear disease. The inner ear is housed in dense bone and subdivided into different fluid-filled compartments, which makes it possible to evaluate the barrier function using MRI. The challenge in inner ear MRI today is to distinguish the inner ear fluids (endolymph and perilymph) using contrast agents and, eventually, identify the pathological changes. A Gd-enhanced T1-weight signal was first detected in labyrinthitis associated with SNHL-induced barrier dysfunction in human after intravenous gadolinium administration (Casselman et al., 1994). However, the low resolution of MRI limited its application. Introduction of high-resolution MRI in mammalian inner ear using a 4.7 T system enabled *in vivo* visualization of cochlea details. MR imaging of guinea pigs has revealed possible perilymph origins, communications between perilymph-containing spaces, and pathological changes in endolymphatic hydrops and perilymphatic fistulae (Counter et al., 2003; Zou et al., 2003a; Zou et al., 2005a; Zou et al., 2003b). High-resolution imaging of guinea pig cochleae using T1 Gd enhancement demonstrated normal and impaired functions of the inner ear barriers (Counter et al., 2000). Great advances in cochlea MRI were realized with the recent introduction of intratympanic and high dose intravenous administration of Gd in animal models and in humans (Pyykko et al., 2010; Zou et al., 2009).

Although mice are widely used in hearing research, such studies have not included inner ears of mouse models. Contrast agent-enhanced MRI has been applied to visualize the mouse central auditory system activity (Watanabe et al., 2008; Yu et al., 2005). High resolution MR imaging of the mouse inner ear *in vivo* could provide new insights into the mechanisms of various inner ear disorders. Of particular interest is the genetic origin hearing loss, such as the connexin 26 mutation, connexion 30 mutation, Caludin 14 knockout, Foxi1 knockout, COCH mutation, as well as age related hearing loss (Ben-Yosef et al., 2003; Cohen-Salmon et al., 2007; Cohen-Salmon et al., 2002; Kudo et al., 2003; Robertson et al., 2008; Teubner et al., 2003; Zheng et al., 1999).

The disadvantages of Gd include its short relaxation and adverse effects. The longitudinal relaxation of gadolinium chelates decreases rapidly at high field strengths, reducing the sensitivity of these contrast agents in high fields (Sosnovik et al., 2008). A high concentration of gadolinium was reported to be ototoxic in a preliminary study (Kakigi et al., 2008). Nanoparticles loaded with contrast agents have aroused enormous interest in recent years and

promise to be useful in novel or improved biomedical applications (Mahmoudi et al., 2011; McCarthy et al., 2007). Such nanoparticles could be traced using high resolution MRI, while serving as a delivery vehicle for clinical therapeutic agents. One promising group of contrast agents is derived from SPIONs. SPION is an effective MRI T2 contrast agent that has been used in high resolution MRI to trace apoptosis and gene transcription in animal models of cerebral ischemia (Liu et al., 2007b; Liu et al., 2008b; Liu et al., 2009; Liu et al., 2007a; Smith et al., 2007). Currently, multifunctional nanoparticles (MFNPs) are in development and are under investigation as a means for controlled, targeted drug delivery to selected cochlear cell populations for SNHL treatment (www.nanoear.org/, 2009). Labeling of these nanoparticles with imaging contrast materials is under investigation for visualization of their distribution in the cochlea *in vivo* (Li et al., 2004; www.nanoear.org/, 2009). SPIONs are potent signal suppressors in T2-weighted MRI sequences that create a negative or dark contrast against the intensely bright signal from proton rich fluids without SPIONs.

2.3.3.2 SPIONs-labelled stem cell tracking

Stem cell therapies hold promise for hearing loss treatment of (Li et al., 2004; Pauley et al., 2008). A major challenge in development of applied clinical stem cell therapy is a lack of efficient cell tracking methods. Even though excellent histological techniques remain the gold standard, no good *in vivo* techniques are currently available to assess transplanted cells for survival, migration, differentiation, and regenerative impact.

Cellular magnetic resonance imaging (CMRI) can be used to track long-term non-invasive temporal-spatial migration within desired organ of transplanted cells labeled with MR contrast agents (Dousset et al., 2006; Ferreira et al., 2008; Petry et al., 2007; Yang et al., 2009). MRI is the most readily accessible tracking method. Under proper conditions, it is safe, reliable, an available in most hospitals. MRI has successfully detected and tracked stem cell migration in brain disease models (Thu et al., 2009; Yang et al., 2009). MRI could be designed to track differentiation, physiological, and pathological state as well as *in vivo* movement of a transplanted stem cell through the body. Given their high sensitivity for cell detection and their excellent biocompatibility, SPIONs are currently recognized as the best contrast agent candidates for non-invasive *in vivo* tracking of labeled cells using MRI (Dousset et al., 2006; Mahmoudi et al., 2011; Petry et al., 2007). Many examples of *in vitro* labeling for various cells have been described, including the following: embryonic stem cells (Rudelius et al., 2003), neural stem cells (Bulte et al., 2001; Jendelova et al., 2004; Rudelius et al., 2003), bone marrow stem cells (Jendelova et al., 2004). After labeling with SPIONs *in vitro*, the maximum of physiological properties of the stem cells must be preserved, some of which some are obligatory, including the following: viability, migration capability, phenotype differentiation, controlled proliferation, and ability to retain the contrast agent for following

the cell, among others. It has been reported that when labelled with SPIONs, cells are unaffected in their viability and proliferating capacities, and labeled human neuronal stem cells differentiate normally into neurons (Bulte et al., 2001). In previous experiment, SPIONs-labeled cells have been followed for up to 8 weeks, which indicates a long lasting label (Jendelova et al., 2004). Labeled olfactory ensheathing cells migrated extensively in normal spinal cord were readily detectable *in vivo* by MR imaging for at least 2 months after transplantation (Lee et al., 2004).

Labeling cells with SPIONs has several potential advantages: their MRI signal has high spatial resolution, and they are nontoxic to cells, as the iron oxide nanoparticles are biodegradable and can be metabolized by cells. Experiments have shown no cytotoxicity upon increasing the concentration of SPIONs in the cell culture media increased up to 250 μg Fe/ml (Lawrence et al., 2000). Magnetic labeling of cells may provide researchers with a tool to elucidate the role or contribution of a specific cell population during either normal and abnormal development or pathological processes. *In vitro* labeling of cells with SPIONs allows for the detection of single labeled cells within target tissues using CMRI (Arbab et al., 2006). *In vitro* experiments have shown that SPION-labeled cells move towards an external magnetic field and magnetically labeled cells can be delivered and retained at a site of interest by applying an external magnetic field (Arbab et al., 2004). The magnetic targeting of either genetically altered cells or cells serving as gene delivery vehicles may be feasible in the future. A likely method for such targeting includes infusion SPION-labeled cells during either angiography or invasive procedures and use of image guidance by placing an external magnet over a predetermined region to maximize cells delivery and retention in target tissue (Arbab et al., 2006).

However, cellular MRI also has its limitations. It is still not sensitive enough to discriminate between a labeled stem cell signal and products of ferritin deposition (Mani et al., 2008). Moreover, MRI technology requires improvement, as each labelled-cell division reduces the concentration of SPIONs within progeny cells. This progressive cell marker dilution via cell division limits the capacity of this method for long-term stem cells tracking. A threshold concentration must be maintained for MRI to image cells. This threshold limits the length of time that MRI can be used to track stem cells *in vivo* (Li et al., 2010). Next-generation magnetic nanoparticles are expected to be truly multifunctional, incorporating therapeutic functionalitiy and further enhancing an already diverse repertoire of abilities (McCarthy et al., 2007). This rapidly growing area of experimental research has the potential to translate from bench to bedside.

2.4 Gene therapy

At present, gene therapy is a promising therapeutic modality for inner diseases (Sun et al., 2011). The concept of gene therapy maybe defined as a technique or approach to introduce a foreign gene or gene-regulatory into the target cells, which results in either a cure for the disease or slowing its progress (Verma et al., 2005. Mulligan, 1993). Gene therapy offers new treatment possibilities for a large number of common acquired and inherited human diseases where conventional clinical procedures are less effective (Gardlik et al., 2005). The study of gene therapy for the inner ear started in the mid-1990s (Fujiyoshi et al., 1994). It may become a treatment option for SNHL in the near future. A number of genes and specific mutations related to hearing loss that are linked to specific locations in the genome have already been identified, and this number is growing as the field rapidly advances (Ryan et al., 2009b). This information provides a basis for therapy centered on genetic approaches. Numerous new discoveries and tremendous advances have been made in inner ear gene therapy. Therapeutic genes encoding proteins for inner ear gene therapy can be divided into two major groups: inner ear protectors and transdifferentiation activators.

Hair cells and SGCs are common pathological sites for inner ear diseases and the major targets for inner ear gene therapy (Brough, 2007). Identification of effective methods that stimulate new functional inner ear hair cell and SGC regeneration would have therapeutic value in treating SNHL. One potential strategy for regenerating hair cells with normal morphological and functional properties is to induce phenotypic transdifferentiation of nonsensory cells that remain in the inner ear (Izumikawa et al., 2005; Shou et al., 2003). To achieve this goal, gene therapy requires technologies capable of gene transfer to the target cochlear cells. Hair cells and supporting cells have common cellular precursors during mammalian embryogenesis (Fekete, 1996; Fekete, 2000; Torres et al., 1998). Differentiated supporting cells are able to change their phenotype and become new hair cells in inner ear (Corwin et al., 1988; Ernfors et al., 1995; Ernfors et al., 1996; Farinas et al., 1994; Liu et al., 2008a; Noushi et al., 2005; Ryals et al., 1988; Staecker et al., 1996; Sun et al., 2011; Wise et al., 2010; Woods et al., 2004). Therefore, supporting cells are an attractive target for interventions designed to produce new hair cells.

SGCs sense the electrical impulses generated by inner hair cells and send them to the brain. Cochlear implants effectively replace the mechanosensory transduction function of lost hair cells and furnish the user with substantial hearing benefit by exerting direct electrical stimulation on SGCs. Although there are controversial clinical reports on the contribution of SGCs to cochlear implant efficacy, at least 10% spiral ganglion cell survival is necessary for current cochlear implants to succeed in helping patients communicate (Khan et al., 2005; Linthicum et al., 1991). Thus, either preventing degeneration or promoting regeneration of deafferented SGCs in the inner ear would also have therapeutic value in treatment of hearing

disorders. Neurotrophic factors are a large group of biologically active proteins, most are able to protect inner ear hair cells and spiral ganglion neurons from damage caused by various pathogenic factors and promote recovery from cochlear injury (Ernfors et al., 1995; Ernfors et al., 1996; Farinas et al., 1994; Sun et al., 2011). Targeted delivery of neurotrophic factor genes to SGCs using functionalized nanoparticles is an efficient method of fulfilling this goal. A large number of documents have demonstrated successful transfection and expression of neurotrophic factors in the inner ear, mediated by both viral and nonviral vectors *in vitro* and *in vivo* (Liu et al., 2008; Noushi et al., 2005; Staecker et al., 1996; Wise et al., 2010). Therefore, neurotrophic factor genes have become the preferred genes for inner ear gene therapy.

2.4.1 Math1 gene and inhibitor of DNA binding/differentiation proteins

2.4.1.1 Math1 gene

The discovery of developmental genes that encode hair cell and neuron differentiation facilitates the design of interventions that promote generation of new hair cells and SGCs. Thus far, one of the most crucial genes for inner ear hair cell differentiation control is the mouse basic helix-loop-helix (bHLH) transcription factor, Math1, a mammalian homolog of Drosophila atonal. The bHLH transcription factor, Math1 (or Atoh1), is both necessary and sufficient for hair cell development in the mammalian cochlea (Bermingham et al., 1999; Zheng et al., 2000b). Previous studies have demonstrated that a dynamic pattern of Math1 expression plays a key role in regulating the number and position of mechanosensory hair cells. Adenovirus-mediated Math1 gene transfection in the inner ear may be the most exciting progress made in inner ear gene therapy; it effectively activated the regeneration of cochlear hair cells in mature mammalian ears (Bermingham et al., 1999). Targeted deletion of the Math1 gene leads to hair cell differentiation failure (Bermingham et al., 1999). *In vitro* Math1overexpression induced generation of new hair cells (Woods et al., 2004; Zheng et al., 2000b). Overexpression of Math1 *in vivo* leads to new hair cell-like cells in the organ of corti (Izumikawa et al., 2008; Kawamoto et al., 2003). These results were were observed using the human Math1 homologue (hath1) *in vitro* (Shou et al., 2003). Previous studies have shown encouraging progress in Math1-based gene therapy that improves auditory dysfunction. Math1-based gene therapy has been proposed for producing functional supernumerary hair cells in mice (Gubbels et al., 2008) and restoring hearing in guinea pigs deafened by ototoxic drugs (Izumikawa et al., 2005). Therefore, Math1 is a good candidate gene for gene-based treatment of SNHL.

Math1 also plays an important role in regulating development of the mammalian nervous system (Flora et al., 2007). Math1 is a positive regulator for the differentiation of cerebellar granule neurons (Ben-Arie et al., 1997; Helms et al., 1998), dorsal commissural interneurons

(Helms et al., 1998), and hindbrain neurons (Benezra et al., 1990; Jones et al., 2006; Kreider et al., 1992; Norton et al., 1998; Rose et al., 2009; Yokota et al., 1999). Thus, the Math1 gene may potentially be used for future studies on spiral ganglion neuron-oriented differentiation. Endogenous stem cells in the inner ear have been identified in a previous study (Li et al., 2003a), but they can spontaneously generate neither hair cells nor spiral ganglion neurons. Modification of inner ear endogenous stem cells with Math1 using a gene delivery technique can potentially be applied in future therapies to treat deafness.

2.4.1.2 Inhibitor of DNA binding/differentiation proteins

Inhibitor of DNA binding/differentiation proteins (Ids) are one family of bHLH transcription factor regulators (Benezra et al., 1990; Jen et al, 1992; Kreider et al., 1992; Sun XH, 1994; Yokota et al., 1999). Math1 is critical for hair cell development and patterns in the organ of Corti. A previous study suggested that Ids play an important role in inhibiting the expression of Math1 and the differentiation of hair cells in developing cochlea (Jones et al., 2006).

Heterodimer formation of Math1-ubiquitous bHLH with ubiquitously expressed bHLH, referred to as E-proteins is essential to induce gene transcription (Benezra et al., 1990; Norton et al., 1998). Ids negatively regulate Math1 function by inhibiting activity of basic bHLH transcription factors. Ids heterodimerize with bHLH transcription factors to inhibit the formation of functional heterodimers (Jones et al., 2006). Although Ids also contain the HLH-dimerization domain that is required for dimerization with other bHLH proteins, they lack the basic DNA-binding domain. Thus, the dimers formed by Ids and bHLHs cannot bind DNA and are inactive. As a result, Ids actively inhibit cellular differentiation (Benezra et al., 1990).

Therefore, Ids are good candidates for regulating Math1 in the cochlea. The target gene can be silenced by short hairpin RNA (shRNA) via mRNA down-regulation, which is similar to small interfering RNA (siRNA). Id shRNA can inhibit the activity of Ids and enhance the Math1 function. Gene-based hair cell regeneration can involve a combination nanoparticle-mediated delivery of the Math1 gene and Id shRNA.

2.4.2 Gene delivery system

A key factor in the success of gene therapy is development of safe and effective gene delivery systems with which to ferry genetic material into target cells and tissue (Verma and Weitzman, 2005; Niidome et al., 2002; Li S and Huang L, 2000). The simplest way for gene delivery is the direct injection of naked DNA that encodes the therapeutic protein into the target tissue (Li and Huang, 2000). However, given this method's low efficiency, it is necessary to develop novel strategies and methods to improve the gene delivery efficiency. A vector can be

described as a system that fulfills several functions, including gene delivery into the target cells and their nuclei, protection of the gene from degradation, and ensuring gene transcription in the cell (Gardlik et al., 2005). Administration of gene therapy vectors requires that they are not only targeted and safe, but also protected from degradation, sequestration, and immune attack, among other events. The ideal DNA vehicle should also be suitable for clinical application. Morever, it must be inexpensive, easy to produce, and purify in large amounts at high concentrations (Gardlik et al., 2005; Neumann et al., 1982; Titomirov et al., 1991).

Two types of gene delivery systems have been employed as gene transfer vehicles, viral vectors and non-viral vectors. The commonly used viruses include, but are not limited to, adenovirus, adeno-associated virus, and retrovirus. The commonly used nonviral vectors are cationic liposomes, cationic polymers, and other inorganic nanoparticles, which typically contain positive charges at their surfaces. Although viral vectors are able to mediate gene transfer with high efficiency, non-viral vectors, which have more advantages over viral vectors, seem to be more promising (Elfinger et al., 2008; Al-Dosari MS and Gao X., 2009). However, neither of the two types of gene delivery system is an ideal too up to now.

2.4.2.1 Electroporation

Plasmid DNA (pDNA) delivery can be enhanced by physical methods that aid passage of the plasmid through the cell membrane. Electroporation is an effective and simple non-viral delivery method that can be applied to different cell types *in vitro* and *in vivo*. The process of electroporation involves exposure of the cell membrane to high-intensity electrical pulses, which can cause transient and localized destabilization of the barrier. During this perturbation, the cell membrane becomes highly permeable to exogenous pDNA present in the surrounding medium. The first *in vitro* and *in vivo* attempts to utilize electroporation in gene transfer were demonstrated in 1982 and 1991 (Neumann et al., 1982; Titomirov et al., 1991), respectively. Electrotransfer can be used to deliver a wide range of potentially therapeutic agents, including drugs, proteins, and oligonucleotides, both RNA and DNA. This technique also has the advantage that, unlike viral vectors, it can be used to target specific tissues with systemic delivery. When the parameters are optimized, this method can generate transfection efficiency equal to that achieved by viral vectors (Andre et al., 2004).

The use of electric pulses to deliver therapeutic molecules to tissues and organs *in vivo* is a rapidly growing field of research. One encouraging applications of electroporation was reported ten years ago by Zheng and Gao, who, using the *in vitro* electroporation, demonstrated that overexpression of Math1 induced robust production of additional hair cells after transfection with the Math1 plasmid (Zheng et al., 2000b). In another recent report,

Gubbels demonstrated that functional auditory hair cells were produced in mammalian cochlea via in utero Math1 gene transfer using *in vivo* electroporation (Gubbels et al., 2008; Liu et al., 2005). Despite the recent progress, one limitation of *in vivo* electroporation-mediated gene transfer to solid tissues is electrodes accessibility to the internal organs, which can induce substantial tissue damage associated with the procedure. Another limitation of electrotransfer is that gene transport into the cell during the time of electropermeability is relatively nonspecific. Thus, plasmid DNA delivery via electroporation is still far from the perfect gene carrier for potential therapeutic applications.

2.4.2.2 Viral vector

Viral techniques use various classes of virus as tools for gene delivery. The underlying concept behind viral vectors is harnessing the innate ability of viruses to deliver genetic material into an infected cell. Viruses introduce their DNA into the cells with high efficiency. Therefore, it is possible to take advantage of this activity by introducing a foreign gene into the virus and then, taking advantage of viral properties, deliver this gene with high efficiency into the target cells. Several viral vectors, including adenovirus (Kawamoto et al., 2003; Huang et al., 2009), adeno-associated virus (Liu et al., 2005), lentivirus (Bedrosian et al., 2006), herpes simplex type I virus, and vaccinia virus (Derby et al., 1999; Praetorius et al., 2002), are highly efficient in gene delivery and providing sustained expression of the transgene.

In previous studies, Most Math1 gene delivery vectors used for hair cell regeneration were adenoviruses. Great achievements and progress related to viral gene delivery systems have been made in inner ear gene therapy (Huang et al., 2009; Izumikawa et al., 2008; Izumikawa et al., 2005; Kawamoto et al., 2003; Liu et al., 2005; Shou et al., 2003; Staecker et al., 2001; Raphael et al., 1996). Although the use of adenovirus vector has been associated with higher transfection efficiency, there are toxicity and safety problems associated with these vectors, such as immunogenicity and insertional mutagenesis (Braun, 2008; Soininen et al., 2010; Verma et al., 2005). Such side effects can result in serious problems or even death (Raper et al., 2003; Thomas et al., 2003). Therefore, the adenovirus vector is not yet regarded as a safe system for inner ear gene delivery. Furthermore, the adenovirus vector has several intrinsic drawbacks, including difficulty in large scale production yields, limited opportunity for repeated administrations due to an acute inflammatory response, limitations on the size of the carried therapeutic genes, and inefficient *in vivo* targeting to specific cells.

2.4.2.3 Nonviral vector

The nonviral vector gene delivery, which uses either synthetic or natural compounds to

deliver DNA into a cell, represent a simple and, more importantly, safer alternative to viral vectors (Mintzer and Simanek, 2009). The materials used in nonviral vectors are generally less toxic and immunogenic than the viral counterparts. The basic unit in a nonviral vector system consists of a backbone with nonviral materials and plasmid DNA, which contains a therapeutic and/or reporter gene.

Nonviral vectors can circumvent some of the problems occurring with viral vectors. Nonviral vectors have no or low toxicity and immunogenicity, and they typically do not pose a threat to safety. Moreover, nonviral vectors also have advantages in their ease of manipulation and large-scale production as well as potential for cell specificity and high flexibility in the size of the delivered gene (Anderson, 1998; Ferber, 2001; Niidome et al., 2002; Schmidt-Wolf et al., 2003; Chattopadhyay et al., 2005). The major disadvantage for all nonviral vectors is low transfection efficiency and transient expression in the host cells. It is likely that future gene therapy protocols will use innovations to improve on the nonviral vector system efficiency, often building upon observations from viral vector transduction.

Among the nonviral vectors, nanoparticle carriers are regarded as the most promising gene carriers (De la Fuente et al., 2008; Farjo et al., 2006; Wang et al., 2006; Ziady et al., 2003). Nanoparticle carriers are are organic or inorganic materials with diameters ranging from 1-1000 nm. It is noteworthy that cationic liposomes and polymers make up the two major and most promising classes of nonviral gene delivery vectors within the category of nanoparticle carriers (Tros de Ilarduya et al., 2010; Godbey et al., 2001). The complexes that they form with DNA are defined as "lipoplexes" or "polyplexes", respectively. They have been extensively investigated and hold great promise as a safe and non-immunogenic approach to gene therapy. Liposomes complexed with LacZ and GFP reporter genes have successfully transfected the tissues of mice and guinea pig cochleae *in vivo* (Jero et al., 2001; Staecker et al., 2001; Wareing et al., 1999). A previous study showed commercial linear polyethylenimine (PEI) is able to transfect the cochlea *in vivo* via cochleostomy and osmotic pump infusion method (Tan et al., 2008). As a strategy for gene therapy, the use of nanoparticle carriers for delivery of therapeutic materials to the inner ear has great potential. Potential candidate nanoparticles, lipid nanocapsules, were observed to distribute in the rat (Zou et al., 2008) and guinea pig (Scheper et al., 2009) cochlear cells in *in vivo* test.

2.4.2.3.1 Liposome and polymers

Use of cationic lipids and cationic polymers for gene transfer was introduced by Felgner and Wu, respectively (Felgner et al., 1987; Wu et al., 1987). Their use has moved rapidly from cell culture transfection to clinical gene therapy applications. The first *in vivo* experiments using cationic lipids were conducted in mice in 1989 (Brigham et al., 1989) and a clinical trial was initiated in 1993 (Nabel et al., 1993). Cationic lipid/DNA complexes (lipoplexes) and

cationic polymer/DNA complexes (polyplexes) used in gene therapy are based on the hypothesis that the complexes adsorb more effectively to the mammalian cell anionic plasma membrane via electrostatic interactions (Gershon et al., 1993; Ruponen et al., 1999; Tros de Ilarduya et al., 2010). Compared with other non-viral delivery systems lipoplexes and polyplexes tend to mediate a higher level of transfection in numerous cell lines. However, the application of liposomes and polymers for inner ear gene delivery is still in its infancy.

Liposomes are made from the same material as a cell membrane and typically contain at least two components: a cationic lipid and a neutral lipid or a "helper lipid". Cationic lipids are amphiphilic molecules containing a positively charged polar headgroup linked, via an anchor, to a hydrophobic domain that generally comprises two alkyl chains. 1, 2-dioleoyl-sn-glycero-3 phosphoethanolamine (DOPE) and cholesterol are often used as neutral lipids. When membrane phospholipids are disrupted, they can reassemble themselves into spheres, smaller than a normal cell, either as bilayers or monolayers. The bilayer structures are liposomes, and the monolayer structures are micelles. Lipoplexes are formed by spontaneous liposomal self-assembly and complexed with DNA. Cationic polymers include polyethylenimine (PEI), cationic dendrimers, natural DNA-binding proteins, and synthetic polypeptides carbohydrate-based polymers, such as chitosan, among others. As most of these are synthetic compounds, the molecular weight can be modified, and ligands can be attached to them. Poly (l-lysine) (PLL) and PEI are among the most widely studied polymers for gene delivery. Cationic polymers differ from cationic lipids in that they do not contain a hydrophobic moiety and are completely soluble in water. The most striking difference between cationic lipids and cationic polymers is the ability of the latter to more efficiently condense DNA into a relatively small size, compared with cationic liposomes (Gershon et al., 1993; Ruponen et al., 1999). This can be crucial for gene transfer, as small particle size may be favorable in improving transfection efficacy, particularly *in vivo*.

Despite numerous applications, elucidation of the cellular pathways mechanisms for cationic lipid- and polymer-mediated transfection has been relatively slow. Rational design of highly efficient liposomes and polymers requires understanding all the interactions between the vector and DNA as well as the cellular pathways and mechanisms involved in DNA cellular entry and nuclear import. Several biological barriers must be overcome to achieve efficient nonviral gene delivery (Bally et al., 1999; Khalil et al., 2006; Pathak et al., 2009). These barriers include binding to the cell surface, traversing the plasma membrane, escaping lysosomal degradation, and overcoming the nuclear envelope. Endocytosis and nuclear entry are two main steps that hinder successful gene therapy, as they play very important roles in gene delivery (Boussif et al., 1995). These pathways have been studied intensely, and endosome escape and nuclear entry have been improved rapidly in recently years (Friend et al., 1996; Kakimoto et al., 2009; Kim et al., 2011; Zabner et al., 1995).

The endosomal escape ability to release DNA into the cytoplasm is a key step in intracellular delivery of DNA by nonviral vectors (Cotten et al., 1992; Friend et al., 1996; Simoes et al., 1999). There is convincing evidence that endocytosis is the major pathway for lipoplex and polyplex entry into the cells before productive gene expression (Friend et al., 1996; Rejman et al., 2006; Simoes et al., 1999; Labat-Moleur et al., 1996). If the plasmid can not be released into the cytoplasm by breaking the endosomal membrane, then it will be transported to the lysosomes, where all DNA is destroyed before achieving its function. Cationic polymers are devoid of a hydrophobic domain, and therefore cannot fuse/destabilize the endosome by direct interaction with the endosomal membrane, as is the case for cationic lipids. The first generation of cationic polymers, such as polylysine or polyarginine, was inefficient in endosomal escape and transfection efficiency. In an effort to increase the efficiency of the endosomal escape efficiency, the second generation of cationic polymers were developed with intrinsic endosomolytic activity, including polyamidoamine dendrimers (PAMAM) (Boussif et al., 1995; Kichler et al., 2001; Tang et al., 1996) and polyethylenimines (PEI) (Boussif et al., 1995; Kichler et al., 2001). PEI and PAMAM can buffer the endosomal interior to some extent, thereby inducing osmotic swelling and rupture. The "proton sponge" hypothesis has found widespread acceptance in past years (Godbey et al., 2000; Boussif et al., 1995). It was also reported that liposomal and polymer transfection efficiency can be increased by targeting DNA release from the endosome with endosomal escape peptides (Moore et al., 2008). These peptides can accommodate multiple functions within short sequences. Peptides offer the capacity for DNA condensation, metabolism blocking, endosomal escape, nuclear localization, and receptor targeting (James et al., 2000; Martin et al., 2007; Tachibana et al., 2002). Furthermore, they are readily synthesized, economically, by numerous commercial custom peptide suppliers.

Transport of the gene construct into the nucleus is also a key stage for gene delivery efficiency. The mechanism transporting the transfecting DNA into the nucleus is still a matter of debate. Many studies have confirmed that, in cells with cytoplasmic plasmid delivery mediated by nonviral vectors, only those with evidence of nuclear plasmid localization showed efficient transgene expression (James et al., 2000; Tachibana et al., 2002). Microinjection of plasmid DNA into the nucleus produced much higher gene expression than when the same plasmid was microinjected into the cytosol (Carlisle et al., 2001; Dean et al., 2005; Pollard et al., 1998). This suggests that the nuclear envelope is a significant barrier against transfection. DNA transport into the nucleus is still not well understood. Molecules of <10 nm can passively diffuse through nuclear pores. This is much smaller than DNA, even when DNA is condensed in lipoplexes or polyplexes. In that case, how is the DNA delivered to the nucleus? The most widely accepted mechanism is that cell division is an important factor in transgene nuclear translocation. During the cell division stage, the nuclear membrane is temporarily disassembled, which allows DNA to diffuse into the nucleus. This is the case for *in vitro* transfection with dividing cells, whereas, *in vivo* transfection typically targets

differentiated nondividing cells. Most cochlear cell populations, especially SGCs and hair cells that are targeted for gene therapy, do not actively undergo cell division during the gene transfer process. Therefore, the infrequent DNA nuclear localization greatly limits the application of liposomes and polymers as carriers for gene therapy.

Nuclear plasmid delivery induced by nanoparticle carriers may be an option for improving transgene expression in nondividing or growth-arrested cells (Carlisle et al., 2001; Dean et al., 2005; Godbey et al., 1999a; Pollard et al., 1998). Pollard et al microinjected PEI–DNA polyplexes into cell's cytoplasm and showed that transfection efficiency was higher compared with either microinjected naked DNA or lipoplexes. This result was interpreted primarily in terms of the ability of PEI to facilitate DNA translocation into the nucleus. It could not be excluded, however, that PEI may aid in nuclear import of DNA via other indirect mechanisms, including enhanced DNA protection and cytoplasmic mobility. Nuclear import of proteins require a nuclear localization signal (NLS), which contains basic amino acids and can be recognized by cytosolic factors to mediate active transport through the nuclear pore complex (Jans et al., 1996; Sebestyen et al., 1998). The same approach can be used to enhance gene delivery to the nucleus, especially for transfection of nondividing cells. It was reported that the nuclear delivery of DNA was increased by coupling of 100 NLS peptides/kilobase pair of DNA (Sebestyen et al., 1998). Development of multifunctional nanoparticles or nanocomplexes for gene delivery promises formulations that mimic the structure and function of viral particles. These formulations offer the best prospects for development of improved efficient vector systems while maintaining the safety characteristics of nonviral formulations (Hart, 2010). Multifunctional nanoparticles functionalized with different peptides that are introduced to overcome different cellular barriers can increase cellular uptake via receptor-mediated endocytosis, endosomal release, and nuclear delivery.

2.4.3 Cellular targeting

Although the development of gene delivery vectors that are capable of efficient delivery is a key factor in the success of gene therapy, targeting the therapeutic carrier to the cells that require treatment is equally vital. This is especially important in the complex inner ear tissues, which contain many cell types that must function in a coordinated manner for hearing. Gene therapy delivered to either the wrong cell type or at the wrong time could be ineffective or even harmful (Ryan and Dazert, 2009a; Friedmann, 1994). Cell-specific gene promoters offer an opportunity to direct gene therapy to a desired cell type. The ideal gene promoter for an inner ear cell type would only be expressed in that cell type. Certain promoters and enhancers that direct gene expressions in cochlear cells have already been identified (Ryan et al., 2009b). Incorporation of targeting ligands to nanoparticles is a promising tool for nonviral gene delivery to a specific tissue or cell type (Elfinger et al., 2008).

Arguably, the most obvious target for gene therapy of the inner ear is the outer hair cells (OHCs). Many of the genes responsible for inherited hearing loss are expressed in the OHCs, and their mutation primarily affects this cell type. Therefore, OHC-specific promoters are of special interest for inner ear gene therapy. One candidate for OHC targeting is prestin, which is a member of the anion solute carrier family 26 (SCL26), with important roles in normal physiology and human pathophysiology (Colvin et al., 1996; Dallos et al., 2002; Oliver et al., 2001; Pasqualetto et al., 2008; Pirvola et al., 1995; Zheng et al., 2000a). Prestin is a transmembrane protein that is highly and exclusively expressed in the lateral plasma membrane of OHCs (Zheng et al., 2000a). It is a unique molecular motor protein that senses membrane potential change and mediates OHC length changes (Dallos et al., 2002; Oliver et al., 2001). Another candidate for OHC targeting is the FGF receptor, FGFR3, splice variant IIIc. FGFs and their receptors (FGFRs) are critically important for normal development of the organ of Corti and may also protect hair cells from ototoxic damage (Colvin et al., 1996; Pirvola et al., 1995). The FGFRs consist of three extracellular immunoglobulin-type domains, a single-span transmembrane domain and an intracellular split tyrosine kinase domain. The FGF receptor, FGFR3, splice variant IIIc, is exclusively expressed in cochlear outer hair cells (Fobian, 2007; O'Leary et al., 2003; Pickles et al., 1998; Schimmang et al., 2003). Therefore, prestin and FGFR3, splice variant IIIc, are useful targets for the nanoparticles delivery in cochlear OHCs. Prestin binding peptides or synthetic FGF ligands can be synthesized and conjugated either to the surface of nanoparticles or directly to plasmid for OHC-targeted delivery.

The SGCs are the only neurons within the cochlea. Thus, a number of genes with expressions that are restricted to neurons could supply promoters for use in targeting applied in gene therapy vectors. This includes many neuron-specific developmental genes. Similarly, a variety of genes encoding neuron-specific proteins, such as the neurotrophin receptor tropomyosin related kinase (Trk) receptor tyrosine kinase, especially TrkB, are expressed only expressed in spiral ganglion cells of the inner (Schimmang et al., 2003). TrkB binding peptides have been developed using either phage display or molecular modeling to mimic the biological functions of brain derived neurotrophic factor (BDNF) and nerve growth factor NGF (Fobian, 2007; O'Leary et al., 2003). Targeted delivery of agents to spiral ganglion cells using TrkB binding peptide-functionalized nanoparticles is an efficient way to either preserve or regenerate deafferented SGCs.

2.5 Stem cell-based therapy

Degeneration of inner ear hair cells and associated neurons results in hearing impairment. There are currently no treatments designed to halt or reverse the progression of hearing loss. These disabilities are incurable, as loss of the hair cells and neuronal cells is currently

irreversible. Stem cell-based therapy is a rapidly growing area of research and has potential applications in treating inner ear disorders (Nakagawa and Ito, 2005). It is considered the ultimate remedy for hearing loss. Although many major hurdles still exist, stem cell-based therapy has the potential to become the gold standard for restoration of hearing loss (Forge et al., 1993; Li et al., 2003a; Malgrange et al., 2002; Oshima et al., 2007; Pauley et al., 2008; Rask-Andersen et al., 2005; Warchol et al., 1993; Zhai et al., 2005; Zhang et al., 2007).

2.5.1 In situ differentiation of inner ear stem cells

In 1988, Corwin and Ryals reported that birds can regenerate hair cells and recover hearing after acoustic trauma (Corwin et al., 1988; Ryals et al., 1988). It was also reported that the adult mammalian vestibular system can regenerate modest hair cells upon damage (Forge et al., 1993; Warchol et al., 1993). These results suggest that unidentified latent or dormant stem cells are retained in the inner ear of adult animals. Li et al. first demonstrated the presence of stem cells in the adult mouse utricle (Li et al., 2003a). Since that time, stem cells have been characterized in the spiral ganglion (Rask-Andersen et al., 2005), the lesser epithelial ridge (Zhai et al., 2005), greater epithelial ridge (Zhang et al., 2007), and in the organ of corti and the stria vascularis (Oshima et al., 2007). Although stem cells are present in the mammalian cochlea (Malgrange et al., 2002; Oshima et al., 2007; Rask-Andersen et al., 2005; Zhai et al., 2005), endogenous cochlear stem cell do not spontaneously generate hair cells or neurons after damage (Reyes et al., 2008; Richardson et al., 2008; Parker et al., 2007; Matsuoka et al., 2006; Hu et al., 2005; Doetzlhofer et al., 2004; Li et al., 2004; Li et al., 2003b; Tateya et al., 2003; Gage, 2000; Zheng et al., 2000b; Thomson et al., 1998; Evans et al., 1981; Martin, 1981). Previous work has shown that hair cells and neurons can be differentiated from endogenous cochlear stem cells *in vitro* (Doetzlhofer et al., 2004; Malgrange et al., 2002; Oshima et al., 2007; Rask-Andersen et al., 2005), particularly in response to treatment with growth factors. However, these approaches are not yet possible in the adult mammalian organ of Corti *in vivo*. To stimulate the proliferation and differentiation in these cochlear stem cells toward a desired cell type, we must discern which genes control the properties of self-renewal and pluripotency and what mechanism control stem cell quiescence in the mammalian cochlea. Math1 is both necessary and sufficient for hair cell development in the mammalian cochlea (Bermingham et al., 1999; Zheng et al., 2000b). A previous study showed that endogenous cochlear stem cell can be converted to hair cells when they were forced to express Math1 (Zhai et al., 2005).

2.5.2 Exogenous stem cell transplantation

Exogenous stem cellular therapy is an intellectually attractive option for replacing damaged sensory epithelia and neurons. Embryonic stem cells (ESCs) and neural stem cells (NSCs) are

two important and potent graft materials, which have a direct phylogenetic root in the inner ear sensory epithelia. Xenografted ESCs, adult NSCs, and fetal dorsal root ganglion survived for certain period following implantation into the vestibulocochlear nerve or inner ears of adult rats and guinea pigs (Hu et al., 2005; Regala et al., 2005). ESCs, which are pluripotent cells derived from the inner cell mass of blastocysts, can grow indefinitely in an undifferentiated state and have the potential to differentiate into all mature cell types, except embryonic tissue (Evans et al., 1981; Martin, 1981; Thomson et al., 1998). Previous results indicate that NSCs have a multipotent capacity and can generate a wide range of cell types for transplantation in a variety of diseases (Clarke et al., 2000; Gage, 2000). Hair cells and neurons can be generated *in vivo* from embryonic stem cells and neural stem cells after transplantation (Li et al., 2003b; Parker et al., 2007; Reyes et al., 2008; Tateya et al., 2003). Embryonic NSCs transduced with the Math1 gene gave rise to both neurons and HCs, following their implantation into normal guinea pig cochleae (Han et al., 2010). ESCs and NSCs replacement therapy, although promising, must overcome potential problems, including immune rejection and post-transplantation immunosuppression (Matsuoka et al., 2006; Richardson et al., 2008). Compared with ESCs, tissue-specific NSCs have less self-renewal capacity and, although they differentiate into multiple lineages, they are not pluripotent. Long-term consequences of ESCs use in cell replacement therapy may include facilitation of tumorigenesis in host tissues (Aoi et al., 2008; Frankel, 2000; Hong et al., 2009; Lanza, 2007; Prockop, 2003). Moreover, ESCs replacement therapy is still highly controversial, and their use in research and therapeutics has been encumbered by ethical considerations (Frankel, 2000; Lanza, 2007). Furthermore, they rely on post-mortem cell harvesting, and typically a low-yield sources of tissue, thus, requiring a large number of animals to produce sufficient cells for transplantation.

2.5.3 Autologous transplantation

Autologous transplantation is a widely accepted and approved technique in regenerative medicine, which can circumvent many problems associated with ESCs. It has the great advantage of avoiding the risk of immune rejection and ethical concerns regarding the use of human embryos. Mesenchymal stem cells and induced pluripotent stem (iPSs) have been recognized as two important promising sources for autologous inner ear hair cell and neuron replacement. Significant breakthrough research has found that activation of a set of stem cell genes can reprogram terminally differentiated cells to acquire properties similar to ESCs (Aoi et al., 2008; Hong et al., 2009; Nishimura et al., 2009; Park et al., 2008; Takahashi et al., 2006; Takahashi et al., 2007; Staecker et al., 2007; Yu et al., 2007). The reprogrammed cells are namely induced iPSs. These iPSs exhibit the morphology and growth properties of ESCs and express ESC marker genes. After transplantation of iPS cell-derived neural progenitors into mouse cochleae, approximately 50% of the iPS cell-derived cells settled in the cochlea and

differentiated into neural lineages (Nishimura et al., 2009). Further, a recent report showed that mechanosensitive sensory hair cell-like cells can be generated from iPSs (Oshima et al., 2010). However, it is unclear whether iPSs will ever be safe for future use in patients. As retroviral transfection necessary to randomly insert “stem cell” genes to form iPSs, there is still a strong risk of tumor formation (Holden et al., 2008). In previous experiments, adult human fibroblasts and adult mouse fibroblasts were induced to become pluripotent stem cells. NIH 3T3 cells (a spontaneously immortalized fibroblast cell line) have the potential to differentiate into SGCs. Therefore, NIH 3T3 cells were selected herein to acquire data for future studies on the SGC-oriented differentiation.

Mesenchymal stem cells (MSCs) are another promising source for autologous inner ear hair cell and neuron replacement (Korbling et al., 2003), and they have been reported to differentiate into multiple lineages and have long been evaluated in clinical practice. MSCs can be readily obtained in abundant quantities for used as an autologous graft material. Previous studies have documented *in vitro* differentiation of bone marrow-derived stem cells into neurons (Jiang et al., 2002). Using this strategy, Naito et al. demonstrated that autologous bone marrow-derived stem cells can survive in the inner ear for up to 4 weeks (Naito et al., 2004). Grafted cells, some of which are expressed a neuronal or glial cell marker, were introduced into the scala tympani and modiolus via microinjection. Another *in vitro* study reports that bone MSCs are progenitors for inner ear hair cells (Jeon et al., 2007). By a combination of growth factor stimulation and expression of Math1, they show that MSCs derived from bone marrow can be induced to differentiate into hair cell-like cells with specific hair cell markers. Trans-differentiation of MSCs into a neuronal and hair cell-like phenotype suggested that MSCs are potential candidates for cell therapy in SNHL.

2.5.4 Perspectives for future research

Cellular therapy is an intellectually attractive option for replacing damaged inner ear hair cells and SGCs. The discovery of adult inner ear stem cells and the generation of hair cells and neurons from exogenous stem cells and iPSs have opened an exciting new avenue for developing of hearing restoration strategies. These findings provide a sound foundation for the development of therapies to treat SNHL. Despite these exciting findings, there are numerous challenges to face and obstacles to overcome before clinical translation. It is conceivable that stem cell-based therapy alone will not be the ultimate solution for the treatment of SNHL. Most likely, future manifestations of biological therapy for hearing loss will probably combine existing cochlear implant with cell-based therapy, or gene/drug therapy (Ciorba et al., 2009; Tang et al., 2006; Patel et al., 2004).

3. AIM OF THE STUDY

The purpose of the study was to diagnose inner ear disease using nanoparticle-based MRI and to evaluate the efficacy of different nanoparticles in gene delivery to treat sensorineural hearing loss.

The original publications covered the following issues:

1. To study inner ear barrier function using different MRI contrast agents;

2. To investigate the ability of nanoparticles to enter the nucleus of cochlear cells for gene delivery;

3. To demonstrate the efficacy of nanoparticle-mediated delivery of the model gene, Math1; and

4. To explore the targetability of TrkB ligand functionalized liposome nanoparticles to spiral ganglion cells.

4. MATERIALS AND METHODS

This chapter briefly describes the main methods used. For more detailed descriptions of the methods, please refer to original publications I-V.

4.1 Plasmid preparation

4.1.1 Math1 Plasmid construction

The Math1 coding fragment was amplified from pCLIG-Math1 plasmid (provided by R. Kageyama Kyoto University, Kyoto, Japan) by PCR using 5'-GCG ATG TCC CGC CTG CTG CA-3' as the forward primer and 5' -AAA ACT GGC CTC ATC AGA GTC-3' as the reverse primer. For generation of an EmGFP C-terminally tagged Math1 expression clone, we used the Gateway recombination system (Invitrogen, USA). The entry clone, pENTR/D-TOPO containing the Math1 open reading frame, was obtained using the pENTR™ Directional TOPO Cloning Kit (Invitrogen, USA). Once the entry clone was obtained, a LR recombination reaction was performed for transfer of Math1 open reading sequence into a Vivid Colors pcDNA 6.2/C-EmGFP-DEST vector to create an EmGFP C-terminally tagged Math1 expression clone. The EmGFP sequence from pcDNA 6.2/CEmGFP- DEST was ligated to the 3' end of the Math1 coding sequence with a short linking peptide (thirteen amino acids). The pcDNA6.2/C- EmGFP-Math1plasmid was first analyzed by PCR (M13 forward primer and M13 reverse primer provided by Invitrogen) to confirm the presence and the size of the insert. The plasmid was sequenced to further verify the integrity of the Math1 gene and its orientation in the vector.

4.1.2 Id2.3 shRNA plasmid preparation

We purchased the plasmid pGeneClip™ hMGFP, which encodes a shRNA to transiently silence the inhibitor of differentiation and DNA binding-2 (Id2) and expresses the reporter gene EGFP (SuperArray, Bioscience Corp, Frederick, MD, USA). The plasmid was propagated in OneShot TOP10 Competent Cells (Invitrogen, Carlsbad, CA, USA) and then extracted using the PureLink™ Plasmid DNA Megaprep kit (Invitrogen, Carlsbad, CA, USA) according to the manufacturer's instructions. The purity and concentration of Id2.3 shRNA Plasmid were determined by spectrophotometer (NanoDrop® ND-1000, USA).

4.2 Cell cultures and treatment

NIH 3T3 cells (ATCC, USA) were cultured in Dulbecco's Modified Eagle's Medium (DMEM) (Sigma, Product Number: D5671) supplemented with 4 mM L-glutamine, 10% fetal bovine serum (FBS), and 1% penicillin-streptomycin (Invitrogen, USA). The cells were cultured at

37°C in a CO_2 incubator. Parts of NIH 3T3 cells were transfected with pCLIG_Math1 plasmid, pcDNA6.2/C-EmGFP-Math1 plasmid, and pcDNA6.2/C-EmGFP-BDNF plasmid using Lipofectamine 2000 for 24h. Parts of NIH 3T3 cells were transfected with pcDNA6.2/C-EmGFP-Math1 plasmid using liposome nanoparticles and HPNPs for 24h, respectively. Lipofectamine-mediated transfection was performed according to the manufacturer's instructions.

Primary cochlear cells were obtained from newborn rats. 1-5-day-old newborn rats were sacrificed by decapitation after deep anesthetization and sterilization with 70% ethanol. The cochleae were isolated and cut into small pieces and then dissociated with a PBS-based solution containing elastase (1 mg/ml, Sigma Aldrich, USA), collagenase type I (1 mg/ml, Sigma Aldrich, USA), and trypsin (0.5 mg/ml, Sigma Aldrich, USA) for 30 min at 37°C. The digestion was terminated by adding 1 ml DMEM-F12 (Sigma Aldrich, USA) containing 10% fetal bovine serum (Sigma Aldrich, USA). After centrifugation for 5 min at 250 x g, the cell pellets were resuspended in 1 ml defined medium [DMEM-F12 with B27 supplement, 1 mM n-acetyl-L-cysteine, penicillin–streptomycin, and 20 ng/ml EGF (Sigma Aldrich, USA)] and plated into a 4-well Lab-Tek®II Chamber Slide (Nalge Nunc International, Naperville, USA) containing 1.0 ml defined medium/well. The cells were cultured at 37°C in a CO_2 incubator overnight. Parts of the cochlear cells were treated with HPNPs which were freshly prepared with cell culture medium at different concentrations (from 3 x 10-9 to 6.25 x 10-6 mol/L) for 24h. Parts of cochlear cells were transfected with the pGeneClip™ hMGFP plasmid using HPNPs at N/P (w/w) ratio of 5:1 and Lipofectamine 2000 (Invitrogen, USA) for 24h, respectively. Parts of cochlear cells were transfected with the pcDNA6.2/C-EmGFP-Math1 plasmid using liposome nanoparticles and Lipofectamine 2000 for 24h, respectively. Parts of the cochlear cells were treated with A_{371}-functionalized liposome nanoparticles (final concentrations: 10 μM, 1.0 μM, and 0.1 μM) and non-functionalized liposome nanoparticles (final concentrations: 10 μM, 1.0 μM, 0.1 μM, and 0.01 μM) without plasmid DNA encapsulation for 2 hours and 24 hours.

Bone marrow mesenchymal stem cells (Biosite, USA) were cultured in Qualified RMSC medium (Biosite, USA) supplemented with 10% FBS and 1% penicillin-streptomycin (Invitrogen, USA). The cells were cultured at 37°C in a CO_2 incubator overnight. MSCs were transfected with the pcDNA6.2/C-EmGFP-Math1 plasmid using Lipofectamine 2000. Fluorescence activated cell sorting was performed to sort for EmGFP positive cells. After 48 h, EmGFP positive cells were plated in a tissue culture dish and treated with 10 ng/ml BDNF and 10 ng/ml glial cell line-derived neurotrophic factor (GDNF) (Invitrogen). After 2 weeks, the cells were counter-stained with neurofilament-200.

After incubation or transfection, all the cells were washed with PBS and fixed with 4% paraformaldehyde for 30 min. The nuclei were stained with 4', 6-Diamidino-2-phenylindole

(DAPI) (10ng/ml, Sigma-Aldrich, USA) for 10 min. Part of cells were counter-stained with 50 μg/ml TRITC-labeled phalloidin (Sigma Aldrich, USA) for 40 min. Finally, all of the cells were mounted with Fluoromount for confocal microscopy.

4.3 Cochlear organotypic culture

Five 1-5-day-old new born rats were used to test HPNPs. The cochlear tissues were treated with HPNPs at concentrations of 2.5 x 10^{-6} mol/L and 1 x 10^{-5} mol/L for 24 hours. Five 1-5-day-old new born rats were treated with liposome nanoparticles carrying plasmid pGeneClip™ hMGFP DNA at concentrations of 1 x 10^{-3} mol/L and 2 x 10^{-4} mol/L for different time points (15 min, 30 min, 120 min, and 120 min, 2 d, and 4 d). The new born rats were decapitated after deep anesthetization and sterilized with 70% ethanol. Similar to the primary cochlear cell culture, each cochlea was isolated, cut into 3-4 pieces, and plated into a 4-well Lab-Tek®II Chamber Slide (Nalge Nunc International, Naperville, USA) containing 1.0 ml defined medium/well. The cochlear tissues were cultured at 37ºC in a CO_2 incubator overnight and then treated with nanoparticles. At the end of the incubation, all of the cochlear tissues were fixed with 4% paraformaldehyde for 30 min. After washing with PBS, the specimens were counter-stained with then DAPI (10 ng/ml) for 10 min. For the HPNPs treated specimens, part of them were counter-stained with TRITC-labeled phalloidin (50 μg/ml) for 40 min and the rest of the specimens were used for Myosin VIIA staining. For the liposome nanoparticles treated specimens, part of them were used for Neurofilament staining. Finally, all of the specimens were mounted with Fluoromount for confocal microscopy.

4.4 In vivo experiment

In the *in vivo* study, eleven male Sprague-Dawley (3-10-month-old) rats weighing 400-750 g with normal Pryer's reflex were supplied by the experimental animal unit, University of Tampere. Six rats were used to test HPNPs. A small piece of gelatin sponge pledget (around 8 mm^3 after saturation) saturated with 10^{-3} mol/L HPNPs were administered to rat the round window membrane for 24 hours. Five rats were used to test liposome nanoparticles. A small piece of gelatin sponge pledget (around 8 mm^3 after saturation) saturated with 10^{-1} mol/L liposome nanoparticles were administered to rat the round window membrane for 24 hours. For intratympanic administration of nanoparticles, animals were under general anesthesia [Domitor (0.5 mg/kg medetomidine hydrochloride, ORION Pharma, Finland) and Ketalar (75 mg/kg ketamine, PFIZER AB, Finland) given intraperitoneally]. After local analgesia with lidocaine, a retro-auricular incision was used to expose the left bulla. A hole was drilled on the bulla with a 2 mm diameter burr. After visualizing the stapedial artery, the round window membrane was identified above the artery. The gelatin sponge saturated with nanoparticles was placed on the round window membrane for 24 hours. The operation was performed under

sterile conditions. Atipamezole hydrochloride (2 mg/kg) was injected intraperitoneally (i.p.) immediately after the operation to accelerate recovery from anesthesia. Saline (2 ml) was administered through subcutaneous injection in the neck. L-Polamivet (0.4 ml/kg) was injected twice a day to relieve pain. Following i.p. injections of pentobarbital (60 mg/kg), cochleae were fixed using cardiac perfusion with 4% paraformaldehyde, and bullae were removed and further fixed for 60min. The cochleae were thoroughly washed with tap water for 30 seconds, opened by breaking the bony wall under a stereomicroscope, and then washed again with PBS for 2x5 min. The bullae were incubated with DAPI (10 µg/ml) for 10 min to stain the nuclei. After washing with PBS for 3x5 min, the round window membrane, lateral wall and modiolus together with the basilar membrane were harvested using a stereomicroscope, placed on glass slides, and mounted with Fluoromount for confocal microscopy.

4.5 Confocal microscopy

The specimens were observed under an Olympus IX70 microscope with ANDOR IQ installed. The excitation filters were 488 nm (blue excitation) and 568 nm (green excitation), and an Ar-Kr laser was used as the excitation source. The corresponding emission filters were 525/50 (FITC) and 607/45 (TRITC). DAPI was excited with a 340-380 nm filter and detected using a 500 LP filter.

4.6 Statistical analysis

Statistical analyses were performed using the SPSS 11.5 software package. Significant differences were identified using one-way analysis of variance, a Bonferroni test was used for pairwise multiple comparison. A difference was considered to be statistically significant at $P<0.05$.

4.7 Synthesis of different nanoparticles

4.7.1 Synthesis of lipoplex nanoparticles

4.7.1.1 Synthesis of lipoplexes with TrkB ligand

The liposome nanoparticles were provided by UH.IB, Helsinki. TrkB ligand peptides (A_{371}) were synthesized by FMOC technology (in Storkbio former inbiolabs, Tallin, Estonia), which have been developed using molecular modeling with the aim of mimicking the biological functions of brain derived neurotrophic factor (BDNF) and nerve growth factor (NGF). The appropriate amounts of the lipid stock solutions in chloroform and the lipid peptide conjugate were mixed in a molar ratio of 0.5:0.44:0.02:0.01:0.03 (Sph: eggPC: DSPE-PEG-2000: lipid-peptide conjugate: TRITC-DHPE) to obtain the desired composition. The solvent was

removed under a stream of nitrogen and the lipid residues was subsequently maintained under reduced pressure for at least 2 h to remove trace amounts of chloroform. The lipid film was hydrated with 5 mM Hepes, 0.1 mM EDTA, pH = 7.4 at 60 ^{0}C for 1h. The lipid mixture at final concentration of 0.1 mM was subjected to focused ultrasound (Covaris, KBiosciences, UK). An average diameter of 182 and 89 nm for lipoplexes with and without targeting peptide (A371), respectively, was determined by dynamic light scattering (Zetasizer, Nano ZS, Malvern Instruments Ltd., UK). Liposome nanoparticles were mixed with plasmid DNA (pGeneClipTM hMGfp) at a lipid/DNA charge ratio (+/-) of 1.2:1 to obtain nanoscale particles, also termed as lipoplexes. The diameter of lipoplexes with and without targeting TrkB ligand peptide was 108 nm and 112 nm, respectively.

4.7.1.2 Synthesis of lipoplexes with Math1 plasmid

Liposome nanoparticles were prepared similar as described above. The liposome nanoparticles were mixed with plasmid DNA (Math1) at a lipid/DNA molar charge ratio (+/-) of 1.2:1 or 2:1 to obtain lipoplexes. The final concentration of lipids in both lipoplexes was 0.1 mM or 1 mM. The following nanoparticles were obtained: LPX (DHAB /eggPC = 1:1), TRITC labeled LPX (DHAB/EggPC/ TRITC = 0.5:0.47:0.03), LPX-PEG (DHAB/ EggPC/ TRITC/ XDSPE-PEG-2000 = 0.5:0.47:0.03:0.01), LPX-DOPE (1.2:1) (DHAB/EggPC/-DOPE = 0.5:0.4:0.1, lipid/DNA molar charge ratio (+/-) of 1.2:1), and LPX-DOPE (2:1) (DHAB/eggPC/DOPE = 0.5:0.4:0.1, lipid/DNA molar charge ratio (+/-) of 2:1). The physi-cal characterization of lipoplexes is included in the original publications (V).

4.7.2 Synthesis of hyperbranched polylysine nanoparticles

The HPNPs were provided by EPFL, Switzerland. Briefly, HPNPs were synthesized by thermal polymerization of *L*-lysine*HCl and labeled with fluorescent dye, FITC (HPNPs without FITC tagged were used for gene transfection). The thermal polymerization of *L*-lysine*HCl was performed at 150 °C in the presence of an alkaline metal base (MOH) to neutralize the amine hydrochloride and to create the corresponding free amino acid base according to the procedure described by Scholl et al (Scholl et al., 2007). Samples were purified by dialysis and gel filtration with a Sephadex Column. The final product was recovered in 85% yield as an orange powder. Before usage *in vitro* or *in vitro*, the powder was dissolved in PBS, resulting in a molecular concentration of 10^{-3}mol/l. The molecular weight, average hydrodynamic diameter, and polydispersity index (PDI) of hyperbranched polylysine nanoparticles were determined by dynamic light scattering (DLS, Zetasizer Nano ZS, Malvern Instruments Ltd., UK): M_n = 22 000 g/mol; hydrodydynamic diameter: 73 nm; PDI = 1.9. The scanning electron microscopy showed the HPNPs spherical morphology and similar size to the DLS measurement. The physical-chemical characterization of polyplexes formed

by complexation of HPNPs and plasmid DNA is included in the original publication (IV).

4.7.3 Synthesis of POA@SPIONs

The SPIONs were provided by KTH, Stockholm. Briefly, a total of 0.903 g FeCl3 • $6H_2O$ (3.34 mmol) and 3.046 g sodium oleate (10.02 mmol) were dissolved in a mixed solvent, including 25 mL ethanol, 20 mL deionized water and 45 mL hexane. The resulting solution was heated to 62°C and refluxed for 4 hours. Then the iron oleate complex containing organic phase was washed with deionized water three times. After the evaporation of hexane, 2.90 g waxy Fe oleate complex (3.23 mmol) and 0.47 g oleic acid (1.67 mmol) were dissolved in 20 mL dioctyl ether at 70°C. The reaction mixture was heated to 290°C for 1.5 hours. A total of 30 ml ethanol was added to the reaction mixture, and the nanoparticles were collected by centrifugation under 6000 rpm. The nanoparticles were purified by centrifugation. Finally, the SPIONs were dispersed in 40 ml tetrahydrofuran (THF) in the presence of 100 µl oleic acid. To achieve transfer from organic phase to water phase, a 2 ml solution of SPIONs in THF was mixed with 2 ml 10 mg/ml Pluronic® F127 aqueous solution at room temperature. After 30 minutes of vigorous agitation, the organic solvent was evaporated overnight to obtain a stable aqueous suspension of SPIONs. The aqueous solution of SPIONs was then dialyzed to remove free-standing PF127 polymers. The particle suspension was filtered by 200 nm syringe filter and stored at 4°C.

4.8 MRI measurements

MRI was performed with a 4.7 T MR scanner with bore diameter of 155 mm (PharmaScan, Bruker BioSpin, Germany) using a dedicated rodent head coil with diameter of 38 mm (for rat and for mice >50 g) and 23 mm (for mice <25 g). The maximum gradient strength was 300 mT/m with an 80-µs rise time. All animal experiments were approved by the Ethical Committee of the University of Tampere (permission: STH527 A ESLH-2006-07528/Ym23). Animal care and experimental procedures were conducted in accordance with the European legislation. All experimental procedures were performed under general anaesthesia. The body temperatures of the animals were maintained by circulating warm water and their respirations were recorded with Physio Tool-1.0.b.2 program (Bruker BioSpin, Germany). Animals were placed in the magnet with the ears positioned at the isocenter.

4.8.1 MRI measurement of Gd-DOTA

Twenty-three albino female FVB mice, weighing from 18 to 55 g were included in this study. For intravenous administration, the gadolinium-tetra-azacyclododecane-tetra-acetic acid (Gd-DOTA, Guerbet, Aulnaysous-Bois, France, 500 mmol/L) was injected into the tail vein (IV) at

dosages of 1.5, 0.75, or 0.3 mmol/kg via canula during MR scanning (Table 1). For intratympanic (IT) delivery, a portion of gelfoam was soaked in Gd-DOTA diluted in physiological saline to concentrations of 500, 100, 50, or 25 mmol/L, and placed in the middle ear cavity against the round window through a myringotomy (Table 1). Excess solution was removed by absorption with a small piece of cotton. It is estimated that the gelfoam pieces measured 1 x 1 x 3.5 mm^3 when wet and contained approximately 5 µl Gd-DOTA, i.e. ranging from 0.014 to 0.0045 mmol/kg. Head coils of either 38 or 23 mm were used, depending on the size of the animal.

T2-weighted two-dimensional (2D) images were acquired with the rapid acquisition with relaxation enhancement (RARE) sequence (TR/TE_{eff} 25,000/40 ms, resolution 0.156 x 0.156 mm^2). T1-weighted 2D images were acquired with RARE sequence (TR/TEeff 500/10 ms, resolution 0.098 x 0.13 mm^2). High resolution T1-weighted three-dimensional (3D) images were acquired with RARE sequence (TR/TEeff 500/43 ms, resolution 0.078 x 0.078 x 0.078 mm^3).

For IT delivery, serial MR imaging was obtained from 1.5 to 4 h after Gd-DOTA administration. 2D and 3D T1-weighted images were acquired. For IV administration, a series of images were acquired with 10 min intervals to study serial dynamic uptake over a period of 120 min following the Gd-DOTA injection in a group of animals using the 38 mm coil. It was noted that the 23 mm coil could potentially limit the animals' ventilatory excursions. Consequently, most of the serial dynamic uptake observations made with the 23 mm coil were performed at longer time intervals, immediately, 90 min, and 180 min after Gd-DOTA injection and using 3D sequences, which reduce the time of acquisition. Animals imaged with the 23 mm coil were removed from the machine between scans (Table 1).

4.8.2 MRI measurement of POA@SPIONs

A total of 26 male Wister rats weighing from 218 to 470 g with normal Prey's (hearing) reflex were included in this study. Overall, the study was designed with three arms of POA@SPIONs administration, including intracochlear (SPIONs-IC), intratympanic (SPIONs-IT) and intravenous (SPIONs-IV) routes. The SPIONs-IC arm was subdivided into two groups based on whether a silicon catheter (SC) or polyurethane catheter (PC) was employed for the IC injection. Animals in the SPIONs-IT arm underwent MRI at varied time intervals following POA@SPIONs administration ranging from day 0 through day 7. T2-weighted 2D images were acquired with RARE 2D sequences (TR/TE_{eff} 2500/40 ms, resolution 0.156 x 0.156 mm^2). T2-weighted 3D images were acquired with RARE 3D sequences (TR/TE_{eff} 500/43 ms, resolution 0.078 x 0.078 x 0.078 mm^3). For IC delivery, 2D T2-weighted images were acquired at different time points post POA@SPIONs administration (1-6 h). 3D T2-weighted imaging was performed in one animal. For IT delivery, 3D T2-weighted images

were acquired at different time points post POA@SPIONs administration in different animals (Table. 2). For IV administration, a series of images were acquired with 30 min intervals over a period of 210 min following the POA@SPIONs injection.

In the SPIONs-IC arm, the left bulla was exposed through a postauricular approach. Working under an operating microscope, a hole was drilled through the bulla with a 2 mm diameter burr. The round window membrane was identified superior to the stapedial artery. The scala tympani in the basal turn was opened with a 0.5 mm cutting burr inferior to the stapedial artery. POA@SPIONs were slowly injected either through a SC group that was connected to a reservoir (tubing outer diameter: 0.64 mm; inner diameter: 0.3 mm; MedEl, Innsbruck, Austria) or through a custom made polyurethane catheter (outer diameter: 0.25 mm; inner diameter: 0.12 mm; AgnTho's AB; PC group). The SC-reservoir drug-delivery system was designed to administer multifunctional nanoparticles into the human cochlea and was, therefore, included in the present study. However, the catheter was excessively large for insertion into the cochlea of a rat, which necessitated our design of an appropriately sized polyurethane catheter drug-delivery system. The catheter tip was inserted into the scala tympani just through the opening and was sealed circumferentially with Histoacryl glue (Aesculap AG, Tuttlingen, Germany). After the glue was dry, 10–20 µl (in SC group) or 5 µ µl (in PC group) POA@SPIONs were slowly instilled over 1 min into the scala tympani. The wound was sutured closed. MRI scanning commenced immediately after the POA@SPIONs administration.

In the SPIONs-IT arm, POA@SPIONs was administered through a postauricular middle ear operation, as described above or through a transcanal approach with a myringotomy over the round window. In the postauricular approach, a small pledget of gelatine sponge (approximately 8 mm^3) soaked in POA@SPIONs was placed against the round window membrane. A muscle plug was used to fill the opening made in the bulla and the wound was sutured closed. In the transcanal approach, an anterior myringotomy was initially made to relieve any air bubbles. A posterior myringotomy was then made and a similar sized gelatine sponge soaked in POA@SPIONs was placed into the round window niche and allowed to fill the posterior middle ear cavity. A control procedure was carried out through a similar approach on the contralateral side and the gelatine sponge was soaked only in physiological saline.

In the SPIONs-IV arm, the lateral tail vein was dilated by soaking the tail in warm water followed by topical application of 70% alcohol. The vein was cannulated with a 30-gauge needle connected to catheter tubing and taped securely into position. Saline containing 5% heparin was initially instilled to maintain patency. Baseline pretreatment MRI scans were obtained as a control. POA@SPIONs were slowly injected intravenously. MRI scanning commenced immediately after the contrast agent administration.

Table 1 Animals were grouped according to administration approaches and dosages of the contrast agent.

Groups/dosages		n	Coil size	Histology/embedding
IT	25 mmol/L	2	23 mm	
	50 mmol/L	2	23 mm	
	100 mmol/L	2	23 mm	
	500 mmol/L	2	23 mm/38 mm	
IV	0.3 mmol/kg	1	23 mm	
	0.75 mmol/kg	3	23 mm/38 mm	
	1.5 mmol/kg	9	23 mm/38 mm	2/paraffin

IT, intratympanic; IV, intravenous; n, number of the animal

Table 2. Animals were grouped according to administration approaches and MRI time post-POA@SPION delivery.

Groups	n	Dosages[†]	MRI time	Ears for histology
SPION-IC:				
SC	3	10-20	Day 0 (1–6 h)	3
PC	6	5 µl/rat	Day 0 (1–6 h)	
SPION-IT:				
Day 0	8	20 µl/rat	Day 0 (2–3 h)	1
Day 1	2	20 µl/rat	Day 1	
Day 3	2	20 µl/rat	Day 0 and 3	
Day 7	2	20 µl/rat	Day 0 and 7	1
SPION-IV	3	2.37 µl/kg	Day 0	

[†]Fe+ concentration: 1.0mg/ml (4.3mM) –1.3mg/ml (5.6mM).

IC: Intracochlear; IT: Intratympanic; IV: Intravenous; PC: Custom-made polyurethane catheter (AgnTho's AB, Sweden); SC: silicon catheter connected to a reservoir (MedEl, Innsbruck, Austria); SPION: Superparamagnetic iron oxide nanoparticle.

5. RESULTS

5. 1. Passage of gadolinium through the mouse inner ear barriers

The mouse inner ear structures delineated by MRI using intratympanic Gd-DOTA administration

T1 and T2 signal characteristics were compared using a 2D imaging protocol in animals with the 23 mm diameter coil. The T2-weighted sequences showed that the inner ear fluids generated a bright signal, including the perilymph in the scala tympani, scala vestibuli, vestibulum, and semicircular canals as well as endolymph in the scala media. The modiolus signal was grey, while the osseous spiral lamina was dark (Fig.1A). The T2 signal was more intense in ears treated with Gd-DOTA. In comparison, T1-weighted images showed that endolymph in the scala media and ampullae of the semicircular canals were dark, while perilymph was bright. The modiolus was also bright, although less than the perilymph. The contralateral non-treated side showed a diffuse grey signal (Fig.1B). The scala tympani and vestibuli were also distinguishable from the scala media in Gd-DOTA contrasted, T1-weighted images using the 38 mm coil.

3D images using T1-weighted sequences revealed greater contrast and detail within the inner ear than 2D images. For example, the lateral wall in the basal turn of the cochlea contained a grey appearing region that likely represents the spiral ligament against the dark endolymph. A dark border appeared between ST and LW in the basal turn near the hook region (Fig.2A). Identification of the lateral wall via MR imaging, located lateral to the perilymph and endolymph, was confirmed by comparison to histological sections. The cochlear aqueduct, which originates in the scala tympani near the round window membrane, was visible (Fig.2). The vestibular perilymph was continuous with the perilymph in the scala vestibuli and semicircular canals; however, the superior semicircular canal was infrequently visible (Figs.2E).

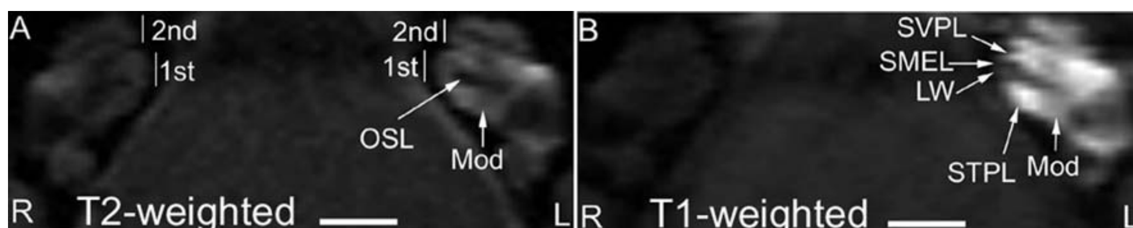

Figure 1. Mouse cochlear structures in coronal 2D MR images with IT administration of Gd-DOTA (23 mm coil) (180 min time point). (A) T2-weighted image shows Gd-DOTA enhanced signal in the cochlea except for the OSL. SM appears slightly darker than the perilymphatic compartments. (B) T1-weighted

image shows much more intense Gd-DOTA enhanced signal in the perilymphatic compartments, ST and SV compared to the bright signal in the T2-weighted image A. SM is dark and clearly distinguishable from the perilymphatic compartments and LW. LW, lateral wall; Mod, modiolus; OSL, osseous spiral lamina; SM, the scala media; ST, the scala tympani; SV, the scala vestibuli; 1st, the basal turn; 2nd, the second turn. Scale bar = 1 mm.

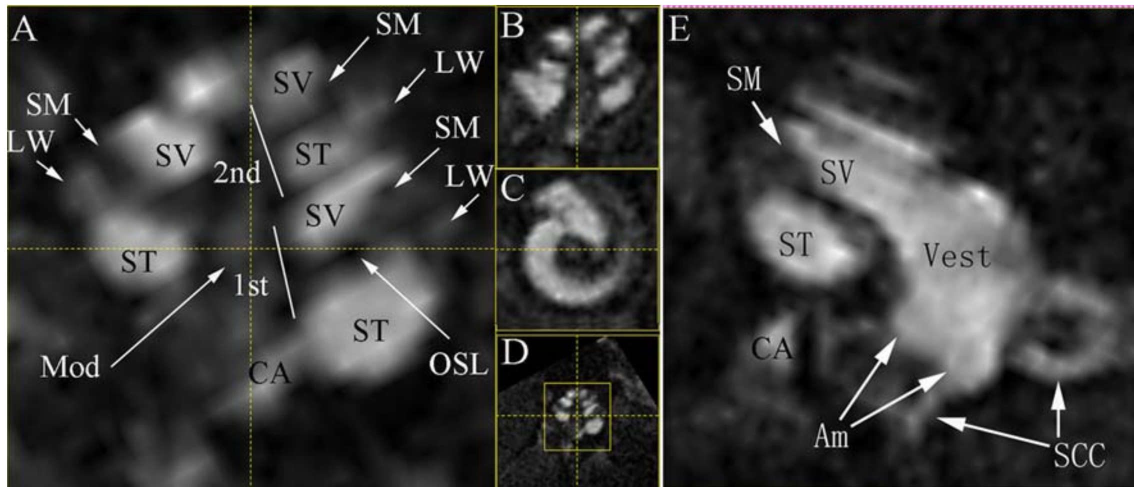

Figure 2. Mouse cochlear and vestibular structures in MPR multi view of T1-weighted images with IT administration of Gd-DOTA (23 mm coil) (180 min time point). Gelfoam soaked with 5 μl, 500 mmol/L Gd-DOTA was placed into the left ear. In the enlarged window A, LW and Mod are slightly highlighted by Gd-DOTA uptake in addition to more pronounced enhancement in ST and SV. The structure adjacent to ST is suspected to be CA with signal intensity similar to ST. LW demonstrated brighter signal than SM. A dark border appeared between ST and LW in the basal turn near the hook region. OSL is seen as a sharp dark line. In the enlarged window E, the vestibular perilymph, including the Vest, Am, and SCC, show obvious uptake of Gd-DOTA. The perilymph in the Vest merges with the perilymph in the basal turn of SV. CA is seen adjacent to the basal turn of the ST. Small window B is a relative perpendicular cut through the centre of plane A. Small window C is a relative axial cut through the centre of the cochlea in window A. Small window D is the minimised image of window A. Am, ampulla; SCC, semicircular canal; Vest, vestibulum. CA, cochlear aqueduct; LW, lateral wall; Mod, modiolus; MPR, multiplanar reconstruction; OSL, osseous spiral lamina; SM, the scala media; ST, the scala tympani; SV, the scala vestibuli; 1st, the basal turn; 2nd, the second turn.

The images were acquired in mice receiving IT administration of Gd-DOTA at concentrations of 500, 100, 50, and 25mmol/L. The signal intensities in the perilymphatic compartments and Gd-DOTA concentrations were linearly correlated ($R = 0.445$, $p < 0.05$, ANOVA test). Gd-DOTA uptake in the scala tympani was consistently higher than in the scala vestibule, while it was variable in the vestibulum.

Dynamic uptake of Gd-DOTA in the mouse inner ear fluids upon intravenous administration

Inner ear images acquired after IV administration of Gd-DOTA were roughly similar to those obtained following IT delivery. Two-dimensional T1-weighted sequences were performed at 10 min intervals in a 38 mm coil and showed a strong linear increase in signal intensity within the perilymph of the scala tympani between 10 and 70 min. The signal enhancement within the perilymphatic compartments reached an initial plateau 80 min after IV administration and continued to slightly increase to a maximum level by 100 min (Fig. 3A).

Three-dimensional images were acquired with T1-weighted sequences using the 23 mm coil. At the time point 0, just after IV injection of Gd-DOTA, the perilymph space did not contain sufficient signal for quantitation. The signal subsequently increased in the perilymph of the scala tympani, scala vestibuli, and vestibulum and showed an increasing trend in intensity from the 90 min to the 180 min scans, but the differences were not statistically significant (Fig. 3B) ($p > 0.05$, Student's t-test). These results were consistent with the 2D observations, wherein Gd-DOTA uptake reached a plateau at approximately 90 min. The higher signal intensities for the perilymph over the endolymph were statistically significant (Fig. 3B) ($p < 0.001$, paired samples t-test). Certain finer details of inner ear structures were better defined following IV administration of Gd-DOTA compared with IT delivery. Uptake within the cochlear apex was slightly greater in the IV group. The cochlear aqueduct and all semicircular canals were better demonstrated in the IV group. However, the signals in the lateral wall and modiolus were slightly higher in the IT group than the IV group.

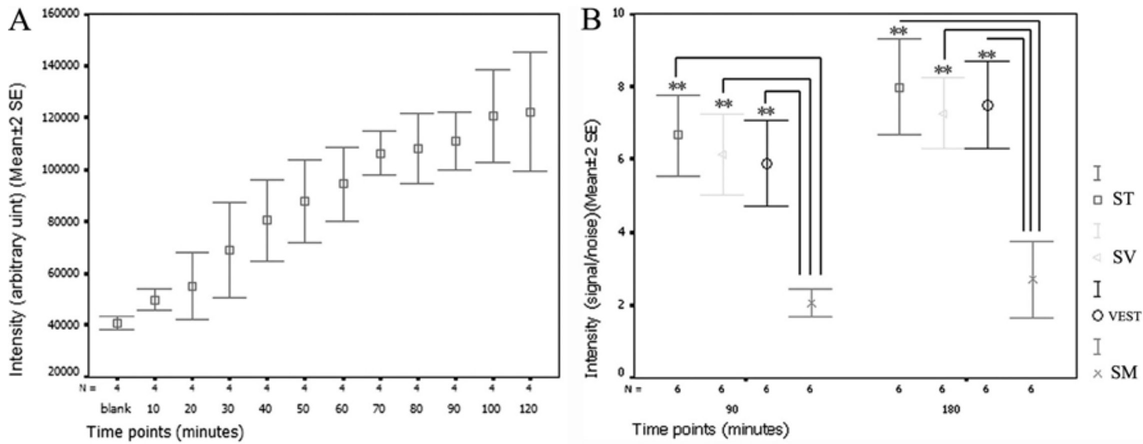

Figure 3. Dynamic uptake of Gd-DOTA in the inner fluids after IV administration at the dosage of 1.5 mmol/kg. (A) Signal intensities of ST plotted versus time imaged with 2D T1-weighted sequences using the 38 mm coil. The uptake reached a plateau after 80 min and stepped to the second one after 100 min. (B) There was slightly increased signal intensity from 90 to 180 min time points when measured with 3D T1-weighted sequences using the 23 mm coil. The uptake in perilymphatic compartments was significantly greater than that in SM (**$p < 0.01$, paired samples t-test). N, number of the ears; SM, the scala media; ST, the scala tympani; SV, the scala vestibuli; Vest, vestibulum.

5. 2. MRI manifestation of novel POA@SPIONs in the rat inner ear

MRI manifestation of POA@SPIONs in the inner ear after IC administration

Without any contrast agent, the inner ear fluids, including perilymph and endolymph, generated an intense signal on T2-weighted MRI. Therefore, the cochlear and vestibular compartments were highlighted on the volume rendering from a T2-weighted 3D scan. In the IC–PC subgroup, 3D rendered images acquired 180 min after IC delivery showed that the areas with high signal in the cochlea and vestibulum were greatly decreased in comparison with the untreated contralateral side. The disappearance of signal for the perilymph signal was attributed to the presence of POA@SPIONs within that compartment. Quantitation of 2D images demonstrated statistically significant decreases in the signal intensity (normalized by the nearby brain signal intensity; POA@SPIONs treatment side vs untreated side) for both the cochlea ($p < 0.001$, paired Student t-test) and ampulla ($p < 0.05$, paired Student t-test) 2 h post-IC injection (Fig. 4). The signal changes persisted over a 6 h observation time (Fig. 4B). In another measurement, the T2 relaxation time (mean ± SD) in the scala vestibuli perilymph after POA@SPIONs (25.608 ± 5.351 ms) treatment was lower than than the untreated side (130.5 ± 71.9 ms). In the IC–SC subgroup, which received a larger injected volume of nanoparticles to compensate for a leak at the round window, the signal decrease in rat the perilymph was greater than in the IC–PC subgroup, which was exposed to a smaller POA@SPION volume (5 µl).

Limited passage of POA@SPIONs through the middle-inner ear barriers

POA@SPIONs were delivered to the round window membrane, and T2-weighted MRI was performed at different time points, from 2 h to 7 days (Table 2). In the 2D MR images, no visible difference was observed between the left inner ears, which were exposed to the round window membrane POA@SPION administration, and the right side, which were exposed to physiological saline (Fig. 5). Quantitation showed no statistically significant difference at 2 h through 7 days post-round window membrane administration ($p > 0.05$, paired t-test). However, the data did show slight decreases in signal intensity for the left cochleae 1 and 3 days after POA@SPIONs delivery and on the left ampullae day 1 through day 7. At 3.5 h post-nanoparticle administration, there was no difference in T2 relaxation time between the cochlea exposed to POA@SPIONs (123.510 ± 4.640 ms) and the untreated cochlea (124.005 ± 22.526 ms). Following this, 1 week later, a slight decrease in T2 relaxation time was observed in the POA@SPION-exposed cochlea (103.255 ± 6.497 ms) compared with the untreated side (121.666 ± 11.677 ms). These data suggest a slight, but insufficient passage of POA@SPIONs through the middle-inner ear barriers.

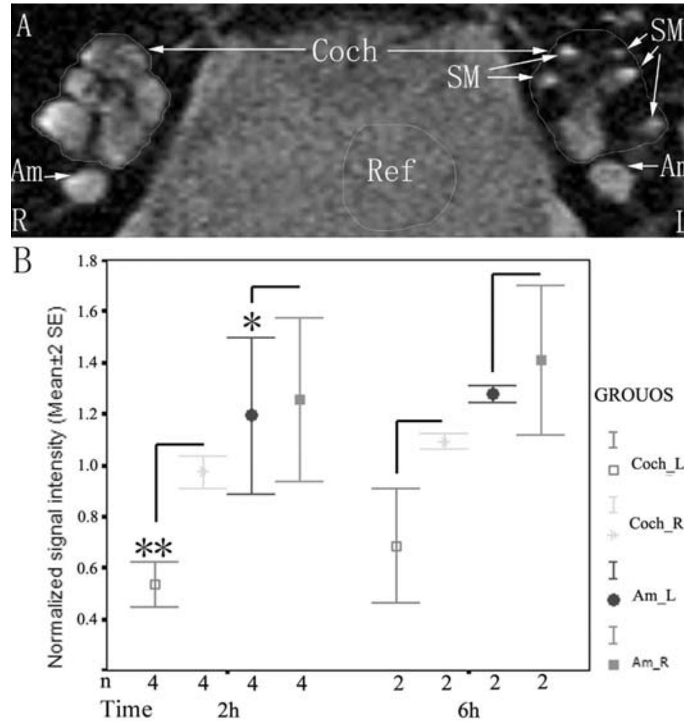

Figure 4. Quantitative comparison of T2-weighted signal intensities of the inner ear between left cochleae receiving intracochlear POA@SPIONs and right nontreated cochleae. Signal in the perilymph of the left cochleae was diminished by the nanoparticles leaving only the endolymph in the scala media with bright signal (A). Quantification showed a significant decrease in the signal intensity in the perilymph of both the cochlea and ampulla at 2 h postintracochlear injection of POA@SPIONs (normalized signal intensity = signal intensity in the region of interest/signal intensity in reference) (B). The signal intensity changes persisted for the 6 h of observation time. $*p < 0.05$; $**p < 0.01$ (paired Student t-test). Am: Ampulla; Coch: Cochlea; IC: Intracochlear; L: Left; PC: Polyurethane catheter; R: Right; Ref: Reference region in brain; SE: Standard error; SM: Scala media.

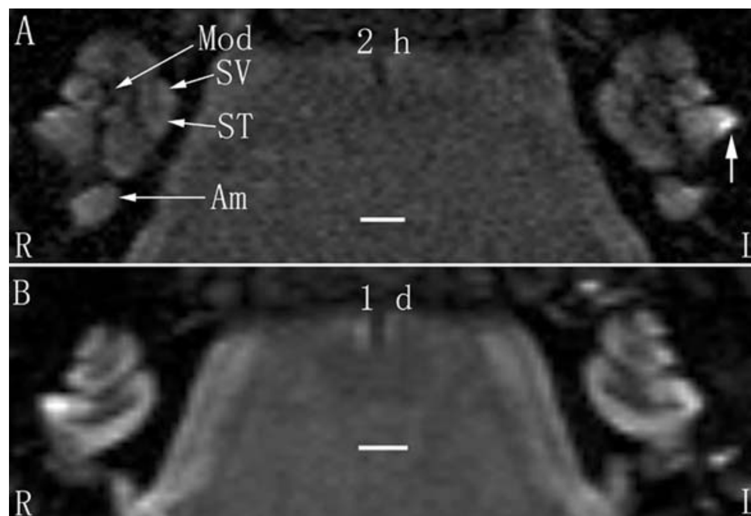

Figure 5. T2-weighted images of the inner ear after intratympanic administration of POA@SPIONs to the left ears. There was no visible signal change observed in the left side (L) compared with the untreated right side (R) at either 2 h **(A)** or 1day **(B)** postadministration. The bright signal in the left cochlea as indicated

by the arrow is of unknown origin and was consistently observed in all cochleae. Am: Ampulla; Mod: Modiolus; ST: Scala tympani; SV: Scala vestibuli.

POA@SPIONs did not pass through the blood-endolymph and blood-perilymph barriers

Before IV injection, baseline T2-weighted images were taken, which showed bright signals in both endolymph and perilymph compartments within the cochlea and vestibular organ. The endolymph was indistinguishable from the perilymph (Fig. 6A). Images of the inner ear acquired at defined time points post-POA@SPIONs IV delivery did not show visible changes, indicating that POA@SPIONs was not detected in the inner ear (Fig. 6B). Quantitation confirmed that no statistically significant signal intensity changes were observed for up to 210 min after IV administration of POA@SPIONs ($p > 0.05$; ANOVA) (Fig. 6C).

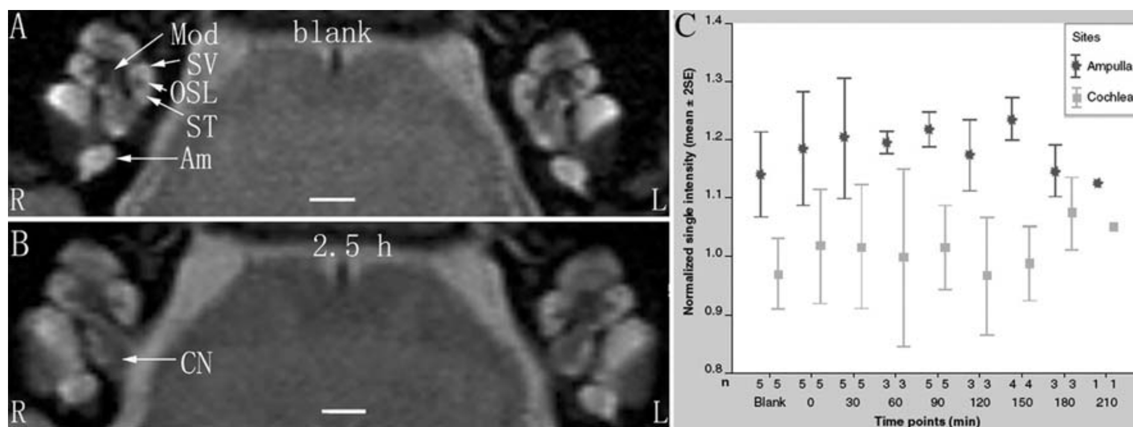

Figure 6. T2-weighted imaging of the inner ear after intravenous POA@SPIONs administration. A baseline image taken before nanoparticle delivery demonstrated the cochlear anatomy and ampulla **(A)**. After 150min, no signal change was observed **(B)**. Signal intensity dynamics (normalized by brain signal intensity) obtained up to 210min did not show statistically significant differences **(C)**.Am: Ampulla; CN: Cochlear nerve; L: Left; Mod: Modiolus; OSL: Osseous spiral lamina; R: Right; SE: Standard error; ST: Scala tympani; SV: Scala vestibuli.

5. 3. Internalization of HPNPs in the cochlear cells both *in vitro* and *in vivo*

Internalization of HPNPs in rat primary cochlear cell culture

After 24 h of incubation, efficient internalization of HPNPs was observed in primary rat cochlear cells at all concentrations tested. The level of HPNPs internalized by the cells was dose-dependent; the higher the HPNP concentration applied to the cell culture medium, the greater fluorescent intensity in the cochlear cells. This positive correlation was statistically significant ($p<0.001$, ANOVA). Nuclear entry of HPNPs was detected in different cochlear cell types, including hair cells and spiral ganglion cells at different concentrations. The higher

the concentration of HPNPs, the more nuclear localization of HPNPS was observed (Fig. 7). In cochlear cells that were incubated with HPNPs at concentrations from 3.87 x 10^{-7} mol/L to 6.25 x 10^{-6} mol/L, a homogenous and condensed distribution of HPNPs was detected throughout the nuclei (Fig. 8). Nuclear permeation of propidium iodide, which indicates cell death, was also observed in cochlear cells treated with HPNPs at this concentration interval (Fig. 8). HPNPs were included in both cytoplasmic and nuclear vesicles when the nanoparticle concentration was below 3.87 x 10^{-7} mol/L (Fig. 7). No permeation of propidium iodide was detected in the nuclei, indicating that these cells are living cells. However, nuclear permeation of propidium iodide was occasionally observed in spiral ganglion cells that were treated with HPNPs at 9.7 x 10^{-8} mol/L. Nucleolin expression was detected in the cochlear cells. Subcellular distribution of nucleolin was in both the cytoplasm and nucleus. An HPNP vesicle pathway from the cytoplasm towards the nucleolin positive nucleolus was also observed.

HPNP internalization in rat cochlear organotypic culture

In cochlear organotypic culture treated with HPNPs for 24 hours, an abundant of HPNPs appeared in diverse cell types: the modiolus, Corti's organ, and the lateral wall (Fig. 9). The hair cell region was demonstrated by myosin 7A staining (Figs. 9A and B). Nuclear entry of HPNPs was frequently observed in these different cell types.

HPNP distribution in adult rat cochlear cell populations after round window membrane permeation

HPNPs were observed in the round window membrane, middle ear mucosa, Corti's organ, spiral ganglion, stria vascularis, spiral ligament, and stapedial artery cells at 24 hours post-round window membrane administration. HPNPs appeared in both layers of the round window membrane (Fig. 10A). A homogenous, condensed distribution of HPNPs was detected in the nuclei, and cytosolic HPNP vesicles were traveling from the outer layer towards the inner layer (Fig. 10A). Additionally, there was a gradient of cytosolic HPNP vesicles from the outer layer to the inner layer (Fig. 10A). More pronounced nuclear entry was also observed in the outer layer of the round window membrane than the inner layer. In the middle ear mucosal cells, HPNPs were observed in both the cytoplasm and nuclei. Distribution was condensed in the nuclei, and vesicles were at low levels in the cytoplasm (Fig. 10B). In the spiral ganglion cells, perinuclear distribution of HPNP vesicles was observed (Fig. 10C). In the Corti's organ, HPNPs were detected in the cytoplasm of outer hair cells, inner hair cells, and supporting cells (Fig. 10D). In the stria vascularis, HPNP vesicles appeared in the tight junctions, cytoplasm, and perinuclear region of the marginal cells (Fig. 10E). In the spiral ligament fibrocytes, HPNPs primarily appeared in the cytoplasm as vesicles (Fig. 10F). An abundant of HPNPs was also detected in the stapedial artery cells and

appeared as vesicles in both the cytoplasm and nuclei (Fig. 10G).

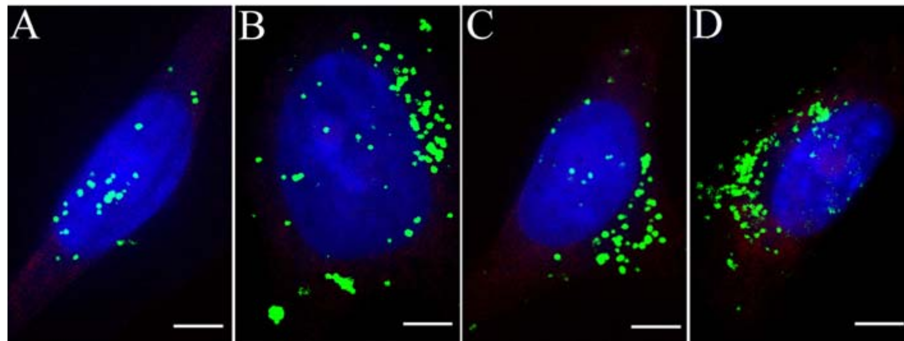

Figure 7. HPNP vesicle formation in both the cytoplasm and nuclei was observed at concentrations below 3.87×10^{-7} mol/L. (A): 3.87×10^{-7} mol/L, (B): 9.7×10^{-8} mol/L, (C): 2.4×10^{-8} mol/L, (D): 3×10^{-9} mol/L. Nuclear permeation of propidium iodide was not detected in these cells. Green: HPNPs. Blue: DAPI. Scale bar = 5 μm.

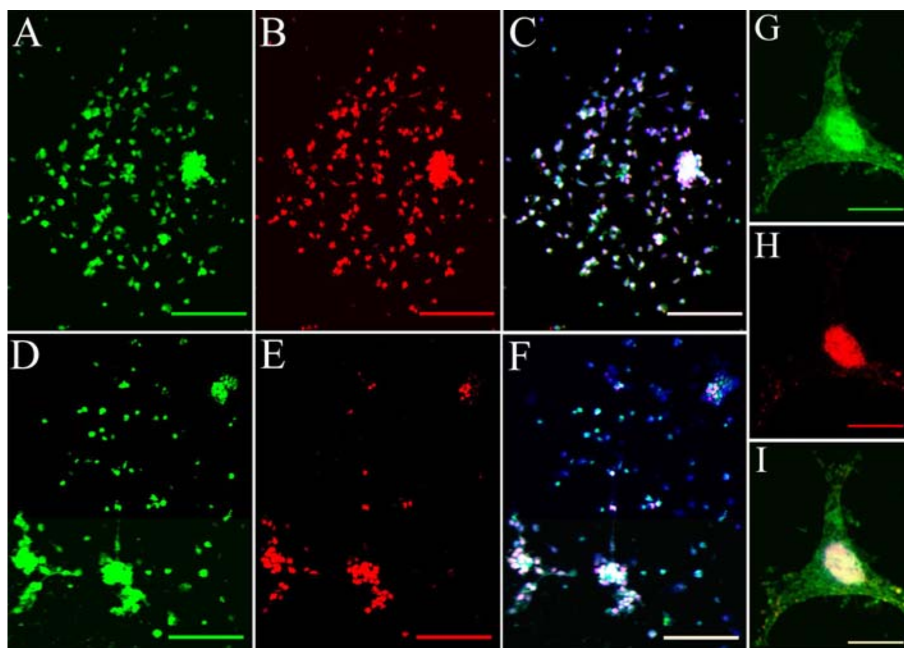

Figure 8. Internalization of HPNPs induced permeation of propidium iodide in the primary cochlear cell culture. (A-C): The cochlear cells were incubated with HPNPs at a concentration of 6.25×10^{-6} mol/L. Nuclear permeation of propidium iodide was observed in all the cells (B). C is the merged images of A and B. (D-F): The cochlear cells were incubated with HPNPs at a concentration of 3.87×10^{-7} mol/L. Nuclear permeation of propidium iodide was observed in most of the cells (E). F is the merged images of D and E. (G-I): Internalization of HPNPs induced permeation of propidium iodide in a single cell (higher magnification). Homogenous and condense distribution of HPNPs was detected in the cytoplasm and entire nucleus (G). (I): merged image. Green: HPNPs. Red: propidium iodide permeation. Blue: DAPI. Scale bars = 100 μm.

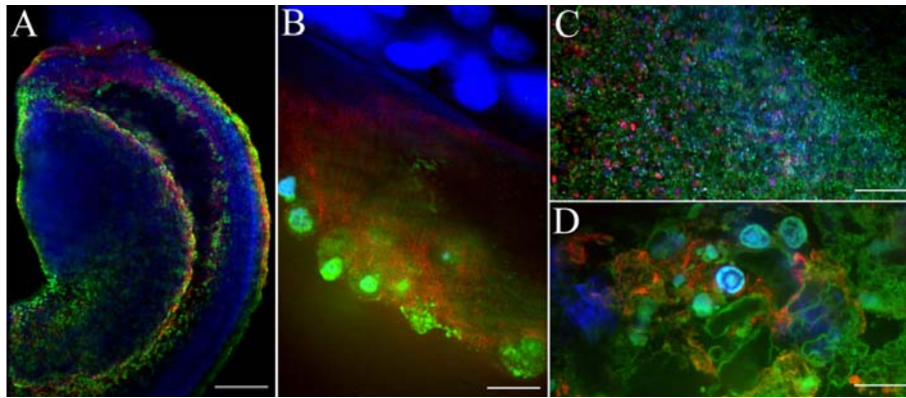

Figure 9. Uptake of HPNPs in the cochlear organotypic culture. Figs. 3A and B are merged images of HPNPs, Myosin 7A, and DAPI in the modiolus (A) and Corti's organ (B). Figs. 3C (low magnification) and D (higher magnification) are merged images of HPNPs, F-actin, and DAPI in the lateral wall. Green: HPNPs; Red: Myosin 3A (A, B), F-actin stained by TRITC-conjugated phalloidin (C, D). Blue: DAPI. Scale bars: A, C =100 μm, B, D =10 μm.

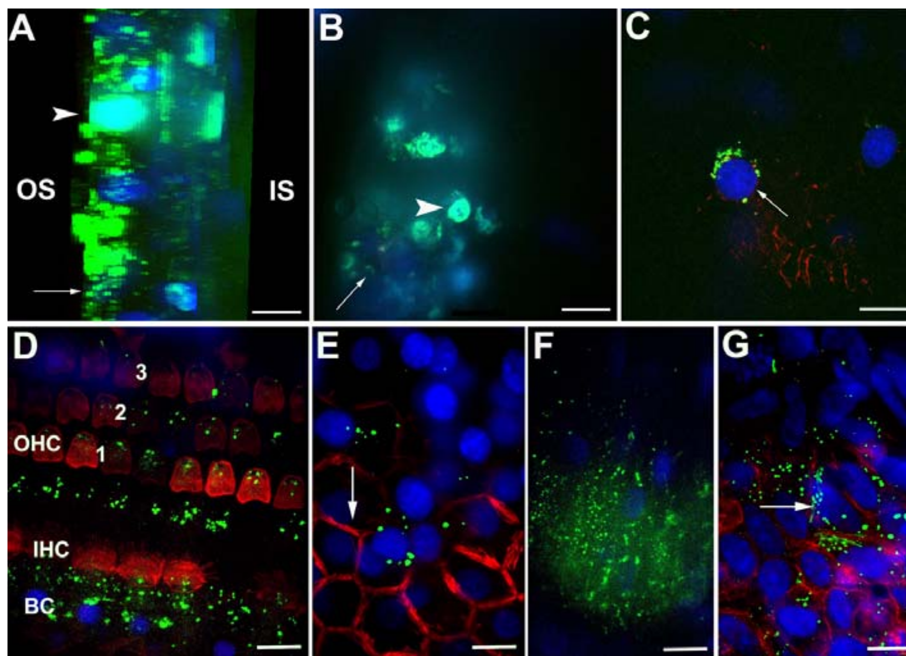

Figure 10. Uptake of HPNPs in the cochlea at 24 hours post-round window membrane administration in an adult rat. A: Lateral view of reconstructed 3D image of the round window membrane showing the gradient distribution of HPNPs, both condensed homogenous nuclear distribution of HPNPs (arrow head) and HPNP vesicles (arrow) were observed. B: Middle ear mucosal uptake of HPNPs. Condensed homogenous nuclear distribution of HPNPs (arrow head) and HPNP vesicles (arrow) were detected. C: Perinuclear distribution of HPNPs was observed in the spiral ganglion cell (arrow). D: HPNPs were found in the Corti's organ, cytoplasmic distribution of HPNPs was observed in the hair cells, and both cytoplasmic and peri-nuclear distribution of HPNPs was detected in the supporting cells (Border cells). E: Both cytoplasmic and nuclear distribution of HPNPs was detected in the stria marginal cells, the typical tight junctions of the stria marginal cells are shown using F-actin staining (arrow). F: Abundant HPNPs were observed in the

spiral ligament fibrocytes. G: Abundant HPNPs were detected in the endothelium of the stapedial artery including the nuclear HPNP vesicles (arrow). Green: HPNPs; Red: TRITC-conjugated phalloidin; Blue: DAPI. BC: Border cell; IHC: inner hair cell; IS: inner side of the RWM; OHC: outer hair cell; OS: outer side of the round window membrane; 1, 2, 3: row 1, row 2, and row 3 of OHC. Scale bar = 10 µm.

HPNP-mediated gene transfection in cell culture

After 24 h of incubation, NIH 3T3 cells were transfected with the pGeneClip^{TM} hMGFP plasmid using HPNPs. To determine the optimum N/P (w/w) ratio, the N/P (w/w) ratio was varied from 1:1 to 6:1. The N/P (w/w) ratios of 4:1 and 5:1 resulted in the maximum level of GFP expression. HPNP-mediated transfection efficiency in NIH 3T3 cells was 29.8% at a 5:1 N/P (w/w) ratio. The HPNP-mediated transfection efficiency in primary cochlear cells was 8.7% at a 5:1 N/P (w/w) ratio, which was higher than the Lipofectamine-mediated transfection efficiency of 6.0%.

5. 4. Math1 expression *in vitro* and intracellular trafficking of the Math1 protein

Lipofectamine-mediated transfection of pcDNA6.2/C-EmGFP-Math1 plasmid in defined cell types

NIH 3T3 cells were transfected with the pcDNA6.2/C-EmGFP-Math1, pcDNA6.2/C-EmGFP-BDNF and PCLIG-Math1 plasmids using Lipofectamine 2000. After 24 h of incubation, variable transfection efficiencies were observed for the three plasmids. The plasmid pcDNA6.2/C-EmGFP-Math1 showed the highest transfection efficiency, 11.7%; pCLIG-Math1 showed the lowest transfection efficiency, 3.0%; and the transfection efficiency of pcDNA6.2/C-EmGFP-BDNF was 7.2%. Using microscopy, the fluorescence of the EmGFP-Math1 fusion protein in NIH 3T3 cells was a vivid emerald, which was bright and easily detected, while EGFP fluorescence in NIH 3T3 cells that was expressed by the PCLIG-Math1 plasmid was faint (Fig. 11G). MSCs and primary cochlear cells were also successfully transfected with pcDNA6.2/C-EmGFP-Math1 plasmids (Figs. 11F and 12). The transfection efficiencies were 2.9% in primary cochlear cells and 5.1% in MSCs. In primary cochlear cell culture, fibrocytes, spiral ganglion neurons, and hair cell-like cells were transfected with the pcDNA6.2/C-EmGFP-Math1 plasmid (Fig. 12). The transfection efficiency of the different cell populations was not quantified; however, fibrocytes and spiral ganglion neurons, the two major populations in the primary cochlear cells, were frequently observed as expressing EmGFP under a confocal microscope.

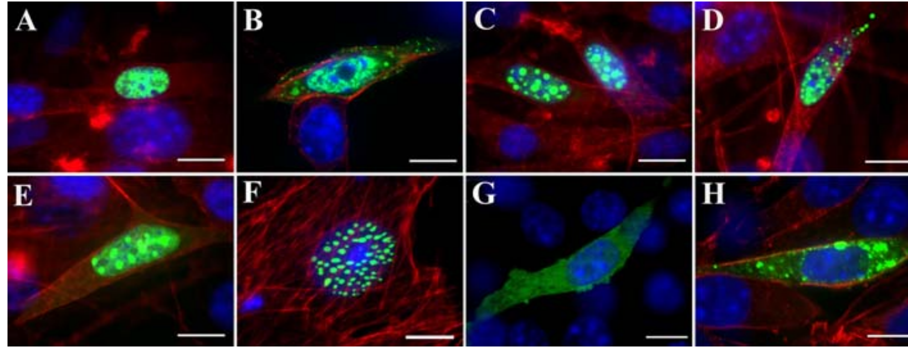

Figure 11. Subcellular localization of EmGFP-Math1 fusion protein in different cell types transfected by pcDNA6.2/C-EmGFP-Math1 plasmid using Lipofectamine. A-E: EmGFP-Math1 expression in NIH 3T3 cells. F: EmGFP-Math1 expression in MSCs. G: EGFP expression in NIH 3T3 cell. H: EmGFP-BDNF expression in NIH 3T3 cell. Green: EmGFP-Math1 (A-F), EGFP (G), EmGFP-BDNF (H); Blue: DAPI. Red: TRITC-phalloidin. Scale bar = 10 μm.

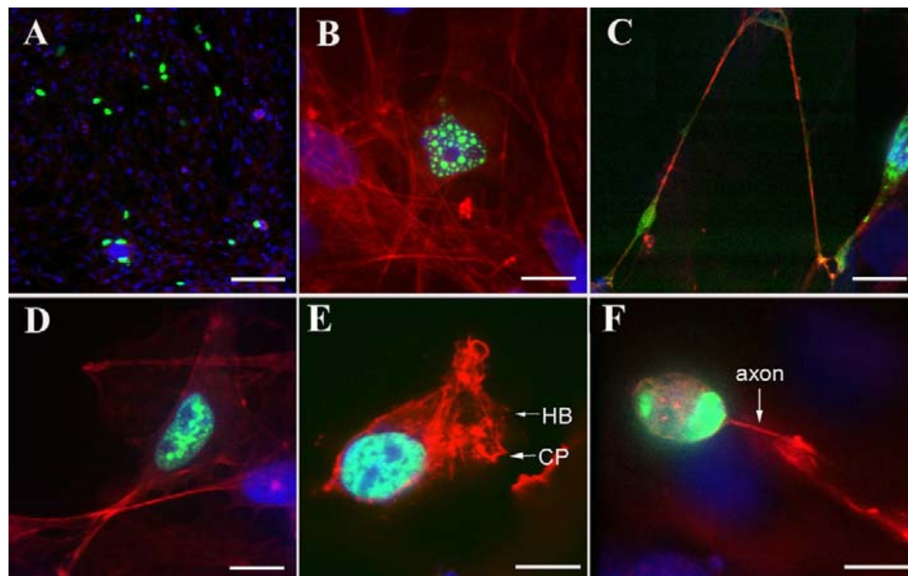

Figure 12. Lipofectamine 2000 mediated transfection of mixed primary cochlear cells by pcDNA6.2/C-EmGFP-Math1 plasmid. A: Lower magnification, transfection efficiency is 2.9%. B, D: fibrocytes. C: In the neuron, EmGFP-Math1 appeared in both the nucleus and axon. E: Outer hair cell-like cell. F: Spiral ganglion cell. Green: EmGFP-Math1; Blue: DAPI; Red: TRITC- phalloidin. HB: hair bundle. CP: cuticular plate. Scale bar = 100 μm (A), 10 μm (B-F).

Subcellular location of the EmGFP-Math1 fusion protein

In most cells, the EmGFP-Math1 fusion protein was primarily localized to the nucleus when transfected by pcDNA6.2/C-EmGFP-Math1 plasmid (Figs. 11A, C, E and F; Figs. 12B and D-F). A unique subcellular localization for EmGFP-Math1 was also observed in certain cell populations: EmGFP-Math1 fusion protein simultaneously appeared in both the nucleus and

cytoplasm (Figs. 11B, D; Fig. 12C). Both cytoplasmic and nuclear EmGFP-Math1 localized to vesicles of varying sizes, with a diameter between 0.4 μm to 2.3 μm (Figs. 11C, D, and F; Fig. 12B). Certain vesicles appeared fused, as both the vesiculated and homogeneous EmGFP-Math1 fusion protein was observed (Fig. 11E). In contrast, NIH 3T3 cells that were transfected with the pCLIG-Math1 plasmid did not show trafficking vesicles, and the EGFP expressed by the pCLIG-Math1 plasmid was localized to the cytoplasm (Fig. 11G). Further, the EmGFP-BDNF fusion protein was localized only to the cytoplasm (Fig. 11H).

MSCs demonstrate a neuronal-like phenotype when transfected with the pcDNA6.2/C-EmGFP-Math1 plasmid

After 10 days of transfection with the pcDNA6.2/C-EmGFP-Math1 plasmid, enhanced volume and polarization were observed in certain MSCs. After two weeks, neuron-like cells with axons and dendrites were observed, while certain cells remained at earlier stages with the appearance of a growth cone. In these cells, the cellular body was spherically shaped (Figs. 13A, B). In the differentiated neuron-like cell, neurofilament was detected, which represents a neural-specific protein (Fig. 13B). In contrast, neither MSCs transfected with the pcDNA6.2/C-EmGFP-CAT plasmid (control plasmid) nor MSCs treated with BDNF and GDNF alone differentiated into neuron-like cells (Figs. 13C, D).

Liposome nanoparticle-mediated Math1 expression in defined cell types

After 24 h of incubation, internalization of TRITC-tagged liposome nanoparticles, LPX-PEG and LPX in NIH 3T3 cells was identified by the appearance of red vesicles in the cytoplasm. Quantitation of the fluorescence intensity showed concentration- dependent internalization of both PEGylated lipoplexes and unPEGylated lipoplexes ($p < 0.05$). However, no significant difference was observed between pegylated lipoplexes and unPEGylated lipoplexes when cells were treated with same concentrations ($p > 0.05$). The EmGFP-Math1 fusion protein was expressed in NIH 3T3 and primary cochlear cells 24 h following transfection (Figs. 13E-H). When the pcDNA6.2/C-EmGFP-Math1 plasmid was delivered with LPX-PEG (PEGylated) and LPX-DOPE (1.2:1) (lipid/plasmid molar charge ratio of 1.2:1) in NIH 3T3 cells, the transfection efficiency was 0.7% and 0.8%, respectively. The two additional lipoplexes, LPX (unPEGylated) and LPX-DOPE (2:1) (lipid/plasmid molar charge ratio of 2:1) showed higher transfection efficiencies 3.8% and 3.6%, respectively. The transfection efficiency of LPX was higher than LPX-PEG. LPX-DOPE (2:1) showed higher transfection efficiency than LPX-DOPE (1.2:1). However, all nanoparticles showed lower transfection efficiencies compared to Lipofectamine 2000.

Subcellular location of the EmGFP-Math1 fusion protein in cells transfected with lipoplexes was similar to cells transfected with Lipofectamine 2000, which was primarily distributed in

the nuclei and sparsely retained within the cytoplasm. Vesicles of various sizes, with diameters between 0.4 µm to 3 µm, appeared in these cells (Figs. 13E, F), and several were fused (Fig. 13E). Vesicles were also observed in both the nucleus and cytoplasm (Fig. 13F).

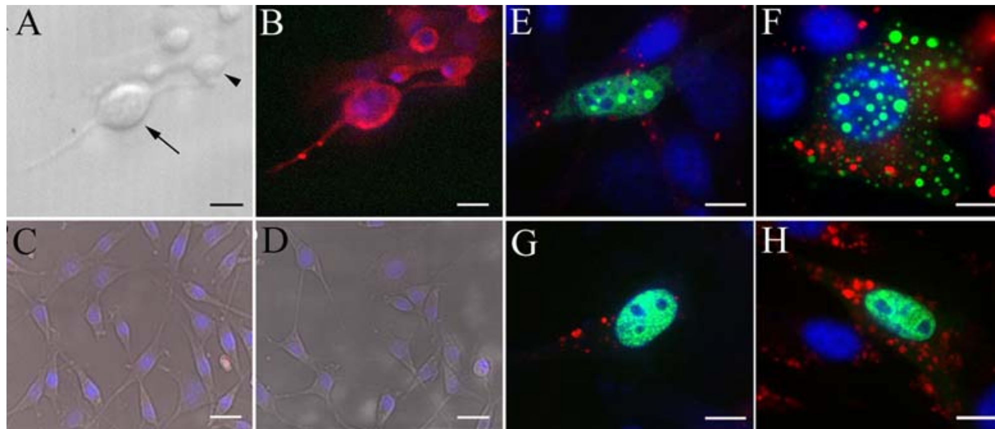

Figure 13. Neuron-like cell differentiation of MSCs transfected with pcDNA6.2/C-EmGFP-Math1 plasmid and liposome nanoparticles mediated transfection of the pcDNA6.2/C-EmGFP-Math1 plasmid**.** A: Bright field image of B. B: Neuron-like cells stained with neurofilament. C: MSCs treated with 10 ng /ml BDNF and 10 ng /ml GDNF alone for two weeks. D: MSCs were transfected with pcDNA6.2/C-EmGFP-CAT plasmid plus treatment with BDNF and GDNF for two weeks. No neurofilament-positive cells were detected in C and D. Liposome nanoparticles mediated transfection of the pcDNA6.2/C-EmGFP-Math1 plasmid in NIH 3T3 cells (E, F: transfection with unPEGylated LPX. H: transfection with PEGylated LPX-PEG), primary cochlear cell (G: transfection with unPEGylated LPX). Arrow heads: unipolar cell indicates neuron-oriented differentiation; Arrow: bipolar shape of the neuron-like cell. Green: EmGFP-Math1; Red: neurofilament (B), liposome nanoparticles (E-H). Blue: DAPI; Scale bars (A-D) = 25µm, (E-H) = 7.5 µm.

5. 5. Internalization of liposome nanoparticles functionalized with the TrkB ligand

Internalization of liposome NPs in primary cochlear cells

Primary cochlea cell culture showed efficient internalization of both A_{371}-functionalized liposome nanoparticles liposome nanoparticles and non-functionalized liposome nanoparticles, which were observed in the primary cochlear cells, including spiral ganglion cells, fibrocytes, and stria vascularis intermediate cells (Fig.15). Cytosolic and perinuclear localization of liposome nanoparticles was observed in different cell types. Internalization differences for liposome nanoparticles were not statistically significant between A_{371}-functionalized liposome nanoparticles and non-functionalized liposome nanoparticles ($p>0.5$). The lipoplex signal intensity was significantly dependent on the lipoplex concentration in the medium ($p<0.01$).

Lipoplex internalization and GFP expression in cochlear explants

Dynamic uptake of liposome nanoparticles in both neurofilaments and spiral ganglion cells was observed, with liposome nanoparticles accumulating in the spiral ganglion satellite cells and gradually appearing on the neurofilament and in the spiral ganglion cells (Fig.14). Abundant distribution of liposome nanoparticles with and without functional TrkB peptides was observed in the neurofilament (Fig.14). Internalization differences for liposome nanoparticles was not statistically significant between A_{371}-functionalized liposome nanoparticles and non-functionalized liposome nanoparticles ($p>0.5$). Likely aggregated EGFP expression was observed in the explants on day 2 post-treatment with A_{371}-functionalized liposome nanoparticles carrying the pGeneClip^{TM} hMGFP plasmid DNA encoding shRNA to transiently silence Id2. More EGFP expression was detected on day 4 post-treatment. EGFP expression was also detected in the explants on day 4 post-treatment with non-functionalized liposome nanoparticles carrying the same plasmid DNA as the A_{371}-functionalized liposome nanoparticles.

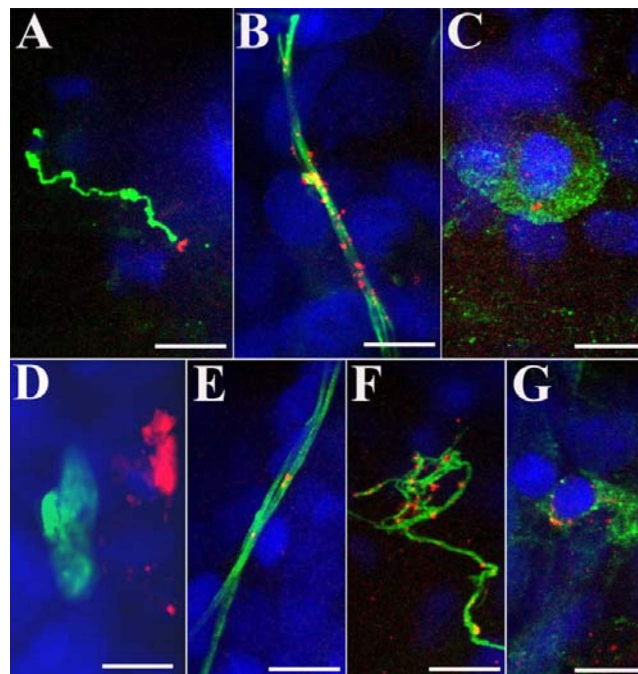

Figure.14. Confocal microscopy showing the internalization of liposome nanoparticles in rat cochlear explants. A_{371}-functionalized liposome nanoparticles carrying plasmid pGeneClip^{TM} hMGFP DNA appeared adjacent to neurofilaments at 1 h post-treatment (A), abundantly attached to neurofilaments at 2h post treatment (B), and distributed in the spiral ganglion cells at 2 h post-treatment (C). Two days post-gene delivery with A_{371}-functionalized liposome nanoparticles carrying plasmid pGeneClip^{TM} hMGFP DNA, Likely EGFP expression was seen in cells (D). Non-functionalized liposome nanoparticles carrying plasmid pGeneClip^{TM} hMGFP DNA attached to neurofilaments (E) at 1 h post-treatment; greatly accumulated on neurofilament (F) and within spiral ganglion cells (G) at 2 h post treatment. Red: liposome nanoparticles; Green: neurofilaments (A-C and E-F), GFP (D); Blue: DAPI. Scale bar =10 µm.

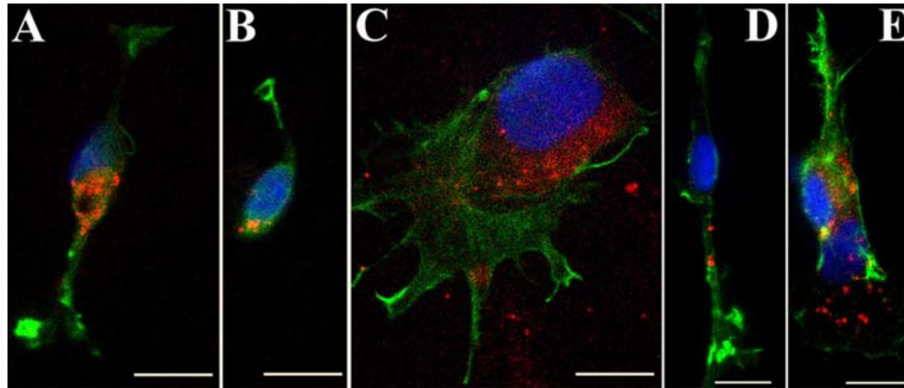

Figure 15. Confocal microscopy showing the internalization of liposome nanoparticles in primary rat cochlear cell cultures. For A371-functionalized liposome nanoparticles without plasmid DNA, efficient uptake was observed in the cytoplasmic and perinuclear regions of type I (A) and type II (B) spiral ganglion cells and stria intermediate cells (C). For the non-functionalized liposome nanoparticles without plasmid DNA, efficient internalization occurred in spiral ganglion cells (D) and fibrocytes (E). Red: liposome nanoparticles; Green: FITC-conjugated phalloidin; Blue: DAPI. Scale bar=10 µm.

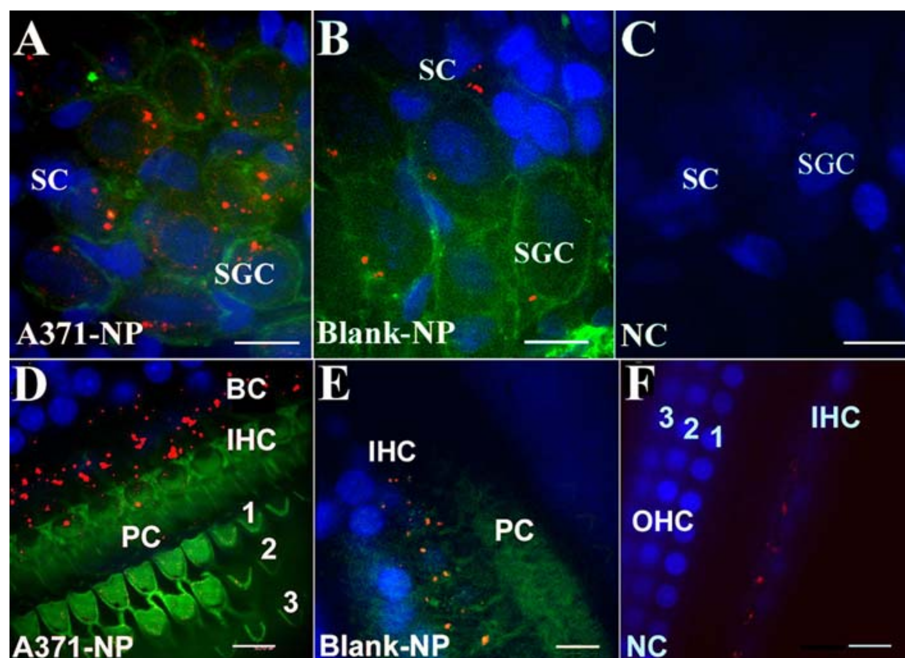

Figure 16. Confocal microscopy showing the distribution of liposome nanoparticles in the spiral ganglion region and hair cell region of the rat cochlea at 24 h post-RWM permeation. Abundant A_{371}-functionalized liposome nanoparticles were detected in the spiral ganglion cells (A) and inner hair cells and adjacent supporting cells (D). After treatment with non-functionalized liposome nanoparticles, fewer liposome nanoparticles appeared in the SGCs (B) and inner hair cells (E). Few liposome nanoparticles were detected in the pillar cells (D and E). In the untreated controls, faint red autofluorescence was also detected in SGCs (C) and the inner hair cells (F). Red: liposome nanoparticles; Green: FITC-conjugated phalloidin; Blue: DAPI. NC: untreated control; SC: satellite cell; SGC: spiral ganglion cell. BC: border cells; IHC: inner hair cell; PC: pillar cell. Scale bar =10 µm.

Lipoplex distribution in cochlear cell populations after round window membrane permeation

In the adult rat cochleae receiving round window membrane permeation with A_{371}-functionalized liposome nanoparticles, greater particle distribution was observed in the spiral ganglion region than in cochleae treated with non-functionalized liposome nanoparticles (Figs.16A, B). This difference was not statistically significant, which likely due to the small sample size ($p>0.05$) (Fig. 17). No EGFP expression was detected in the spiral ganglion cell and spiral ganglion satellite cells with lipoplex internalization. In the inner hair cell region, there was significantly greater uptake of functionalized liposome nanoparticles than non-functionalized liposome nanoparticles ($p<0.05$) (Figs. 16D, E and Fig.17). Lipoplex uptake was also observed in the lateral wall, including the spiral ligament and stria vascularis, but was not significantly different between the functionalized and non-functionalized liposome nanoparticles ($p>0.05$) (Fig.17). No uptake was detected in the outer hair cell region for cochleae treated with either A_{371}-functionalized liposome nanoparticles or non-functionalized liposome nanoparticles (Fig. 16).

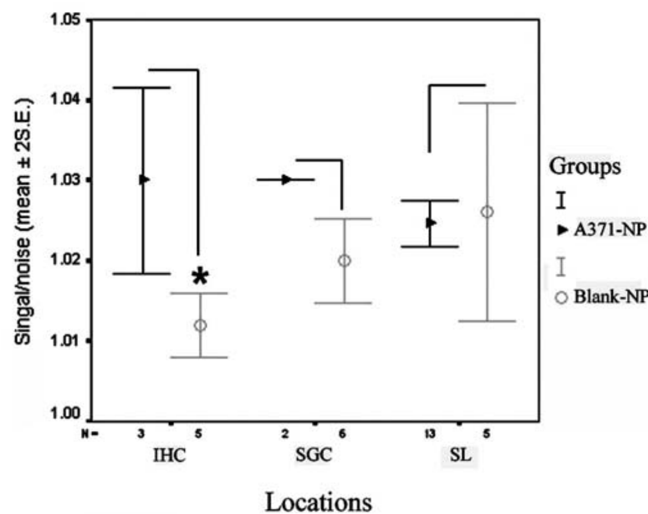

Figure 17. Quantification of the lipoplexes distribution in different cell populations of adult rat cochleae at 24h post-round window membrane permeation. There was a significantly greater distribution of A_{371}-functionalized liposome nanoparticles compared to non-functionalized liposome nanoparticles in the inner hair cells. There was also a tendency toward enhanced distribution of A_{371}-functionalized liposome nanoparticles compared to non-functionalized liposome nanoparticles in the spiral ganglion cells. There was no difference in the nanoplex distribution in the spiral ligament of the lateral wall. IHC: inner hair cell; SGC: spiral ganglion cell; SL: spiral ligament.

6. DISCUSSION

6. 1. Difference in gadolinium permeability of perilymphatic and endolymphatic barriers and indication for diagnosis

This experiment is the first to show MR imaging with visualization of uptake of Gd-DOTA administered by IV or IT routes in the perilymph of the mouse. Gd-DOTA administered intratympanically passed through the round window membrane efficiently and appeared in the perilymphatic spaces of the cochlea and vestibule but not in the endolymphatic spaces. This finding is in agreement with previous MRI results from the inner ears of guinea pigs and humans (Zou et al., 2009; Zou et al., 2005a). High resolution visualisation of the contrast-enhanced perilymphatic space allows for some investigation into the process by which contrast material may pass through the round window membrane into the inner ear. High resolution scanning with the 4.7 T machine revealed some details of the soft tissues within the lateral wall of the cochlea. A dark border was revealed between ST and LW in the basal turn near the hook region. This structure might represent the tissues that did not pass Gd-DOTA such as the stria vascularis and the twisted basilar membrane near the hook region. However, this appearance needs to be elucidated in further studies.

The intravenous administration of Gd-DOTA demonstrated passage through the blood-perilymph barrier, but not through the blood-endolymph barrier, which is also consistent with results in guinea pigs and humans (Counter et al., 2003; Counter et al., 2000; Zou et al., 2009). The dynamic uptake of Gd-DOTA into the perilymph of the mouse and humans has been seen to occur more slowly than in the guinea pig. It is possible that there is some structurally based regulation of this uptake and that these results reflect the closer genetic similarities between the mouse and humans. In addition to the cochlear glomeruli of Schwalbe within the modiolus, saccular capillaries and capillaries in the spiral limbus may contribute to the uptake of Gd-DOTA in the mouse perilymph (Franz et al., 1993). In humans, injury to the inner ear appeared to accelerate the rate of gadolinium uptake into the perilymph following IV injection, which indicated a possible change in the regulation of the blood-perilymph barrier (Zou et al., 2009).

Some slight differences were observed in the uptake of Gd-DOTA within the lateral wall and modiolus between IV and IT administrations. One of the differences was that the IT delivered Gd-DOTA may more efficiently pass into the ‘‘perimodiolar lymph”, it could indicate that the barrier between the scala tympani and the modiolus is more porous than the potential IV route of passage through the cochlear glomeruli of Schwalbe within the modiolus. The second difference was that more Gd-DOTA accessed to the lateral wall after IT administration than IV approach suggested a more efficient transport from round window membrane to the spiral

ligament extracellular space than from the local capillaries to the extracellular space. A difference in efficiency of passage of Gd-DOTA into the modiolus and lateral wall would raise the possibility that drug delivery to these areas of the cochlea might be similarly favored by IT route. There are other potential advantages of IT administration over IV. IT treatment is likely to cause less systemic effects because of its local administration and lower dose requirement. The total dose of Gd-DOTA required for visualisation of the inner ear using the IT route was significantly less than IV administration, with Gd-DOTA maximum 0.014 mmol/kg for IT versus 1.5 mmol/kg for IV.

In principle, IV administration of Gd-DOTA might be used to investigate the integrity of the stria vascularis, especially the intercellular junctions of strial marginal cells and endothelium of strial capillaries. Interference with the endothelial barrier of the capillaries supplying the stria vascularis, which is a component of the blood-endolymph barrier, has resulted in an intrastrial electric shunt that ablated endocochlear potentials and induced hearing loss (Cohen-Salmon et al., 2007). Rupture of Reissner's membrane has been shown to produce bright signal within the scala media using IV gadolinium (Zou et al., 2003a; Zou et al., 2003b). This disruption of the endo-perilymph barrier caused a mixing of endolymph with perilymph and eliminated endocochlear potentials (Jin et al., 1990).

6. 2. POA@SPION are a "super" MR contrast agent for inner ear imaging

The inner ear endolymph and perilymph of the cochlea and vestibular organ where most of the nanoparticles should appear are known to generate very bright signals on T2-weighted images (Counter et al., 2003; Counter et al., 1999). POA@SPIONs was demonstrated to be an efficient T2 contrast agent within the rat inner ear. When infused into the perilymph, there was a consistent dramatic reduction of signal intensity on T2-weighted images compared with the persisting bright signal of the endolymph, which did not take up POA@SPIONs and lacked the negative contrast effect. These results support previous work that POA@SPIONs is a potent T2 negative contrast agent in vivo(Qin et al., 2007). POA@SPION, when introduced into the perilymph compartment, caused a marked suppression of T2 signal that produced the effect of showing the endolymphatic compartment as a bright, isolated structure. It is apparent that significant amounts of POA@SPIONs did not pass through the perilymph–endolymph barrier into the endolymph, resulting in a remarkable opportunity to observe the isolated endolymphatic space with bright T2 signal compared with the darkened perilymph, which contained POA@SPIONs. It suggests the potential for studying the integrity of the perilymph-endolymph barriers, such as Reissner's membrane, which might be injured during acute endolymphatic hydrops or impulse noise exposure (Flock et al., 2003; Fraysse et al., 1980; Konishi et al., 1982; Valk et al., 2006; Zou et al., 2003b).

Intracochlear delivery of nanoparticles to investigate their distribution as potential drug or gene carriers has been reported by workers in the Nanoear consortium (Scheper et al., 2009; www.nanoear.org/, 2009). Although the IC administration of POA@SPIONs is an invasive procedure, not suitable for an office setting, it may be applied clinically as a diagnostic or therapeutic agent in the future, perhaps in conjunction with cochlear implantation. Therefore, the information acquired from IC delivery is important both in present animal studies to track nanoparticles through the cochlea and to plan for future clinic work with cochlear implants. POA@SPIONs have demonstrated sufficient contrast effects and IC distribution to justify their further development as a label to trace the passage of drugs, genes, and nanoparticles within the inner ear *in vivo*. Application of therapy into the middle ear which is a minimally invasive approach would be favorable for use in the out-patient clinic, but probably depend upon passage through the middle-inner ear barriers (round window and oval window) in order to access the inner ear. It has been reported that positively enhancing T1 MRI contrast agents, gadolinium chelates, have excellent passage through the middle–inner ear barriers after IT administration in guinea pigs (Zou et al., 2009; Zou et al., 2005a), rats (Zou et al., 2010) and humans (Zou et al., 2009; Zou et al., 2005a). However, the longitudinal relaxivity (r1) of gadolinium chelates decreases rapidly at high field strengths, reducing the sensitivity of these contrast agents at high field (Sosnovik et al., 2008). Besides, Gadolinium is not practical in molecular imaging, which requires high magnetic field strength. Finally, a high concentration of gadolinium was reported to be ototoxic in a preliminary study (Kakigi et al., 2008). The permeation of nanoparticles through the middle-inner ear barriers of the rat has been observed with lipid nanocapusules (Zou et al., 2008). Nanoparticles that would be detectable with MRI would provide an excellent means to evaluate the efficacy of their transport through the middle-inner ear barriers *in vivo*. Although the passage of naked POA@SPIONs through the middle-inner ear barriers was inefficient in this study, it is possible that if they were to be downsized or manufactured with altered surface characteristics (charge and ligands) similar to other nanoparticles, POA@SPIONs may penetrate the middle-inner ear barriers more efficiently in future studies (www.nanoear.org/, 2009).

The IV route is another desirable approach to introduce contrast agents that may be taken up into the perilymph or endolymph under normal or pathological circumstances. Gadolinium has been shown to enhance the perilymphatic space in T1 MR images after IV injection (Counter et al., 2003; Counter et al., 1999). The integrity of the blood-perilymph and blood-endolymph barriers, which are critical for the proper functioning of inner ear physiology, can be studied with contrast agents. These barriers may become 'leaky' when injured and their integrity could be evaluated with the use of contrast imaging agents that do not normally pass through. As an example, changes in the blood-perilymph barrier or blood-endolymph barrier permeability to gadolinium have been observed in MRI (Counter et al., 2000; Mark et al., 1992). POA@SPIONs delivered intravenously did not produce detectable signal changes within the inner ear, suggesting that neither the blood-perilymph barrier nor blood–

endolymph barrier were permeable to them. Their larger particle size and differences in surface properties, in comparison to Gd-DOTA, likely contribute to the difficulties in transport through the blood-perilymph barrier. The doses of gadolinium that have been employed for IV use have been in excess of those typically given in clinical circumstances (Counter et al., 1999; Zou et al., 2009). There are concerns that high doses of IV gadolinium might increase the risk of adverse effects, such as nephrogenic systemic fibrosis (High et al., 2007; Thakral et al., 2009). However, the potential for toxicity from SPIONs can be limited by manipulating the polymer/iron mass ratio (Mahmoudi et al., 2009b). The concentration of $Fe3^{+}$ in POA@SPIONs (4.3–5.6 mM) is far below the maximum levels previously tested and no toxicity has yet been demonstrated at any concentrations (Mahmoudi et al., 2009a). As opposed to gadolinium, SPIONs do not lose T2 contrast effects at higher Tesla strengths. For all of these reasons, POA@SPIONs remains an important contrast agent that should be studied as an alternative to gadolinium. By conjugating with different ligands, POA@SPIONs may be developed that will penetrate the different inner ear barriers and that may serve as a molecule-specific contrast agent to detect pathologic molecular expression within the inner ear of proteins such as TNF- alpha and VEGF (Zou et al., 2005b).

6. 3. Nuclear entry of HPNPs into the cochlear cells

The success of nonviral gene therapy has been largely limited by inefficient gene delivery to cochlear cells due to the nuclear envelope barrier. Our primary intention in this study was to demonstrate the potential for HPNPs as carriers to deliver genes to cochlear cell nuclei. Although it has been discovered that nanoparticles can enter the cytoplasm of cochlear cells, nuclear delivery remains problematic (Scheper et al., 2009; Zou et al., 2008). HPNPs were detected in both cochlear cell cytoplasm and nuclei in primary cell culture, in organotypic culture, and *in vivo* via intratympanic administration. The results herein contrast the results of an *in vivo* study performed in guinea pigs using hyperbranched polylysine nanoparticles (Scheper et al., 2009). A likely explanation is that the HPNP's nuclear entry is concentration-dependent; in the *in vivo* study, cochlear cells were exposed to much lower HPNP concentrations than *in vitro*. The cells that are integrated into the organ may behave differently than individual cells. Nuclear localization of HPNPs was intense in rat round window membrane cells but was rarely observed in cochlear cells. The different HPNP delivery methods and the biological differences between rats and guinea pigs should also be considered as explanations for the results.

Concentration-dependent toxicity was observed in the primary cochlear cell culture, and most of the cells died when treated with concentrations greater than 3.87×10^{-7} mol/L. Spiral ganglion cells died when treated with HPNPs at 9.7×10^{-8} mol/L. This finding indicates that spiral ganglion cells might be more vulnerable to HPNP treatment as neurons are highly

sensitive to hazardous substance exposure. In primary cochlear cells incubated with higher HPNP concentrations, homogenous nuclear staining with propidium iodide indicated cell death. No permeation of propidium iodide was detected in the nuclei when the cochlear cells were treated with HPNPs at concentrations less than 3.87 x 10^{-7} mol/L, verifying the viability of these cells. Furthermore, the nuclear distribution of HPNP vesicles indicated the active transport of HPNP into living cells. It should also be pointed out that HPNP-containing vesicles are only detectable in living cells, as passive diffusion of HPNPs into the nuclei following cell death would not generate HPNP-containing vesicles but would show a homogenous distribution. As a result, HPNP nuclear entry was a meaningful biological process instead of a consequence of cell death.

There are several potential mechanisms behind HPNP-mediated gene transfection's greater efficiency than liposomes. First, HPNPs can condense DNA into a relatively smaller size than cationic liposomes, which is crucial for gene transfer. Second, HPNPs have a better ability to mediate endosomal escape than liposomes via the "proton sponge" hypothesis (Boussif et al. 1995). Finally, HPNPs transport the plasmid into the nucleus directly and induce high transfection efficiency, as the nuclear localization of HPNPs is observed. However, it could not be excluded that, as mentioned in the review, HPNPs may aid in the nuclear import of DNA via other indirect mechanisms, including enhanced DNA protection and cytoplasmic mobility.

Regarding the mechanism of nuclear import, there are several potential pathways. Nuclear localization signal (NLS)-mediated nuclear transport of HPNPs is a potential mechanism (Berry et al., 2007; Tkachenko et al., 2003). NLS-mediated nuclear transport requires certain cytosolic factors and ATP (Adam et al., 1990; Cserpan et al., 1995). Although the nuclear pore complex (NPC) can only transport macromolecules with diameters of up to 39 nm (Pante et al., 2002), the PDI of HPNPs is large (PDI = 1.9), which means that a certain amount of HPNPs have sizes less than 39 nm. Conformational change is expected in HPNPs with sizes greater than 39 nm, which is different from the solid rigid gold nanoparticles that were employed to investigate nuclear pore complex transportation (Pante et al., 2002).

In addition, HPNPs may also enter the nucleus through other unknown NPC-independent mechanisms. Robert's work proved that large size (122 nm-203 nm) polyplexes could also enter the nucleus (Carlisle et al., 2001). He inhibited nuclear pore function by co-microinjection of wheat germ agglutinin (WGA). The failure of WGA to inhibit PEI/DNA complexes suggests that PEI/DNA may enter the nuclei of cells through an NPC-independent mechanism. One such potential mechanism by which HPNPs mediate nuclear entry may be that they are internalized and transported into the nucleus via nucleolin binding. Nucleolin is a ubiquitous eukaryotic protein that is conserved from yeast to mammals and is found in the nucleoli and nucleoplasm, as well as on the cell surface (Ginisty et al., 1999; Mongelard et al.,

2007). Nucleolin is able to shuttle between the plasma membrane, and cytoplasm, as well as the nucleus, and it regulates many aspects of DNA and RNA metabolism (Ginisty et al., 1999; Srivastava et al., 1999). It has been reported that nucleolin is the cell surface target of DNA nanoparticles and that nucleolin is essential for the internalization and/or transport of the DNA nanoparticle from the cell surface into the nucleus (Chen et al., 2008). This process was also indicated in our study, as demonstrated by the HPNP vesicle pathway from the cytoplasm towards nucleolin-positive nucleolus. A recent report showed that the nucleolin-mediated cellular trafficking of DNA nanoparticles is lipid raft- and microtubule-dependent and can be modulated by glucocorticoid (Chen et al., 2010). Another potential NPC-independent mechanism for HPNP nuclear internalization in cochlear cells is nuclear envelope penetration or fusion (Godbey et al., 1999a; Godbey et al., 1999b; Verma et al., 2010). It is possible that the internalized cytoplasmic HPNPs are retained and tethered to the inner surface of the vesicles and, thereafter, are transported into the nuclei by molecular machines (such as dyneins) along cytoskeletal tracks (Godbey et al., 1999a; Godbey et al., 1999b; Verma et al., 2010).

Finally, HPNP internalization by cochlear cells was not specific for a cell population. This finding did not meet our goal of targeted gene delivery into the cochlea. However, HPNP functionalization with peptides specific for a definite cellular cochlear population may introduce the targetability of these nanoparticles. Herein, in the present studt, potential targetability with TrkB affinity peptide-functionalized liposome nanoparticles was observed in the spiral ganglion and inner hair cell regions of adult rat cochleae. Additionally, validating results were observed by our NanoEar project partner in spiral ganglion neurons using PEG-PCL polysome nanoparticles functionalized with the same peptide (Roy et al., 2010). HPNPs can also be included in other nanoparticles to achieve both ideal targetability and efficient gene expression.

6. 4. Importance of nuclear localization of Math1 in transcription

PCR amplification, gene sequencing, and Western blot analysis confirmed the structure, integrity, and gene expression capacity of the newly constructed plasmid pcDNA6.2/C-EmGFP-Math1. Using Lipofectamine, this novel pcDNA6.2/C-EmGFP-Math1 plasmid induced significantly higher transfection efficiencies than the pCLIG-Math1 plasmid, which was developed using the Moloney murine leukemia virus. An additional advantage of pcDNA6.2/C-EmGFP-Math1 is that EmGFP is fused to the Math1 protein, thus, it is possible to observe subcellular localization of the EmGFP-tagged Math1 protein. Furthermore, mutations have been introduced into GFP that further enhance and shift its spectral properties such that they emit vivid emerald fluorescence, thus, GFP is easier to visualize.

Several cell types, including NIH 3T3 cells, MSCs, and primary cochlear cells, showed efficient transfection of the pcDNA6.2/C-EmGFP-Math1 plasmid using lipofectamine. In addition, NIH 3T3 and primary cochlear cells were successfully transfected with the pcDNA6.2/C-EmGFP-Math1 plasmid using liposome nanoparticles. This result proved that the new Math1 plasmid is valuable for non-viral-vector-mediated Math1 gene delivery. NIH 3T3 cells demonstrated the highest transfection efficiency among all cell types tested, using either lipofectamine or liposome nanoparticles. There is important significance in using autologous fibroblasts for the cell replacement deafness treatment mediated by Oct3/4, Sox2, c-Myc, Klf4, and Math1 (Oshima et al., 2010; Takahashi et al., 2006). Poor transfection efficiencies in primary cochlear cells, compared with other cell types, can be explained by cell cycle-correlated gene transfection efficiency, in which the more differentiated the cell is, the worse the transfection efficiency is for gene delivery. Usually, non-dividing cells are more difficult to transfect than dividing cells, and this can be attributed to the absence of mitotic activity in non-dividing cells. In dividing cells, DNA is passively transported into the nucleus during the M-phase in cell division, during which the nuclear membrane temporarily disintegrates (Tseng et al., 1999). For non-dividing cells, the presence of an intact nuclear membrane limits the entry of pDNA into the nucleus. The mechanism of pDNA cyto-nucleoplasmic transport into non-dividing cells is likely a process mediated by the interaction of soluble cytoplasmic factors with minimal nuclear transport machinery (Munkonge et al., 2009).

A unique subcellular localization of EmGFP-fused Math1 was observed in the transfected cells. In certain cells, EmGFP-Math1 fusion proteins were detected in both the nuclei and cytoplasm. Their multiple locations within a single cell suggest that Math1 proteins are transported from the cytoplasm to the nucleus. In the majority of the cells, EmGFP-Math1 fusion proteins appeared in the nucleus, suggesting that the cytoplasmic-nuclear transport event was rapid. This observation strongly supports the fusion of EmGFP onto Math1 does not disrupt Math1 intracellular trafficking. We cannot confirm whether EmGFP-Math1 enters the neucleus through the nuclear pore complex. However, the fact that EmGFP-Math1 fusion proteins were encapsulated into the vesicles was in accordance with the nuclear transport mechanism of vesicle fusion events (Zuleger et al., 2008). The simultaneous appearance of vesiculated and homogeneous EmGFP-Math1 fusion proteins in the same nuclei demonstrated the process of vesicle fusion events. Therefore, promoting vesicle fusion may be important in realizing the function of each Math1 molecule. Likely, Ca2+ and inositol 1, 4, 5-trisphosphate (IP3) receptors contribute to this effort (Sullivan et al., 1993).

It has been reported that Math1-fused GFP induces the development of hindbrain neurons in mice (Rose et al., 2009). EmGFP fusing to the C-terminal end of Math1 should not disrupt the interaction between Math1 and chromosomal E-box, at the N-terminal end of Math1. We were unable to evaluate the binding efficacy of the Math1 protein to the chromosomal E-box

directly, although it is a critical step in Math1 transcription. Our observation that MSCs differentiated into neural progenitor cells and then into neuron-like cells, following treatment with BDNF and GDNF, further supported a preserved transcription function for EmGFP-fused Math1. It has been reported that the role of Math1 protein in these sequential events is to direct neural progenitor differentiation (Flora et al., 2007). The maturation of the differentiated neural progenitor is maintained by BDNF and GDNF treatment, which induces neural cone growth (Anderson et al., 2006). Although neural-oriented differentiation of MSCs without Math1 stimulation has been reported, agents other than BDNF and/or GDNF (such as retinoid acid and β - mercaptoethanol) have been added to the cell culture medium (Sanchez-Ramos, 2002). However, BDNF and GDNF do not necessarily induce MSC differentiation alone, and the role for Math1 has not been diproved in our study. MSCs are a source of progenitors for inner ear hair cells in cell replacement treatment (Jeon et al., 2007). The modification of MSCs with Math1, BDNF, and GDNF using a non-viral gene delivery technique may be applied in future therapies for deafness.

Liposome nanoparticles are a beneficial application of *in vivo* gene therapy. However, the transfection efficiency of pcDNA6.2/C-EmGFP-Math1 plasmid mediated by liposome nanoparticles was lower than commercial Lipofectamine-mediated transfection. The following four characteristics should be considered: “endosomal escaping”, nanoparticle size, the surface charge of the nanoparticles, and the PEGylation effect in the medium. Endocytosis has been reported to be the major pathway of lipoplex internalization (Elouahabi et al., 2005; Rejman et al., 2006). The endosomal escape function, or ability to release DNA into the cytoplasm, is one of the key steps in the intracellular delivery of DNA by nonviral vectors (Cotten et al., 1992). The tested lipoplexes likely lacked the “endosomal escaping” capacity. If the pcDNA6.2/C-EmGFP-Math1 plasmid cannot be released into the cytoplasm by breaking the endosomal membrane, then it may be diretced to lysosomes where DNA is destroyed before executing its function. Lipoplex size was reported to be a major factor influencing *in vitro* lipofection efficiency (Almofti et al., 2003; Ross et al., 1999). Lipoplex size plays a key role in gene transfer to actively endocytosising cells (Rejman et al., 2006; Ross et al., 1999). Our results showed that a 255 nm lipoplex has higher transfection efficiency than other lipoplex sizes. This finding is consistent with previous reports showing that optimal transfection efficiencies are obtained *in vitro* with lipoplexes 200 – 400 nm in size (Ma et al., 2007; Zhdanov et al., 2002). The relatively large lipoplexes induce higher transfection efficiencies, as the larger size facilitates membrane contact and fusion (Escriou et al., 1998). Furthermore, larger lipoplexes may delay DNA dissociation from the lipid, thereby enhancing DNA transfection efficiency (Lian et al., 2003).
The surface charge of the lipoplexes is also an important parameter that can influence transfection efficiency (Ma et al., 2007). It has been reported that by increasing the lipid/DNA charge ratio, the lipoplex size decreases and it becomes more stable (Simberg et al., 2004). The size and stability of the lipoplexes depend on the cationic lipid/DNA charge ratio used in

lipoplex preparation (Eastman et al., 1997; Radler et al., 1997; Turek et al., 2000). The impact on lipoplex transfection efficiency of the lipid/DNA ratio is realized primarily by influences on lipoplex size and lipoplex stability. LPX-DOPE (2:1) has a higher lipid/DNA molar charge ratio than LPX-DOPE (1.2:1), while the former has a smaller size. In our experiment, the transfection efficiency of LPX-DOPE (2:1) was higher than LPX-DOPE (1.2:1). This result indicates that a lipid/DNA molar charge ratio of 2:1 is favorable for endocytosis and is more stable, which protects the plasmid DNA from degradation by cellular nucleases.

The PEGylation of liposome nanoparticles can protect DNA against degradation by serum, but it also inhibits the transfection capacity (Pedroso de Lima et al., 2001). In our study, unPEGylated LPX showed higher transfection efficiency than PEGylated LPX-PEG, which was inconsistent with a previous report (Kwon et al., 2010). PEGylation affects transfection efficiency by adversely interacting with the intracellular trafficking of nanoparticles (Kwon et al., 2010; Mishra et al., 2004). However, a recent report showed that lipoplex PEGylation did not hamper internalization but did interfered with the intracellular release of DNA from lipoplexes (Jellema et al., 2010). No difference in internalization was observed between PEGylated and unPEGylated lipoplexes in our study, supporting the second hypothesis. Our results indicate that PEGylation affects the release of DNA but not the internalization of nanoparticles.

6. 5. Targetability of TrkB ligand-functionalized liposome nanoparticles

In primary cochlear cell culture and explants, no cell type-specific internalization of A_{371}-functionalized liposome nanoparticles was observed. The uptake of non-functionalized liposome nanoparticles in the cochlear cells was as efficient as A_{371}-functionalized liposome nanoparticles. This finding indicates that the TrkB receptor pathway is not involved in the internalization of liposome nanoparticles in spiral ganglion cells, although TrkB internalization occurs upon binding to BDNF. There are two possible explanations for the different behavior of A_{371} peptide-functionalized liposome nanoparticles and BDNF in spiral ganglion cells. First, as a modification of the natural sequence of amino acids 8_4-100 from the structure of NGF, A_{371} does not have the full functionality of either NGF or BDNF. Second, coupling the peptide to liposome nanoparticles significantly increases the size of A_{371}, such that it is much larger than BDNF and NGF. The large size of A_{371}-coupled liposome nanoparticles may prevent internalization of TrkB upon binding. As they were equally exposed to the liposome nanoparticles, every cell population displayed the same amount of internalization.

For the *in vivo* study, the relative accumulation of A_{371}-functionalized liposome nanoparticles in the spiral ganglion and inner hair cell regions was the result of targeting. In our previous

study, we observed the round window membrane permeation of lipid nanocapsules PEGylated with DSPE-PEG- 2000, the same coating material used for liposome nanoparticles herein. In the earlier study, we showed that the nanocapsules primarily appeared in the spiral ganglion region, correlated nerve fibers, the inner hair cell region, and the spiral ligaments of the lateral wall (Zou et al., 2008). Thus, there is a greater chance that the cells and tissues in these regions were exposed to nanoparticles upon round window membrane permeation. In the case of A_{371}-functionalized liposome nanoparticles, affinity for TrkB at the surface of spiral ganglion cells and neuron peripheral processes enhanced the distribution of the liposome nanoparticles in the spiral ganglion and inner hair cell regions (Tan et al., 2006). We propose the following mechanism for lipoplex distribution: after permeating the porous modiolar wall of the scala tympani, A_{371}-functionalized liposome nanoparticles bind to TrkB on non-myelinated type II spiral ganglion cells and certain peripheral processes, and the level of liposome nanoparticles along the nerve pathway was enhanced (Rask-Andersen et al., 2006; Zou et al., 2008). This process supplies more liposome nanoparticles to the inner hair cell region (Zou et al., 2008). Movement of liposome nanoparticles along nerve fibers was demonstrated in the cochlear explant study, which showed that an abundance of liposome nanoparticles were attached to neurofilaments. The access of nanoparticles to the lateral cochlear wall was directly related to the round window membrane and perilymph and was not limited by the nerve pathway (Zou et al., 2008). Therefore, internalization of non-functionalized liposome nanoparticles in spiral ligament fibrocytes and lateral wall intermediate cells was as efficient as that of A_{371}-functionalized liposome nanoparticles.

In the cells successfully transfected by liposome nanoparticles, pGeneClipTM hMGFP plasmid DNA encoding shRNA transiently silenced Id_2 in the host cells. Id_2 (E47 protein) is reportedly involved in cell survival, cell cycle progression, lipid metabolism, stress response, and lymphoid maturation (Schwartz et al., 2006). The poor gene transfection efficiency of liposome nanoparticles can be attributed to the absence of mitotic activity in most cochlear cell populations during the gene transfer process. Many studies have confirmed that, in cells with non-viral vector-mediated cytoplasmic plasmid delivery, only those cells with evidence of nuclear plasmid localization showed efficient transgene expression (James et al., 2000; Tachibana et al., 2002). Typically, transfection efficiency is facilitated in dividing cell populations, wherein the nuclear envelope disassembles during mitosis, thus largely eliminating this barrier. For non-dividing cochlear cells, the intact nuclear membrane limits the nuclear entry of the cytoplasmic plasmid delivered by liposome nanoparticles. Poor gene transfection efficiency for liposome nanoparticles might be resolved by using nuclear localization signal peptides. Furthermore, efficient internalization of hyperbranched polylysine nanoparticles was observed in both the cochlear cell cytoplasm and the nuclei of cochlear cell culture, cochlear organotypic culture, and *in vivo*. Thus, nuclear gene delivery induced by hyperbranched polylysine nanoparticles is also an option for improving transgene expression in *in vivo*.

7. SUMMARY AND CONCLUSIONS

The summary and conclusions to be drawn from the main findings in the present studies are as follows:

1. Contrast agent MRI is capable of discerning fine structures of the inner ear and inner ear barrier function in mice. The normal blood-endolymph barrier is tighter than the blood-perilymph barrier. This finding can be applied to future investigations into the pathological mechanisms for SNHL in different etiologies in mouse models. POA@SPIONs are a promising T2 negative contrast agent that is detectable within the rat inner ear by MRI. Normal blood-perilymph, blood-endolymph, and perilymph-endolymph barriesr restrict the passage of POA@SPIONs. Novel POA@SPIONs may be further surface modified by peptides or antibodies to increase their use as diagnostic agents and traceable therapeutic nanoparticle in SNHL molecular imaging.

2. HPNPs were efficiently internalized by the cochlear cells in primary cell culture, in organotypic culture, and *in vivo*. Both the cytoplasm and nucleus showed HPNP distribution This finding suggests that HPNPs have a potential use in gene delivery to the cochlea.

3. Plasmid pcDNA6.2/C-EmGFP-Math1 is suitable for non-viral gene delivery of Math1. Unique intracellular trafficking of Math1 was demonstrated using this novel plasmid. The modification of MSCs by Math1 gene delivery, together with BDNF and GDNF treatment, is an option for cell replacement treatment of cochlear spiral ganglion cell loss in deafness.

4. The potential targetability of TrkB ligand-functionalized liposome nanoparticles was observed in rat cochlea but not in primary cochlear cell culture and cochlear explants. However, gene transfection efficiency mediated by liposome nanoparticles was poor. Further improvement in transfection efficacy and targetability should be realized by nanoparticles functionalized with peptides or antibodies.

8. ACKNOWLEDGEMENTS

This study was carried out at the Department of Otolaryngology, Medical School, University of Tampere, Finland. I wish to express my deepest and sincere gratitude to the head of the Department of Otolaryngology, coordinator of NanoEar project, and my co-supervisor, Professor Ilmari Pyykkö, for the excellent facilities and friendly working environment. I am deeply grateful that he offered me many opportunities to participate in the NanoEar's courses and conferences in Finland and abroad, from which I have both enjoyed and professionally benefitted a lot. His support, guidance, sense of humor, swift decisions, and the occasional gentle push have made all of my work possible.

My deepest and sincere gratitude is also expressed to my supervisor, Docent Jing Zou M.D, PhD. He has taught me scientific thinking and, more importantly, how to bring this thinking from the level of a hypothesis into something that can be tested in the lab and, finally, presented in a scientific journal. I am also grateful for his never-ending enthusiasm towards my projects, encouragement, patience, and the motivating discussions that we have had during these years. His meticulous scholarship, which is, to me, worthy of emulation, will benefit me for lifetime.

I am deeply grateful to the members of my thesis committee, Professor Seppo Parkkila and Professor Dennis Poe for their advice, support and discussions during my thesis project. I sincerely thank my reviewers Docent Maija Vihinen-Ranta and Docent Petri Mattila for their valuable suggestions and positive comments, which have given me great encourage-ment for my future. I also want to acknowledge Docent Antti Annisalo for the honor of having him as my opponent.

I wish to express my great thanks to the partners of the NanoEar project in Finland and abroad. I especially thank Professor Mamoun Muhammed's group in Sweeden, Professor Paavo Kinnunen's group in Helsinki and Professor Harm-Anton Klok's group in Switzerland. Due to their timely and continuous provision of perfect nanoparticles for me, my work proceeded smoothly and my thesis could be completed successfully. Elena is warmly thanked for her greatful help during construction of Math1 plasmid.

I am also very thankful to all my current and former colleagues who work at NanoEar group. They are acknowledged for encouragement during the process of writing my thesis, for inspiring conversations about science and livelihood, but also for providing an example of how to combine research and family life successfully. I want to thank them for sharing the best and worst moments in the lab during these years.

I would like to express my sincere thankfulness to Henna Kankkunen and Piia Reku, my current and former colleague and secretary of the NanoEar project. They provided much help and supports during the years.

I sincerely thank the staff of the animal lab. They provided rats for me in time and took care of the rats after surgery, which made my *in vivo* experiments possible.

I would like to thank all the people who work in the medical school for help me during my thesis. I am very thankful to the technicians in the FM3 and B-building for always being so helpful and for keeping things running. I want to acknowledge Tomi Malmström and Toni vormisto for their endurance in solving my computer and network related problems.

I want to thank my friends for reminding that there is a world outside laboratory as well. I sincerely thank all my Chinese friends for the nice dinners that we have enjoyed together. Liang Zhang was thanked for the good advice and support during my studies and thesis project, but more importantly for friendship during the year. The special thanks belong to Shanjun Chen, who gave me lots of kindly technical support.

Finally, my warmest thanks go to my wife Ya Zhang. She gave me lots of emotional and intellectual support during the years of my research. I wish to express my sincere and deep gratitude to my parents for their continuous understanding and encouragement.

This study was supported by the European Community 6th Framework Programme on Research, Technological Development and Demonstration (Nanotechnology-based Targeted Drug Delivery. Contract number: NMP4-CT-2006-026556; project acronym: NANOEAR).

Tampere, June 2011
Weikai Zhang

9. REFERENCES

Adam SA, Marr RS, Gerace L. 1990. Nuclear protein import in permeabilized mammalian cells requires soluble cytoplasmic factors. J Cell Biol 111, 807-16.

Almofti, MR, Harashima H, Shinohara Y, Almofti A, Li W, Kiwada H. 2003. Lipoplex size determines lipofection efficiency with or without serum. Mol Membr Biol 20, 35-43.

Al-Dosari MS, Gao X. 2009. Nonviral gene delivery: principle, limitations, and recent progress. Aaps J 11, 671-81.

Anderson M, Bostrom M, Pfaller K, Glueckert R, Schrott-Fischer A, Gerdin B, Rask-Andersen, H. 2006. Structure and locomotion of adult in vitro regenerated spiral ganglion growth cones-- a study using video microscopy and SEM. Hear Res 215, 97-107.

Anderson, WF. 1998. Human gene therapy. Nature 392, 25-30.

Andre F, Mir LM. 2004. DNA electrotransfer: its principles and an updated review of its therapeutic applications. Gene therapy 11(Suppl 1), S33-42.

Aoi T, Yae K, Nakagawa M, Ichisaka T, Okita K, Takahashi K, Chiba T, Yamanaka S. 2008. Generation of pluripotent stem cells from adult mouse liver and stomach cells. Science 321, 699-702.

Arbab AS, Liu W, Frank JA. 2006. Cellular magnetic resonance imaging: current status and future prospects. Expert Rev Med Devices 3, 427-39.

Arbab AS, Jordan EK, Wilson LB, Yocum GT, Lewis BK, Frank JA. 2004. In vivo trafficking and targeted delivery of magnetically labeled stem cells. Hum Gene Ther 15, 351-60.

Bally MB, Harvie P, Wong FM, Kong S, Wasan EK, Reimer DL. 1999. Biological barriers to cellular delivery of lipid-based DNA carriers. Adv Drug Deliv Rev 38, 291-315.

Batts SA, Raphael Y. 2007. Transdifferentiation and its applicability for inner ear therapy. Hear Res 227, 41-7.

Bedrosian JC, Gratton MA, Brigande JV, Tang W, Landau J, Bennett J. 2006. In vivo delivery of recombinant viruses to the fetal murine cochlea: transduction characteristics and long-term effects on auditory function. Mol Ther 14, 328-35.

Ben-Arie N, Bellen HJ, Armstrong DL, McCall AE, Gordadze PR, Guo Q, Matzuk MM, Zoghbi HY. 1997. Math1 is essential for genesis of cerebellar granule neurons. Nature 390, 169-72.

Ben-Yosef T, Belyantseva IA, Saunders TL, Hughes ED, Kawamoto K, Van Itallie CM, Beyer LA, Halsey K, Gardner DJ, Wilcox ER, Rasmussen J, Anderson JM, Dolan DF, Forge A, Raphael Y, Camper SA, Friedman TB. 2003. Claudin 14 knockout mice, a model for autosomal recessive deafness DFNB29, are deaf due to cochlear hair cell degeneration. Human molecular genetics 12, 2049-61.

Benezra R, Davis RL, Lockshon D, Turner DL, Weintraub H. 1990. The protein Id: a negative regulator of helix-loop-helix DNA binding proteins. Cell 61, 49-59.

Bermingham NA, Hassan BA, Price SD, Vollrath MA, Ben-Arie N, Eatock RA, Bellen HJ, Lysakowski A, Zoghbi HY. 1999. Math1: an essential gene for the generation of inner ear hair cells. Science 284, 1837-41.

Berry CC, de la Fuente JM, Mullin M, Chu SW, Curtis AS. 2007. Nuclear localization of HIV-1 tat functionalized gold nanoparticles. IEEE Trans Nanobioscience 6, 262-9.

Borkholder DA. 2008. State-of-the-art mechanisms of intracochlear drug delivery. Curr Opin Otolaryngol Head Neck Surg 16, 472-7.

Boussif O, Lezoualc'h F, Zanta MA, Mergny MD, Scherman D, Demeneix B, Behr JP. 1995. A versatile vector for gene and oligonucleotide transfer into cells in culture and in vivo: polyethylenimine. Proc Natl Acad Sci U S A 92, 7297-301.

Braun S. 2008. Muscular gene transfer using nonviral vectors. Curr Gene Ther 8, 391-405.

Brigham KL, Meyrick B, Christman B, Magnuson M, King G, Berry LC Jr. 1989. In vivo transfection of murine lungs with a functioning prokaryotic gene using a liposome vehicle. Am J Med Sci 298, 278-81.

Brough DE. 2007. Methods of gene therapy for treating disorders of the ear by administering a vector encoding an atonal-associated factor. U.S. Patent 2007141029.

Bulte JW, Douglas T, Witwer B, Zhang SC, Strable E, Lewis BK, Zywicke H, Miller B, van Gelderen P, Moskowitz BM, Duncan ID, Frank JA. 2001. Magnetodendrimers allow endosomal magnetic labeling and in vivo tracking of stem cells. Nat Biotechnol 19, 1141-7.

Carlisle RC, Bettinger T, Ogris M, Hale S, Mautner V, Seymour LW. 2001. Adenovirus hexon protein enhances nuclear delivery and increases transgene expression of polyethylenimine/plasmid DNA vectors. Mol Ther 4, 473-83.

Casselman JW, Kuhweide R, Dehaene I, Ampe W, Devlies F. 1994. Magnetic resonance examination of the inner ear and cerebellopontine angle in patients with vertigo and/or abnormal findings at vestibular testing. Acta Otolaryngol Suppl 513, 15-27.

Chattopadhyay D, Mitra S, Maitra, A. (2005) A method using inorganic nanoparticles as non-viral vectors for gene therapy. Patent WO/2005/123142. Available at www.wipo.int/pctdb/en/wo.jsp?WO=2005123142 (accessed March 2011).

Chen X, Kube DM, Cooper MJ, Davis PB. 2008. Cell surface nucleolin serves as receptor for DNA nanoparticles composed of pegylated polylysine and DNA. Mol Ther 16, 333-42.

Chen X, Shank S, Davis PB, Ziady AG. 2010. Nucleolin-mediated cellular trafficking of DNA nanoparticle is lipid raft and microtubule dependent and can be modulated by glucocorticoid. Mol Ther 19, 93-102.

Ciorba A, Astolfi L, Jolly C, Martini A. 2009. Cochlear Implants and Inner Ear Based Therapy. Eur J Nanomedicine 2, 25-28.

Cohen-Salmon M, Regnault B, Cayet N, Caille D, Demuth K, Hardelin JP, Janel N, Meda P, Petit C. 2007. Connexin30 deficiency causes instrastrial fluid-blood barrier disruption within the cochlear stria vascularis. Proc Natl Acad Sci U S A 104, 6229-34.

Cohen-Salmon M, Ott T, Michel V, Hardelin JP, Perfettini I, Eybalin M, Wu T, Marcus DC, Wangemann P, Willecke K, Petit C. 2002. Targeted ablation of connexin26 in the inner ear epithelial gap junction network causes hearing impairment and cell death. Curr Biol 12, 1106-11.

Colvin JS, Bohne BA, Harding GW, McEwen DG, Ornitz DM. 1996. Skeletal overgrowth and deafness in mice lacking fibroblast growth factor receptor 3. Nat Genet 12, 390-7.

Corwin JT, Cotanche DA. 1988. Regeneration of sensory hair cells after acoustic trauma. Science 240, 1772-4.

Cotten M, Wagner E, Zatloukal K, Phillips S, Curiel DT, Birnstiel ML. 1992. High-efficiency receptor-mediated delivery of small and large (48 kilobase gene constructs using the endosome-disruption activity of defective or chemically inactivated adenovirus particles. Proc Natl Acad Sci U S A 89, 6094-8.

Counter SA, Zou J, Bjelke B, Klason T. 2003. 3D MRI of the in vivo vestibulo-cochlea labyrinth during Gd-DTPA-BMA uptake. Neuroreport 14, 1707-12.

Counter SA, Bjelke B, Klason T, Chen Z, Borg E. 1999. Magnetic resonance imaging of the cochlea, spiral ganglia and eighth nerve of the guinea pig. Neuroreport 10, 473-9.

Counter SA, Bjelke B, Borg E, Klason T, Chen Z, Duan ML. 2000. Magnetic resonance imaging of the membranous labyrinth during in vivo gadolinium (Gd-DTPA-BMA) uptake in the normal and lesioned cochlea. Neuroreport 11, 3979-83.

Cserpan I, Udvardy A. 1995. The mechanism of nuclear transport of natural or artificial transport substrates in digitonin-permeabilized cells. J Cell Sci 108 (Pt 5), 1849-61.

Dallos P, Fakler B. 2002. Prestin, a new type of motor protein. Nat Rev Mol Cell Biol 3, 104-11.

Damadian R, Goldsmith M., Minkoff L. 1977. NMR in cancer: XVI. FONAR image of the live human body. Physiol Chem Phys 9, 97-100, 108.

Davidson HC. 2001. Imaging evaluation of sensorineural hearing loss. Semin Ultrasound CT MR 22, 229-49.

de Felipe MM, Feijoo Redondo AF, Garcia-Sancho J, Schimmang T, Alonso MB, 2011. Cell- and gene-therapy approaches to inner ear repair. Histol Histopathol 2011 26, 923-40.

De la Fuente M, Csaba N, Garcia-Fuentes M, Alonso MJ. 2008. Nanoparticles as protein and gene carriers to mucosal surfaces. Nanomedicine (Lond) 3, 845-57.

Dean DA, Strong DD, Zimmer WE. 2005. Nuclear entry of nonviral vectors. Gene therapy 12, 881-90.

Derby ML, Sena-Esteves M, Breakefield XO, Corey DP. 1999. Gene transfer into the mammalian inner ear using HSV-1 and vaccinia virus vectors. Hear Res 134, 1-8.

Djourno A, Eyries C. 1957. Prothèse auditive par excitation à distance du nerf sensoriel à l'aide d'un bobinage inclus à demeure. Presse Med. 35, 1417-1423.

Doetzlhofer A, White PM, Johnson JE, Segil N, Groves AK. 2004. In vitro growth and differentiation

of mammalian sensory hair cell progenitors: a requirement for EGF and periotic mesenchyme. Dev Biol 272, 432-47.

Dousset V, Brochet B, Deloire MS, Lagoarde L, Barroso B, Caille JM, Petry KG. 2006. MR imaging of relapsing multiple sclerosis patients using ultra-small-particle iron oxide and compared with gadolinium. AJNR Am J Neuroradiol 27, 1000-5.

Eastman SJ, Siegel C, Tousignant J, Smith AE, Cheng SH, Scheule RK. 1997. Biophysical characterization of cationic lipid: DNA complexes. Biochim Biophys Acta 1325, 41-62.

Elfinger M, Uzgun S, Rudolph C. 2008. Nanocarriers for Gene Delivery - Polymer Structure, Targeting Ligands and Controlled-Release Devices. Curr Nanosci 4, 322-353

Elouahabi A, Ruysschaert JM. 2005. Formation and intracellular trafficking of lipoplexes and polyplexes. Mol Ther 11, 336-47.

Ernfors P, Van De Water T, Loring J, Jaenisch R. 1995. Complementary roles of BDNF and NT-3 in vestibular and auditory development. Neuron 14, 1153-64.

Ernfors P, Duan ML, ElShamy WM, Canlon B. 1996. Protection of auditory neurons from aminoglycoside toxicity by neurotrophin-3. Nature medicine 2, 463-7.

Escriou V, Ciolina C, Lacroix F, Byk G, Scherman D, Wils P. 1998. Cationic lipid-mediated gene transfer: effect of serum on cellular uptake and intracellular fate of lipopolyamine/DNA complexes. Biochim Biophys Acta 1368, 276-88.

Evans MJ, Kaufman MH. 1981. Establishment in culture of pluripotential cells from mouse embryos. Nature 292, 154-6.

Farinas I, Jones KR, Backus C, Wang XY, Reichardt LF. 1994. Severe sensory and sympathetic deficits in mice lacking neurotrophin-3. Nature 369, 658-61.

Farjo R, Skaggs J, Quiambao AB, Cooper MJ, Naash MI. 2006. Efficient non-viral ocular gene transfer with compacted DNA nanoparticles. PLoS One 1, e38.

Fekete DM. 1996. Cell fate specification in the inner ear. Curr Opin Neurobiol 6, 533-41.

Felgner PL, Gadek TR, Holm M, Roman R, Chan HW, Wenz M, Northrop JP, Ringold GM, Danielsen M. 1987. Lipofection: a highly efficient, lipid-mediated DNA-transfection procedure. Proc Natl Acad Sci U S A 84, 7413-7.

Fekete DM. 2000. Making sense of making hair cells. Trends Neurosci 23, 386.

Ferber, D. 2001. Gene therapy. Safer and virus-free? Science 294, 1638-42.

Ferreira L, Karp JM, Nobre L, Langer, R. 2008. New opportunities: the use of nanotechnologies to manipulate and track stem cells. Cell Stem Cell 3, 136-46.

Flock A, Flock B. 2003. Micro-lesions in Reissner's membrane evoked by acute hydrops. Audiol Neurootol 8, 59-69.

Flora A, Garcia JJ, Thaller C, Zoghbi HY. 2007. The E-protein Tcf4 interacts with Math1 to regulate

differentiation of a specific subset of neuronal progenitors. Proc Natl Acad Sci U S A 104, 15382-7.

Fobian K. 2007. Roles of nGf-derived peptides in neuritogenesis and neuronal survival. Roskilde university; 2007, Roskilde

Forge A, Li L, Corwin JT, Nevill G. 1993. Ultrastructural evidence for hair cell regeneration in the mammalian inner ear. Science 259, 1616-9.

Frankel MS. 2000. In search of stem cell policy. Science 287, 1397.

Franz P, Aharinejad S, Bock P, Firbas W. 1993. The cochlear glomeruli in the modiolus of the guinea pig. Eur Arch Otorhinolaryngol 250, 44-50.

Fraysse BG, Alonso A, House WF. 1980. Meniere's disease and endolymphatic hydrops: clinical-histopathological correlations. Ann Otol Rhinol Laryngol Suppl 89, 2-22.

Friedmann T. 1994. Gene Therapy: Fact and Fiction in Biology's New Approaches to Disease CSHL Press.

Friend DS. Papahadjopoulos D, Debs RJ. 1996. Endocytosis and intracellular processing accompanying transfection mediated by cationic liposomes. Biochim Biophys Acta 1278, 41-50.

Fujiyoshi T, Hood L, Yoo TJ. 1994. Restoration of brain stem auditory-evoked potentials by gene transfer in shiverer mice. Ann Otol Rhinol Laryngol 103, 449-56.

Gage FH. 2000. Mammalian neural stem cells. Science 287, 1433-8.

Gardlik R, Palffy R, Hodosy J, Lukacs J, Turna J, Celec P. 2005. Vectors and delivery systems in gene therapy. Med Sci Monit 11, RA110-21.

Gershon H, Ghirlando R, Guttman SB, Minsky A. 1993. Mode of formation and structural features of DNA-cationic liposome complexes used for transfection. Biochemistry 32, 7143-51.

Giesel FL, Mehndiratta A, Locklin J, McAuliffe MJ, White S, Choyke PL, Knopp MV, Wood BJ, Haberkorn U, von Tengg-Kobligk H. 2009. Image fusion using CT, MRI and PET for treatment planning, navigation and follow up in percutaneous RFA. Exp Oncol 31, 106-14.

Ginisty H, Sicard H, Roger B, Bouvet P. 1999. Structure and functions of nucleolin. J Cell Sci 112 (Pt 6), 761-72.

Godbey WT, Mikos AG. 2001. Recent progress in gene delivery using non-viral transfer complexes. J Control Release 72, 115-25.

Godbey WT, Wu KK, Mikos AG. 1999a. Tracking the intracellular path of poly(ethylenimine)/DNA complexes for gene delivery. Proc Natl Acad Sci U S A 96, 5177-81.

Godbey, W.T., Wu, K.K., Mikos, A.G. 1999b. Poly(ethylenimine) and its role in gene delivery. J Control Release 60, 149-60.

Godbey WT, Barry MA., Saggau P, Wu KK, Mikos AG. 2000. Poly(ethylenimine)-mediated transfection: a new paradigm for gene delivery. J Biomed Mater Res 51, 321-8.

Grobner T. 2006. Gadolinium--a specific trigger for the development of nephrogenic fibrosing dermopathy and nephrogenic systemic fibrosis? Nephrol Dial Transplant 21, 1104-8.

Gubbels SP, Woessner DW, Mitchell JC, Ricci AJ, Brigande JV. 2008. Functional auditory hair cells produced in the mammalian cochlea by in utero gene transfer. Nature 455, 537-41.

Han Z, Yan JM., Chi FL, Cong N, Huang YB, Gao Z, Li W. 2010. Survival and fate of transplanted embryonic neural stem cells by Atoh1 gene transfer in guinea pigs cochlea. Neuroreport 21, 490-496.

Hart SL. 2010. Multifunctional nanocomplexes for gene transfer and gene therapy. Cell Biol Toxicol 26, 69-81.

Helms AW, Johnson JE. 1998. Progenitors of dorsal commissural interneurons are defined by MATH1 expression. Development 125, 919-28.

Hibino, H., Kurachi, Y. 2006. Molecular and physiological bases of the K+ circulation in the mammalian inner ear. Physiology (Bethesda) 21, 336-45.

High WA, Ayers RA., Chandler J, Zito G, Cowper SE. 2007. Gadolinium is detectable within the tissue of patients with nephrogenic systemic fibrosis. J Am Acad Dermatol 56, 21-6.

Hinshaw WS, Bottomley PA, Holland GN. 1977. Radiographic thin-section image of the human wrist by nuclear magnetic resonance. Nature 270, 722-3.

Holden C, Vogel G. 2008. Cell biology. A seismic shift for stem cell research. Science 319, 560-3.

Hong H, Takahashi K, Ichisaka T, Aoi T, Kanagawa O, Nakagawa M, Okita K, Yamanaka S. 2009. Suppression of induced pluripotent stem cell generation by the p53-p21 pathway. Nature 460, 1132-5.

Hu Z, Wei D, Johansson CB, Holmstrom N, Duan M, Frisen J, Ulfendahl M. 2005. Survival and neural differentiation of adult neural stem cells transplanted into the mature inner ear. Exp Cell Res 302, 40-7.

Huang Y, Chi F, Han Z, Yang J, Gao W, Li Y. 2009. New ectopic vestibular hair cell-like cells induced by Math1 gene transfer in postnatal rats. Brain Res 1276, 31-8.

Izumikawa M, Batts SA, Miyazawa T, Swiderski DL, Raphael Y. 2008. Response of the flat cochlear epithelium to forced expression of Atoh1. Hear Res 240, 52-6.

Izumikawa M, Minoda R, Kawamoto K, Abrashkin KA, Swiderski DL, Dolan DF, Brough DE, Raphael Y. 2005. Auditory hair cell replacement and hearing improvement by Atoh1 gene therapy in deaf mammals. Nat med 11, 271-6.

James MB, Giorgio TD. 2000. Nuclear-associated plasmid, but not cell-associated plasmid, is correlated with transgene expression in cultured mammalian cells. Mol Ther 1, 339-46.

Jans DA, Hubner S. 1996. Regulation of protein transport to the nucleus: central role of phosphorylation. Physiol Rev 76, 651-85.

Jellema RK, Bomans P, Deckers N, Ungethum L, Reutelingsperger CP, Hofstra L, Frederik PM. 2010. Transfection efficiency of lipoplexes for site-directed delivery. J Liposome Res 20, 258-67.

Jen Y, Weintraub H, Benezra R. 1992 Overexpression of Id protein inhibits the muscle differentiation program: in vivo association of Id with E2A proteins. Genes Dev 6,1466 –1479.

Jendelova P, Herynek V, Urdzikova L, Glogarova K, Kroupova J, Andersson B, Bryja V, Burian M, Hajek M, Sykova E. 2004. Magnetic resonance tracking of transplanted bone marrow and embryonic stem cells labeled by iron oxide nanoparticles in rat brain and spinal cord. J Neurosci Res 76, 232-43.

Jeon SJ, Oshima K, Heller S, Edge AS. 2007. Bone marrow mesenchymal stem cells are progenitors in vitro for inner ear hair cells. Mol Cell Neurosci 34, 59-68.

Jero J, Tseng CJ, Mhatre AN, Lalwani AK. 2001. A surgical approach appropriate for targeted cochlear gene therapy in the mouse. Hear Res 151, 106-114.

Jiang Y, Jahagirdar BN, Reinhardt RL, Schwartz RE, Keene C.D, Ortiz-Gonzalez XR, Reyes M, Lenvik T, Lund T, Blackstad M, Du J, Aldrich S, Lisberg A, Low WC, Largaespada DA., Verfaillie CM. 2002. Pluripotency of mesenchymal stem cells derived from adult marrow. Nature 418, 41-9.

Jin XM, Guo YQ, Huangfu MS. 1990. Electrocochleography in an experimental animal model of acute endolymphatic hydrops. Acta Otolaryngol 110, 334-41.

Jones JM, Montcouquiol M, Dabdoub A, Woods C, Kelley MW. 2006. Inhibitors of differentiation and DNA binding (Ids) regulate Math1 and hair cell formation during the development of the organ of Corti. J Neurosci 26, 550-8.

Kakigi A, Nishimura M, Takeda T, Okada T, Murata Y, Ogawa Y. 2008. Effects of gadolinium injected into the middle ear on the stria vascularis. Acta Otolaryngol 128, 841-5.

Kakimoto S, Hamada T, Komatsu Y, Takagi M, Tanabe T, Azuma H, Shinkai S, Nagasaki T. 2009. The conjugation of diphtheria toxin T domain to poly(ethylenimine) based vectors for enhanced endosomal escape during gene transfection. Biomaterials 30, 402-8.

Kawamoto K, Ishimoto S, Minoda R, Brough DE, Raphael Y. 2003. Math1 gene transfer generates new cochlear hair cells in mature guinea pigs in vivo. J Neurosci 23, 4395-400.

Khalil IA, Kogure K, Akita H, Harashima H. 2006. Uptake pathways and subsequent intracellular trafficking in nonviral gene delivery. Pharmacol Rev 58, 32-45.

Khan AM, Handzel O, Burgess BJ, Damian D, Eddington DK, Nadol JB Jr. 2005. Is word recognition correlated with the number of surviving spiral ganglion cells and electrode insertion depth in human subjects with cochlear implants? Laryngoscope115, 672-7.

Kichler A, Leborgne C, Coeytaux E, Danos O. 2001. Polyethylenimine-mediated gene delivery: a mechanistic study. J Gene Med 3, 135-44.

Kim TI, Rothmund T, Kissel T, Kim SW. 2011. Bioreducible polymers with cell penetrating and endosome buffering functionality for gene delivery systems. J Control Release 152, 110-9.

Klingebiel R, Bockmuhl U, Werbs M, Freigang B, Vorwerk W, Thieme N, Lehmann R. 2001. Visualization of inner ear dysplasias in patients with sensorineural hearing loss. Acta Radiol 42, 574-81.

Klose AD, Beattie BJ, Dehghani H, Vider L, Le C, Ponomarev V, Blasberg R. 2010. In vivo bioluminescence tomography with a blocking-off finite-difference SP3 method and MRI/CT coregistration. Medical physics 37, 329-38.

Konishi T, Salt AN, Hamrick PE. 1982. Effects of exposure to noise on permeability to potassium of the endolymph-perilymph barrier in guinea pigs. Acta Otolaryngol 94, 395-401.

Korbling M, Estrov Z. 2003. Adult stem cells for tissue repair - a new therapeutic concept? N Engl J Med 349, 570-82.

Kreider BL, Benezra R, Rovera G, Kadesch T. 1992. Inhibition of myeloid differentiation by the helix-loop-helix protein Id. Science 255, 1700-2.

Kudo T, Kure S, Ikeda K, Xia AP, Katori Y, Suzuki M, Kojima K, Ichinohe A, Suzuki Y, Aoki Y, Kobayashi T, Matsubara Y. 2003. Transgenic expression of a dominant-negative connexin26 causes degeneration of the organ of Corti and non-syndromic deafness. Hum Mol Genet 12, 995-1004.

Kwon EJ, Lasiene J, Jacobson BE, Park IK, Horner PJ, Pun SH. 2010. Targeted nonviral delivery vehicles to neural progenitor cells in the mouse subventricular zone. Biomaterials 31, 2417-24.

Labat-Moleur F, Steffan AM, Brisson C, Perron H, Feugeas O, Furstenberger P, Oberling F, Brambilla E, Behr JP. 1996. An electron microscopy study into the mechanism of gene transfer with lipopolyamines. Gene Ther 3, 1010–1017.

Lanza R. 2007. Stem cell breakthrough: don't forget ethics. Science 318, 1865.

Lauterbur PC. 1973. Image formation by induced local interactions. Examples employing nuclear magnetic resonance. Clin Orthop Relat Res, 3-6.

Lawrence MJ, Rees GD. 2000. Microemulsion-based media as novel drug delivery systems. Adv Drug Deliv Rev 45, 89-121.

Lee IH, Bulte JW, Schweinhardt P, Douglas T, Trifunovski A, Hofstetter C, Olson L, Spenger C. 2004. In vivo magnetic resonance tracking of olfactory ensheathing glia grafted into the rat spinal cord. Exp Neurol 187, 509-16.

Leonova EV, Raphael Y. 1997. Organization of cell junctions and cytoskeleton in the reticular lamina in normal and ototoxically damaged organ of Corti. Hear Res 113, 14-28.

Li H, Liu H, Heller S. 2003a. Pluripotent stem cells from the adult mouse inner ear. Nat Med 9, 1293-9.

Li H, Roblin G, Liu H, Heller S. 2003b. Generation of hair cells by stepwise differentiation of embryonic stem cells. Proceedings of the National Academy of Sciences of the United States of America 100, 13495-500.

Li H, Corrales CE, Edge A, Heller S. 2004. Stem cells as therapy for hearing loss. Trends Mol Med 10, 309-15.

Li S and Huang L. 2000. Nonviral gene therapy: Promises and challenges. Gene Ther 7, 31–34.

Li SC, Tachiki LM, Luo J, Dethlefs BA, Chen Z, Loudon WG. 2010. A biological global positioning

system: considerations for tracking stem cell behaviors in the whole body. Stem Cell Rev 6, 317-33.

Lian T, Ho RJ. 2003. Design and characterization of a novel lipid-DNA complex that resists serum-induced destabilization. J Pharm Sci 92, 2373-85.

Linthicum FH Jr, Fayad J, Otto SR, Galey FR, House WF. 1991. Cochlear implant histopathology.Am J Otol 12, 245-311.

Liu CH, Kim YR, Ren JQ, Eichler F, Rosen BR, Liu PK. 2007b. Imaging cerebral gene transcripts in live animals. J Neurosci 27, 713-22.

Liu CH, You Z, Ren J, Kim YR, Eikermann-Haerter K, Liu PK. 2008b. Noninvasive delivery of gene targeting probes to live brains for transcription MRI. Faseb J 22, 1193-203.

Liu CH, You Z, Liu CM, Kim YR, Whalen MJ, Rosen BR, Liu PK. 2009. Diffusion-weighted magnetic resonance imaging reversal by gene knockdown of matrix metalloproteinase-9 activities in live animal brains. J Neurosci 29, 3508-17.

Liu CH, Huang S, Cui J, Kim YR, Farrar CT, Moskowitz MA, Rosen BR, Liu PK. 2007a. MR contrast probes that trace gene transcripts for cerebral ischemia in live animals. Faseb J 21, 3004-15.

Liu Y, Okada T, Shimazaki K, Sheykholeslami K, Nomoto T, Muramatsu S, Mizukami H, Kume A, Xiao S, Ichimura K, Ozawa K. 2008a. Protection against aminoglycoside-induced ototoxicity by regulated AAV vector-mediated GDNF gene transfer into the cochlea. Mol Ther 16, 474-80.

Liu Y, Okada T, Sheykholeslami K, Shimazaki K, Nomoto T, Muramatsu S, Kanazawa T, Takeuchi K, Ajalli R, Mizukami H, Kume A, Ichimura K, Ozawa K. 2005. Specific and efficient transduction of Cochlear inner hair cells with recombinant adeno-associated virus type 3 vector. Mol Ther 12, 725-33.

Logothetis NK. 2008. What we can do and what we cannot do with fMRI. Nature 453, 869-78.

Ma B, Zhang S, Jiang H, Zhao B, Lv H. 2007. Lipoplex morphologies and their influences on transfection efficiency in gene delivery. J Control Release 123, 184-94.

Mahmoudi M, Shokrgozar M, Simchi A. 2009a. Multiphysics flow modeling and in vitro toxicity of iron oxide nanoparticles coated with poly(vinyl alcohol). J. Phys. Chem C113, 2322-2331.

Mahmoudi M, Simchi A, Milani AS, Stroeve, P. 2009b. Cell toxicity of superparamagnetic iron oxide nanoparticles. J Colloid Interface Sci 336, 510-8.

Mahmoudi M, Hosseinkhani H, Hosseinkhani M, Boutry S, Simchi A, Journeay WS, Subramani K, Laurent S. 2011. Magnetic resonance imaging tracking of stem cells in vivo using iron oxide nanoparticles as a tool for the advancement of clinical regenerative medicine. Chem Rev 111, 253-80.

Maiorana CR, Staecker H. 2005. Advances in inner ear gene therapy: exploring cochlear protection and regeneration. Curr Opin Otolaryngol Head Neck Surg13, 308-12.

Makimoto K, Takeda T, Silverstein H. 1978. Chemical composition in various compartments of inner ear fluid. Arch Otorhinolaryngol 220, 259-64.

Malgrange B, Belachew S, Thiry M, Nguyen L, Rogister B, Alvarez ML, Rigo JM, Van De Water TR,

Moonen G, Lefebvre PP. 2002. Proliferative generation of mammalian auditory hair cells in culture. Mech Dev 112, 79-88.

Mani V, Adler E, Briley-Saebo KC, Bystrup A, Fuster V, Keller G, Fayad ZA. 2008. Serial in vivo positive contrast MRI of iron oxide-labeled embryonic stem cell-derived cardiac precursor cells in a mouse model of myocardial infarction. Magn Reson Med 60, 73-81.

Mark AS, Seltzer S, Nelson-Drake J, Chapman JC, Fitzgerald DC, Gulya AJ. 1992. Labyrinthine enhancement on gadolinium-enhanced magnetic resonance imaging in sudden deafness and vertigo: correlation with audiologic and electronystagmographic studies. Ann Otol Rhinol Laryngol 101, 459-64.

Martin GR. 1981. Isolation of a pluripotent cell line from early mouse embryos cultured in medium conditioned by teratocarcinoma stem cells. Proc Natl Acad Sci U S A 78, 7634-8.

Martin ME, Rice KG. 2007. Peptide-guided gene delivery. Aaps J 9, E18-29.

Matsuoka AJ, Kondo T, Miyamoto RT, Hashino E. 2006. In vivo and in vitro characterization of bone marrow-derived stem cells in the cochlea. Laryngoscope 116, 1363-7.

McCarthy JR, Kelly KA, Sun EY, Weissleder R. 2007. Targeted delivery of multifunctional magnetic nanoparticles. Nanomedicine (Lond) 2, 153-67.

McClay JE, Booth TN, Parry DA, Johnson R, Roland P. 2008. Evaluation of pediatric sensorineural hearing loss with magnetic resonance imaging. Arch Otolaryngol Head Neck Surg 134, 945-52.

Mendonca-Dias MH, Gaggelli E, Lauterbur PC. 1983. Paramagnetic contrast agents in nuclear magnetic resonance medical imaging. Semin Nucl Med 13, 364-76.

Mintzer MA, Simanek EE. 2009. Nonviral vectors for gene delivery. Chem Rev 109, 259-302.

Mishra S, Webster P, Davis ME. 2004. PEGylation significantly affects cellular uptake and intracellular trafficking of non-viral gene delivery particles. Eur J Cell Biol 83, 97-111.

Mongelard F, Bouvet P. 2007. Nucleolin: a multiFACeTed protein. Trends Cell Biol 17, 80-6.

Moore NM, Sheppard CL, Barbour TR, Sakiyama-Elbert SE. 2008. The effect of endosomal escape peptides on in vitro gene delivery of polyethylene glycol-based vehicles. J Gene Med 10, 1134-49.

Marsot-Dupuch K, Meyer B. 2001. Cochlear implant assessment: imaging issues. Eur J Radiol 40, 119-32.

Mulligan RC. 1993. The basic science of gene therapy. Science 260, 926–932.

Munkonge FM, Amin V, Hyde SC, Green AM, Pringle IA, Gill DR, Smith JW, Hooley RP, Xenariou S, Ward MA, Leeds N, Leung KY, Chan M, Hillery E, Geddes DM, Griesenbach U, Postel EH, Dean DA, Dunn MJ, Alton EW. 2009. Identification and functional characterization of cytoplasmic determinants of plasmid DNA nuclear import. J Biol Chem 284, 26978-87.

Nabel GJ, Nabel EG, Yang ZY, Fox BA, Plautz GE, Gao X, Huang L, Shu S, Gordon D, Chang AE. 1993. Direct gene transfer with DNA-liposome complexes in melanoma: expression, biologic activity, and lack of toxicity in humans. Proc Natl Acad Sci U S A 90, 11307-11.

Nakagawa T, Ito J. 2005. Cell therapy for inner ear diseases. Curr Pharm Des11, 1203-7.

Naito Y, Nakamura T, Nakagawa T, Iguchi F, Endo T, Fujino K, Kim TS, Hiratsuka Y, Tamura T, Kanemaru S, Shimizu Y, Ito J. 2004. Transplantation of bone marrow stromal cells into the cochlea of chinchillas. Neuroreport 15, 1-4.

Neumann E, Schaefer-Ridder M., Wang Y, Hofschneider P. 1982. Gene transfer into mouse lyoma cells by electroporation in high electric fields. EMBO J 1, 841-845.

Niidome T, Huang L. 2002. Gene therapy progress and prospects: nonviral vectors. Gene Ther 9, 1647-52.

Nishimura K, Nakagawa T, Ono K, Ogita H, Sakamoto T, Yamamoto N, Okita K, Yamanaka S, Ito J. 2009. Transplantation of mouse induced pluripotent stem cells into the cochlea. Neuroreport 20, 1250-4.

Norton JD, Atherton GT. 1998. Coupling of cell growth control and apoptosis functions of Id proteins. Mol Cell Biol 18, 2371-81.

Noushi F, Richardson RT, Hardman J, Clark G, O'Leary S. 2005. Delivery of neurotrophin-3 to the cochlea using alginate beads. Otol Neurotol 26, 528-33.

Okano T, Nakagawa T, Kita T, Endo T, Ito J. 2006. Cell-gene delivery of brain-derived neurotrophic factor to the mouse inner ear. Mol Ther 14, 866-71.

O'Leary PD, Hughes RA. 2003. Design of potent peptide mimetics of brain-derived neurotrophic factor. J Biol Chem 278, 25738-44.

Oliver D, He DZ, Klocker N, Ludwig J, Schulte U, Waldegger S, Ruppersberg JP, Dallos P, Fakler B. 2001. Intracellular anions as the voltage sensor of prestin, the outer hair cell motor protein. Science 292, 2340-3.

Oshima K, Grimm CM, Corrales CE, Senn P, Martinez Monedero R, Geleoc GS, Edge A, Holt JR, Heller S. 2007. Differential distribution of stem cells in the auditory and vestibular organs of the inner ear. J Assoc Res Otolaryngol 8, 18-31.

Oshima K, Shin K, Diensthuber M, Peng AW, Ricci AJ, Heller S. 2010. Mechanosensitive hair cell-like cells from embryonic and induced pluripotent stem cells. Cell 141, 704-16.

Pante N, Kann M. 2002. Nuclear pore complex is able to transport macromolecules with diameters of about 39 nm. Mol Biol Cell 13, 425-34.

Park IH, Zhao R, West JA, Yabuuchi A, Huo H, Ince TA, Lerou PH, Lensch MW, Daley GQ. 2008. Reprogramming of human somatic cells to pluripotency with defined factors. Nature 451, 141-6.

Parker MA, Corliss DA, Gray B, Anderson JK, Bobbin RP, Snyder EY, Cotanche DA. 2007. Neural stem cells injected into the sound-damaged cochlea migrate throughout the cochlea and express markers of hair cells, supporting cells, and spiral ganglion cells. Hear Res 232, 29-43.

Pasqualetto E, Seydel A, Pellini A, Battistutta R. 2008. Expression, purification and characterisation of the C-terminal STAS domain of the SLC26 anion transporter prestin. Protein Expr Purif 58, 249-56.

Patel NP, Mhatre AN, Lalwani AK. 2004. Biological therapy for the inner ear. Expert Opin Biol Ther 4, 1811-9.

Pathak A, Patnaik S, Gupta KC. 2009. Recent trends in non-viral vector-mediated gene delivery. Biotechnol J 4, 1559-72.

Pauley S, Kopecky B, Beisel K, Soukup G, Fritzsch B. 2008. Stem cells and molecular strategies to restore hearing. Panminerva Med 50, 41-53.

Pedroso de Lima MC, Simoes S, Pires P, Faneca H, Duzgunes N. 2001. Cationic lipid-DNA complexes in gene delivery: from biophysics to biological applications. Adv Drug Deliv Rev 47, 277-94.

Petry KG, Boiziau C, Dousset V, Brochet, B. 2007. Magnetic resonance imaging of human brain macrophage infiltration. Neurotherapeutics 4, 434-42.

Pickles JO, Harter C, Rebillard G. 1998. Fibroblast growth factor receptor expression in outer hair cells of rat cochlea. Neuroreport 9, 4093-5.

Pirvola U, Cao Y, Oellig C, Suoqiang Z, Pettersson RF, Ylikoski J. 1995. The site of action of neuronal acidic fibroblast growth factor is the organ of Corti of the rat cochlea. Proc Natl Acad Sci U S A 92, 9269-73.

Poe D, Zou J, Zhang W, Qin J, Usama AR, Fornara A, Muhammed M, Pyykko I. 2009. MRI of the Cochlea with Superparamagnetic iron oxide nanoparticles compared to Gadolinium chelate contrast agents in a rat model. Eur J Nanomedicine 2, 7-13.

Pollard H, Remy JS, Loussouarn G, Demolombe S, Behr JP, Escande D. 1998. Polyethylenimine but not cationic lipids promotes transgene delivery to the nucleus in mammalian cells. J Biol Chem 273, 7507-11.

Popper A, Fay R. 1996. The cochlea, Springer Handbook of auditory research ed. by peter dallos, (1996).

Praetorius M, Knipper M, Schick B, Tan J, Limberger A, Carnicero E, Alonso MT, Schimmang T. 2002. A novel vestibular approach for gene transfer into the inner ear. Audiol Neurootol 7, 324-34.

Prockop DJ, Gregory CA, Spees JL. 2003. One strategy for cell and gene therapy: harnessing the power of adult stem cells to repair tissues. Proc Natl Acad Sci U S A 100 Suppl 1, 11917-23.

Pyykko I, Zou J, Poe D, Nakashima T, Naganawa S. 2010. Magnetic resonance imaging of the inner ear in Meniere's disease. Otolaryngol Clin North Am 43, 1059-80.

Qin J, Laurent S, Jo Y, Roch A, Mikhaylova M, Zaver M, Bhujwalla Z, Muller RN, Mamoun M. 2007. A High-performance magnetic resonance imaging T2 contrast agent. Adv. Mater. 19, 1874-1878

Radler JO, Koltover I, Salditt T, Safinya CR. 1997. Structure of DNA-cationic liposome complexes: DNA intercalation in multilamellar membranes in distinct interhelical packing regimes. Science 275, 810-4.

Raper SE, Chirmule N, Lee FS, Wivel NA, Bagg A, Gao GP, Wilson JM, Batshaw ML. 2003. Fatal

systemic inflammatory response syndrome in a ornithine transcarbamylase deficient patient following adenoviral gene transfer. Mol Genet Metab 80, 148-58.

Raphael Y, Frisancho JC, Roessler BJ. 1996. Adenoviral-mediated gene transfer into guinea pig cochlear cells in vivo. Neurosci Lett 207, 137-41.

Rask-Andersen H, Schrott-Fischer A, Pfaller K, Glueckert R. 2006. Perilymph/ modiolar communication routes in the human cochlea. Ear Hear 27, 457-65.

Rask-Andersen H, Bostrom M, Gerdin B, Kinnefors A, Nyberg G, Engstrand T, Miller JM, Lindholm D. 2005. Regeneration of human auditory nerve. In vitro/in video demonstration of neural progenitor cells in adult human and guinea pig spiral ganglion. Hear Res 203, 180-91.

Regala C, Duan M, Zou J, Salminen M, Olivius P. 2005. Xenografted fetal dorsal root ganglion, embryonic stem cell and adult neural stem cell survival following implantation into the adult vestibulocochlear nerve. Exp Neurol 193, 326-33.

Rejali D, Lee VA, Abrashkin KA, Humayun N, Swiderski DL, Raphael Y. 2007. Cochlear implants and ex vivo BDNF gene therapy protect spiral ganglion neurons. Hear Res 228, 180-7.

Rejman J, Conese M, Hoekstra D. 2006. Gene transfer by means of lipo- and polyplexes: role of clathrin and caveolae-mediated endocytosis. J Liposome Res 16, 237-47.

Reyes JH, O'Shea KS, Wys NL, Velkey JM, Prieskorn DM, Wesolowski K, Miller JM, Altschuler RA. 2008. Glutamatergic neuronal differentiation of mouse embryonic stem cells after transient expression of neurogenin 1 and treatment with BDNF and GDNF: in vitro and in vivo studies. J Neurosci 28, 12622-31.

Richardson RT, Wise AK, Andrew JK, O'Leary SJ. 2008. Novel drug delivery systems for inner ear protection and regeneration after hearing loss. Expert Opin Drug Deliv 5, 1059-76.

Robertson NG, Jones SM, Sivakumaran TA, Giersch AB, Jurado SA, Call LM, Miller, CE, Maison SF, Liberman MC, Morton CC. 2008. A targeted Coch missense mutation: a knock-in mouse model for DFNA9 late-onset hearing loss and vestibular dysfunction. Hum Mol Genet 17, 3426-34.

Roehm PC, Hansen MR. 2005. Strategies to preserve or regenerate spiral ganglion neurons. Curr Opin Otolaryngol Head Neck Surg13, 294-300.

Rose MF, Ren J, Ahmad KA, Chao HT, Klisch TJ, Flora A, Greer JJ, Zoghbi HY. 2009. Math1 is essential for the development of hindbrain neurons critical for perinatal breathing. Neuron 64, 341-54.

Ross PC, Hui SW. 1999. Lipoplex size is a major determinant of in vitro lipofection efficiency. Gene Ther 6, 651-9.

Roy S, Johnston AH, Newman TA, Glueckert R, Dudas J, Bitsche M, Corbacella E, Rieger G, Martini A, Schrott-Fischer A. 2010. Cell-specific targeting in the mouse inner ear using nanoparticles conjugated with a neurotrophin-derived peptide ligand: potential tool for drug delivery. Int J Pharm 390, 214-24.

Rudelius M, Daldrup-Link HE, Heinzmann U, Piontek G, Settles M, Link TM, Schlegel J. 2003. Highly efficient paramagnetic labelling of embryonic and neuronal stem cells. Eur J Nucl Med Mol Imaging 30, 1038-44.

Ruponen M, Yla-Herttuala S, Urtti A. 1999. Interactions of polymeric and liposomal gene delivery systems with extracellular glycosaminoglycans: physicochemical and transfection studies. Biochim Biophys Acta 1415, 331-41.

Ryals BM, Rubel EW. 1988. Hair cell regeneration after acoustic trauma in adult Coturnix quail. Science 240, 1774-6.

Ryan AF, Wickham M.G, Bone RC. 1979. Element content of intracochlear fluids, outer hair cells, and stria vascularis as determined by energy-dispersive roentgen ray analysis. Otolaryngol Head Neck Surg 87, 659-65.

Ryan AF, Mullen LM, Doherty JK. 2009b. Cellular targeting for cochlear gene therapy. Adv Otorhinolaryngol 66, 99-115.

Ryan AF, Dazert S. 2009a. Gene therapy for the inner ear: challenges and promises. Adv Otorhinolaryngol 66, 1-12.

Sanchez-Ramos JR. 2002. Neural cells derived from adult bone marrow and umbilical cord blood. J Neurosci Res 69, 880-93.

Scheper V, Wolf M, Scholl M, Kadlecova Z, Perrier T, Klok HA, Saulnier P, Lenarz T, Stover T. 2009. Potential novel drug carriers for inner ear treatment: hyperbranched polylysine and lipid nanocapsules. Nanomedicine (Lond) 4, 623-35.

Schimmang T, Tan J, Muller M, Zimmermann U, Rohbock K, Kopschall I, Limberger A, Minichiello L, Knipper M. 2003. Lack of Bdnf and TrkB signalling in the postnatal cochlea leads to a spatial reshaping of innervation along the tonotopic axis and hearing loss. Development 130, 4741-50.

Schmidt-Wolf GD, Schmidt-Wolf IG. 2003. Non-viral and hybrid vectors in human gene therapy: an update. Trends Mol Med 9, 67-72.

Scholl M, Nguyen T, Bruchmann B, Klok H-A. 2007. The thermal polymerization of amino acids revisited; Synthesis and structural characterization of hyperbranched polymers from L-lysine. J Polym Sci 45, 5494-5508.

Schroeder T. 2008. Imaging stem-cell-driven regeneration in mammals. Nature 453, 345-51.

Schwartz R, Engel I, Fallahi-Sichani M, Petrie HT, Murre C. 2006. Gene expression patterns define novel roles for E47 in cell cycle progression, cytokine-mediated signaling, and T lineage development. Proc Natl Acad Sci U S A 103, 9976-81.

Sebestyen MG, Ludtke JJ, Bassik MC, Zhang G, Budker V, Lukhtanov EA, Hagstrom JE, Wolff JA. 1998. DNA vector chemistry: the covalent attachment of signal peptides to plasmid DNA. Nat Biotechnol 16, 80-5.

Shepherd RK, Roberts LA, Paolini AG. 2004. Long-term sensorineural hearing loss induces functional changes in the rat auditory nerve. Eur J Neurosci 20, 3131-3140.

Shibata SB and Raphael Y. 2010. Future approaches for inner ear protection and repair. J Commun Disord 43, 295-310.

Shou J, Zheng JL, Gao WQ. 2003. Robust generation of new hair cells in the mature mammalian inner ear by adenoviral expression of Hath1. Mol Cell Neurosci 23, 169-79.

Simberg D, Weisman S, Talmon Y, Barenholz Y. 2004. DOTAP (and other cationic lipids): chemistry, biophysics, and transfection. Crit Rev Ther Drug Carrier Syst 21, 257-317.

Simoes S, Pires P, Duzgunes N, Pedrosa de Lima MC. 1999. Cationic liposomes as gene transfer vectors: barriers to successful application in gene therapy. Curr Opin Mol Ther 1, 147-57.

Simons JP, Mandell DL, Arjmand EM. 2006. Computed tomography and magnetic resonance imaging in pediatric unilateral and asymmetric sensorineural hearing loss. Arch Otolaryngol Head Neck Surg 132, 186-92.

Smith BR, Heverhagen J, Knopp M, Schmalbrock P, Shapiro J, Shiomi M, Moldovan NI., Ferrari M., Lee SC. 2007. Localization to atherosclerotic plaque and biodistribution of biochemically derivatized superparamagnetic iron oxide nanoparticles (SPIONs) contrast particles for magnetic resonance imaging (MRI). Biomed Microdevices 9, 719-27.

Smith TA, Mehaffey MG, Kayda DB, Saunders JM, Yei S, Trapnell BC, McClelland A, Kaleko M. 1993. Adenovirus mediated expression of therapeutic plasma levels of human factor IX in mice. Nat Genet 5, 397–402.

Soininen P, Hanzlikova M, Paukkunen M, Lecklin A, Mannisto PT, Raasmaja A. 2010. Sample purification improves the analysis of nonviral in vivo gene transfection. Plasmid 63, 27-30.

Sosnovik DE, Nahrendorf M, Weissleder R. 2008. Magnetic nanoparticles for MR imaging: agents, techniques and cardiovascular applications. Basic Res Cardiol 103, 122-30.

Srivastava M, Pollard HB. 1999. Molecular dissection of nucleolin's role in growth and cell proliferation: new insights. Faseb J 13, 1911-22.

Staecker H, Li D, O'Malley BW Jr, Van De Water TR. 2001. Gene expression in the mammalian cochlea: a study of multiple vector systems. Acta Otolaryngol 121, 157-63.

Staecker H, Praetorius M, Baker K, Brough DE. 2007. Vestibular hair cell regeneration and restoration of balance function induced by math1 gene transfer. Otol Neurotol 28, 223-31.

Staecker H, Kopke R, Malgrange B, Lefebvre P, Van de Water TR. 1996. NT-3 and/or BDNF therapy prevents loss of auditory neurons following loss of hair cells. Neuroreport 7, 889-94.

Sullivan KM, Busa WB, Wilson KL. 1993. Calcium mobilization is required for nuclear vesicle fusion in vitro: implications for membrane traffic and IP3 receptor function. Cell 73, 1411-22.

Sun H, Huang A, Cao S. 2011. Current Status and Prospects of Gene Therapy for the Inner Ear. Hum Gene Ther. [Epub ahead of print]

Sun XH. 1994. Constitutive expression of the Id1 gene impairs mouse B cell development. Cell 79, 893–900.

Tachibana R, Harashima H, Ide N, Ukitsu S, Ohta Y, Suzuki N, Kikuchi H, Shinohara Y, Kiwada H. 2002. Quantitative analysis of correlation between number of nuclear plasmids and gene expression activity after transfection with cationic liposomes. Pharm Res 19, 377-81.

Takahashi K, Yamanaka S. 2006. Induction of pluripotent stem cells from mouse embryonic and adult fibroblast cultures by defined factors. Cell 126, 663-76.

Takahashi K, Tanabe K, Ohnuki M, Narita M, Ichisaka T, Tomoda K, Yamanaka S. 2007. Induction of pluripotent stem cells from adult human fibroblasts by defined factors. Cell 131, 861-72.

Tan BT, Foong KH, Lee MM, Ruan R. 2008. Polyethylenimine-mediated cochlear gene transfer in guinea pigs. Arch Otolaryngol Head Neck Surg 134, 884-91.

Tan J, Shepherd RK. 2006. Aminoglycoside-induced degeneration of adult spiral ganglion neurons involves differential modulation of tyrosine kinase B and p75 neurotrophin receptor signaling. Am J Pathol 169, 528-43.

Tang LS, Montemayor C, Pereira FA. 2006. Sensorineural hearing loss: potential therapies and gene targets for drug development. IUBMB Life 58, 525-30.

Tang MX, Redemann CT, Szoka FC Jr. 1996. In vitro gene delivery by degraded polyamidoamine dendrimers. Bioconjug Chem 7, 703-14.

Tateya I, Nakagawa T, Iguchi F, Kim TS, Endo T, Yamada S, Kageyama R, Naito Y, Ito J. 2003. Fate of neural stem cells grafted into injured inner ears of mice. Neuroreport 14, 1677-81.

Teubner B, Michel V, Pesch J, Lautermann J, Cohen-Salmon M, Sohl G, Jahnke K, Winterhager E, Herberhold C, Hardelin JP, Petit C, Willecke K. 2003. Connexin30 (Gjb6)-deficiency causes severe hearing impairment and lack of endocochlear potential. Hum Mol Genet 12, 13-21.

Thakral C, Abraham JL. 2009. Gadolinium-induced nephrogenic systemic fibrosis is associated with insoluble Gd deposits in tissues: in vivo transmetallation confirmed by microanalysis. J Cutan Pathol 36, 1244-54.

Thomas CE, Ehrhardt A, Kay MA. 2003. Progress and problems with the use of viral vectors for gene therapy. Nat Rev Genet 4, 346-58.

Thomson JA, Itskovitz-Eldor J, Shapiro SS, Waknitz MA, Swiergiel JJ, Marshall, VS, Jones JM. 1998. Embryonic stem cell lines derived from human blastocysts. Science 282, 1145-7.

Thu MS, Najbauer J, Kendall SE, Harutyunyan I, Sangalang N, Gutova M, Metz MZ, Garcia E, Frank RT, Kim SU, Moats RA, Aboody KS. 2009. Iron labeling and pre-clinical MRI visualization of therapeutic human neural stem cells in a murine glioma model. PLoS One 4, e7218.

Titomirov AV, Sukharev S, Kistanova E. 1991. In vivo electroporation and stable transformation of skin cells of newborn mice by plasmid DNA. Biochim Biophys Acta 1088, 131-4.

Tkachenko AG, Xie H, Coleman D, Glomm W, Ryan J, Anderson MF, Franzen S, Feldheim DL. 2003. Multifunctional gold nanoparticle-peptide complexes for nuclear targeting. J Am Chem Soc 125, 4700-1.

Torres M, Giraldez F. 1998. The development of the vertebrate inner ear. Mech Dev 71, 5-21.

Tros de Ilarduya C, Sun Y, Duzgunes N. 2010. Gene delivery by lipoplexes and polyplexes. Eur J Pharm Sci 40, 159-70.

Tseng WC, Haselton FR, Giorgio TD. 1999. Mitosis enhances transgene expression of plasmid delivered by cationic liposomes. Biochim Biophys Acta 1445, 53-64.

Turek J, Dubertret C, Jaslin G, Antonakis K, Scherman D, Pitard B. 2000. Formulations which increase the size of lipoplexes prevent serum-associated inhibition of transfection. J Gene Med 2, 32-40.

Valk WL, Wit HP, Albers FW. 2006. Rupture of Reissner's membrane during acute endolymphatic hydrops in the guinea pig: a model for Meniere's disease? Acta Otolaryngol 126, 1030-5.

Van de Water TR, Staecker H, Halterman MW, Federoff HJ. 1999. Gene therapy in the inner ear. Mechanisms and clinical implications. Ann N Y Acad Sci 884, 345-60.

Verma, A., Stellacci, F. 2010. Effect of surface properties on nanoparticle-cell interactions. Small 6, 12-21.

Verma IM, Weitzman MD. 2005. Gene therapy: twenty-first century medicine. Annu Rev Biochem 74, 711-38.

Wang Y, Gao S, Ye WH, Yoon HS, Yang YY. 2006. Co-delivery of drugs and DNA from cationic core-shell nanoparticles self-assembled from a biodegradable copolymer. Nat Mater 5, 791-6.

Warchol ME, Lambert PR, Goldstein BJ, Forge A, Corwin JT. 1993. Regenerative proliferation in inner ear sensory epithelia from adult guinea pigs and humans. Science 259, 1619-22.

Wareing M, Mhatre AN, Pettis R, Han JJ, Haut T, Pfister MH, Hong K, Zheng WW, Lalwani AK. 1999. Cationic liposome mediated transgene expression in the guinea pig cochlea. Hear Res 128, 61-9.

Watanabe T, Frahm J, Michaelis T. 2008. Manganese-enhanced MRI of the mouse auditory pathway. Magn Reson Med 60, 210-2.

White PM, Doetzlhofer A, Lee YS, Groves AK, Segil N. 2006. Mammalian cochlear supporting cells can divide and trans-differentiate into hair cells. Nature 441, 984-7.

Wise AK, Hume CR, Flynn BO, Jeelall YS, Suhr CL, Sgro BE, O'Leary SJ, Shepherd RK, Richardson RT. 2010. Effects of localized neurotrophin gene expression on spiral ganglion neuron resprouting in the deafened cochlea. Mol Ther 18, 1111-22.

Woods C, Montcouquiol M, Kelley MW. 2004. Math1 regulates development of the sensory epithelium in the mammalian cochlea. Nat Neurosci 7, 1310-8.

Wu GY, Wu CH. 1987. Receptor-mediated in vitro gene transformation by a soluble DNA carrier system. J Biol Chem 262, 4429-32.

www.nanoear.org/. 2009. Nanoear: 3g-nanotechnology based targeted drug delivery using the inner ear as a model target organ (2009).

Wyatt C, Soher B, Maccarini P, Charles HC, Stauffer P, Macfall J. 2009. Hyperthermia MRI temperature measurement: evaluation of measurement stabilisation strategies for extremity and breast tumours. Int J Hyperthermia 25, 422-33.

Yang J, Liu J, Niu G, Chan KC, Wang R, Liu Y, Wu EX. 2009. In vivo MRI of endogenous stem/

progenitor cell migration from subventricular zone in normal and injured developing brains. Neuroimage 48, 319-28.

Yang Y, Nunes FA, Berencsi K, Furth EE, Gonczol E, Wilson JM. 1994. Cellular immunity to viral antigens limits E1-deleted adenoviruses for gene therapy. Proc Natl Acad Sci USA 91, 4407–4411.

Yang Y, Yang Y, Yanasak N, Schumacher A, Hu TC. 2010. Temporal and noninvasive monitoring of inflammatory-cell infiltration to myocardial infarction sites using micrometer-sized iron oxide particles. Magn Reson Med 63, 33-40.

Yokota Y, Mansouri A, Mori S, Sugawara S, Adachi S, Nishikawa S, Gruss P. 1999. Development of peripheral lymphoid organs and natural killer cells depends on the helix-loop-helix inhibitor Id2. Nature 397, 702-6.

Yu J, Vodyanik MA, Smuga-Otto K, Antosiewicz-Bourget J, Frane JL, Tian S, Nie J, Jonsdottir GA, Ruotti V, Stewart R, Slukvin II, Thomson JA. 2007. Induced pluripotent stem cell lines derived from human somatic cells. Science 318, 1917-20.

Yu X, Wadghiri YZ, Sanes DH, Turnbull DH. 2005. In vivo auditory brain mapping in mice with Mn-enhanced MRI. Nat Neurosci 8, 961-8.

Zabner J, Fasbender AJ, Moninger T, Poellinger KA, Welsh MJ. 1995. Cellular and molecular barriers to gene transfer by a cationic lipid. J Biol Chem 270, 18997-9007.

Zhai S, Shi L, Wang BE, Zheng G, Song W, Hu Y, Gao WQ. 2005. Isolation and culture of hair cell progenitors from postnatal rat cochleae. J Neurobiol 65, 282-93.

Zhang Y, Zhai SQ, Shou J, Song W, Sun JH, Guo W, Zheng GL, Hu YY, Gao WQ. 2007. Isolation, growth and differentiation of hair cell progenitors from the newborn rat cochlear greater epithelial ridge. J Neurosci Methods 164, 271-9.

Zhdanov RI, Podobed OV, Vlassov VV. 2002. Cationic lipid-DNA complexes-lipoplexes-for gene transfer and therapy. Bioelectrochemistry 58, 53-64.

Zheng J, Shen W, He DZ, Long KB, Madison LD, Dallos P. 2000a. Prestin is the motor protein of cochlear outer hair cells. Nature 405, 149-55.

Zheng JL, Gao WQ. 2000b. Overexpression of Math1 induces robust production of extra hair cells in postnatal rat inner ears. Nat Neurosci 3, 580-6.

Zheng QY, Johnson KR, Erway LC. 1999. Assessment of hearing in 80 inbred strains of mice by ABR threshold analyses. Hear Res 130, 94-107.

Ziady AG, Gedeon CR, Miller T, Quan W, Payne JM, Hyatt SL, Fink TL, Muhammad O, Oette S, Kowalczyk T, Pasumarthy MK, Moen RC, Cooper MJ, Davis PB. 2003. Transfection of airway epithelium by stable PEGylated poly-L-lysine DNA nanoparticles in vivo. Mol Ther 8, 936-47.

Zou J, Ramadan UA, Pyykko I. 2010. Gadolinium uptake in the rat inner ear perilymph evaluated with 4.7 T MRI: a comparison between transtympanic injection and gelatin sponge-based diffusion through the round window membrane. Otol Neurotol 31, 637-41.

Zou J, Pyykko I, Sutinen P, Toppila E. 2005b. Vibration induced hearing loss in guinea pig cochlea:

expression of TNF-alpha and VEGF. Hear Res 202, 13-20.

Zou J, Poe D, Bjelke B, Pyykko I. 2009. Visualization of inner ear disorders with MRI in vivo: from animal models to human application. Acta Otolaryngol Suppl, 22-31.

Zou J, Pyykko I., Bretlau P, Klason T, Bjelke B. 2003a. In vivo visualization of endolymphatic hydrops in guinea pigs: magnetic resonance imaging evaluation at 4.7 tesla. Ann Otol Rhinol Laryngol 112, 1059-65.

Zou J, Pyykko I, Bjelke B, Dastidar P, Toppila E. 2005a. Communication between the perilymphatic scalae and spiral ligament visualized by in vivo MRI. Audiol Neurootol 10, 145-52.

Zou J, Pyykko I, Counter SA, Klason T, Bretlau P, Bjelke B. 2003b. In vivo observation of dynamic perilymph formation using 4.7 T MRI with gadolinium as a tracer. Acta Otolaryngol 123, 910-5.

Zou J, Saulnier P, Perrier T, Zhang Y, Manninen T, Toppila E, Pyykko I. 2008. Distribution of lipid nanocapsules in different cochlear cell populations after round window membrane permeation. J Biomed Mater Res B Appl Biomater 87, 10-8.

Zuleger N, Korfali N, Schirmer EC. 2008. Inner nuclear membrane protein transport is mediated by multiple mechanisms. Biochem Soc Trans 36, 1373-7.

10. ORIGINAL PUBLICATIONS